UNIVERSITY OF OSLO
Department of Physics

Master thesis 2007

Cooling of Neutron Stars

Sutharsan Arumugam

June 2007

Preface

Neutron stars are some of the densest manifestations of massive objects in the universe. They are ideal astrophysical laboratories for testing theories of dense matter physics and provide connections among nuclear physics, particle physics and astrophysics. Neutron stars may exhibit conditions and phenomena not observed elsewhere, such as hyperon-dominated matter, deconfined quark matter, superfluidity and superconductivity with critical temperatures near $10^{10}\,\mathrm{K}$, opaqueness to neutrinos, and magnetic fields in excess of $10^{13}\,\mathrm{G}$.

Current understanding of the structure of neutron stars is defined by existing mathematical models. On the basis of current models, the matter at the surface of a neutron star is composed of ordinary atomic nuclei as well as electrons. The "atmosphere" of the star is roughly one meter thick, below which one encounters a solid "crust". Proceeding inward, one encounters nuclei with ever increasing numbers of neutrons; such nuclei would quickly decay on Earth, but are kept stable by tremendous pressures. Proceeding deeper, one comes to a point called neutron drip ($\rho_{\mathrm{d}} \approx 4.3 \times 10^{11}\,\mathrm{g/cm^3}$) where free neutrons leak out of nuclei. In this region, there are nuclei, free electrons, and free neutrons. The nuclei become smaller and smaller until the core is reached, by definition the point where they disappear altogether. The exact nature of the superdense matter in the core is still not well understood. The core material could be a superfluid mixture of neutrons with a few protons and electrons, or it could incorporate high-energy particles like pions and kaons in addition to neutrons, or it could be composed of strange matter incorporating quarks heavier than up and down quarks, or it could be quark matter not bound into hadrons. However so far observations have neither indicated nor ruled out such exotic states of matter.

The main objective of this thesis is to investigate the cooling mechanism that causing energy loss from a neutron star. The study of neutron star cooling is potentially an important source of information about the interior constitution of neutron stars. To start with, we briefly describe the formation, structure, internal composition and evolution of neutron stars. We then aim at calculating the rate of energy loss associated with the neutrino emission from the neutron star.

Our treatment is suitable for beginning graduate students or advanced undergraduates in physics and mathematics. No prior knowledge of astrophysics or general relativity is needed. Instead, we introduce the necessary concepts and mathematical tools which are of relevance in the calculations. We do assume that the reader has familiarity with classical and relativistic mechanics, statistical mechanics, and quantum field theory.

Acknowledgments

First I would like to thank Professor Morten Hjorth-Jensen for his everlasting encouragement and guidance throughout this thesis. For collaboration in the development of numerical algorithms I am very thankful to my co-student Jon Thonstad. I have greatly benefited from discussions with Professor Jan Olav Eeg and other colleagues. I would like to thank all of them for their help, and particularly Sigurd Kirkevold Næss who gave me invaluable criticism and suggestions. Finally, I will be forever grateful to my family: Kasi, Selva, Sunthar, Theeban, and Karthika, and particularly to my mother, Selva, for her support and encouragement throughout my life. With these in mind, I dedicate this thesis to my family.

— Sutharsan Arumugam

Contents

Chapter 1

Introduction

Neutron stars are born in supernova explosions and the interior temperatures initially exceed $T \sim 10^{11}\,\mathrm{K}$. As the neutron star cools down to $10^{10} - 10^{9}\,\mathrm{K}$, neutrinos begin to stream freely and essentially leave the star without further interaction. As a consequence, after about 30 s, the long-term cooling of neutron stars is controlled by neutrino emission. This stage lasts up to about 10^5 years of age, when cooling by emission of photons becomes more effective. Photon emission overtakes neutrinos only when the internal temperature falls to $\sim 10^8\,\mathrm{K}$, with a corresponding surface temperature roughly two orders of magnitude smaller. Importantly, the neutron stars remain luminous enough during the cooling, so that the surface temperature can be extracted from space telescope data and the theoretical cooling curves can be confronted with observations. During the last years there have been made intense efforts to measure the surface temperatures of neutron stars by the orbiting Einstein Observatory (HEAO-2) and the German ROSAT satellite. The thermal evolution of a neutron star can in principle yield significant information about the interior constitution of matter and structure of the neutron star.

As mentioned above, the characteristic way of energy loss from a neutron star is expected to proceed via the emission of neutrinos. The important neutrino-emitting process leading to the cooling of neutron stars is the so-called direct Urca process:

$$n \longrightarrow p + e^- + \bar{\nu}_e, \qquad\qquad p + e^- \longrightarrow n + \nu_e.$$

These are the well known β-decay of the neutron and electron capture on protons. But these processes are not usually allowed on the surface of a neutron star because the densities are too low to ensure momentum conservation. Thus, for a long time, the dominant mode of neutrino emission is thought to be the so-called modified Urca process:

$$n + n \longrightarrow n + p + e^- + \bar{\nu}_e, \qquad\qquad n + p + e^- \longrightarrow n + n + \nu_e.$$

These processes are basically the direct Urca process, with the addition of a bystander particle whose sole purpose is to enhance the phase space. My fellow master-student, Jon Thonstad, has studied this type of processes in his master thesis.

Besides the processes stated above, there exist several other neutrino-emitting processes, like neutrino pair bremsstrahlung:

$$n + n \longrightarrow n + n + \nu + \bar{\nu}, \qquad n + p \longrightarrow n + p + \nu + \bar{\nu}.$$

Like the modified Urca process, the neutrino pair bremsstrahlung plays a crucial role in neutron star cooling. All these processes together make the so-called standard cooling scenario for a neutron star.

In this project we are considering a non-rotating star that mostly consists of neutrons and protons as well as electrons. In the first turn, we will focus on the direct Urca process and study the β-decay of the neutron. We take aim at calculating the neutrino emissivities due to the direct Urca process. For this purpose we are going to construct a numerical program which is able to carry out a five-dimensional integration over the phase space. Afterwards, we will go on to study the neutrino pair bremsstrahlung in detail. In this regard, we will set up all the Feynman diagrams contributing to this process. We will then work out the corresponding Feynman amplitudes analytically. As a principal stage, we are going to develop a generic code for calculating the Feynman amplitude of any process. In preparing this numerical tool, I have cooperated with my co-student Jon Thonstad. And last, but not least, we will calculate the rate of energy loss associated with the neutrino emission from neutrino pair bremsstrahlung.

The properties of neutron stars are determined by the equation of state (EoS) for dense matter. Properties like the mass range, the mass-radius relationship, the crust thickness and the cooling rate can all be extracted from the EoS. The same EoS is also crucial in calculating the energy released in a supernova explosion. The properties of dense matter and the associated EoS are reasonably well understood in the density regime below the saturation density ρ_0. In the high-density range above ρ_0, the physical properties of matter are still uncertain so that the associated EoS is only very poorly known.

Concerning the energy loss by the neutrino emission, a qualitative and approximate description was already carried out by Friman and Maxwell in 1979[1]. In their work, they have applied a nucleon-nucleon interaction that consists of a long-range, one-pion-exchange tensor part and a short-range part parametrized with nuclear Fermi liquid (Landau) parameters. However, a proper treatment would be here to introduce the many-body contributions from the EoS in order to generate a medium modified interaction. This effective interaction may be parametrized by means of γ-matrices and be used directly in the calculation of neutrino emissivities. This approach will eventually give a consistent relation between the EoS and neutrino emissivities. In calculating the rate of neutrino emission, we thus apply various equations of state and composition of matter in order to include the many-body correlations in an effective way. We will in the following work out a general formalism and a calculational scheme that may be carried out to determine the neutrino emissivities of any process, with a given effective interaction.

The layout of this thesis is as follows. The basic concepts and properties of neutron stars are covered in Chapter 2. In entering on this chapter, we briefly discuss the characteristics of neutron stars, followed by a historical overview. We further describe the formation, structure, internal composition, equation of state and cooling of neutron stars. In Chapter 3 we give a substantial treatment of the direct Urca process. We will here take a closer look at the β-decay of the neutron and evaluate the corresponding matrix element. This chapter concludes with the calculation of neutrino emissivity by the direct Urca process. Chapter 4 is devoted to the detailed analysis of neutrino pair bremsstrahlung, where we first evaluate the corresponding Feynman amplitudes and then go for the neutrino emissivities. In Chapter 5 we present the numerical results obtained for neutrino emissivities and sketch the key features of the numerical methods. Concluding remarks and suggestions for future work are given in Chapter 6. Finally, the calculational details which frequently occur in the following chapters, are worked out in Appendix A.

Chapter 2

Neutron Stars

Neutron stars inherit the class of compact objects that incorporate white dwarfs and black holes. They are "born" when normal stars "die" as most of their nuclear fuel has been consumed. All three species of compact object differ from normal stars in two fundamental ways. First, since they do not burn nuclear fuel, they cannot support themselves against gravitational collapse by generating thermal pressure. Instead, white dwarfs are supported by the pressure of degenerate electrons, while neutron stars are supported largely by the pressure of degenerate neutrons. Black holes, on the other hand, are completely collapsed stars – that is, stars that could not find any means to hold back the inward pull of gravity and therefore collapsed to singularities. All three objects represent the final stage of stellar evolution.

The second characteristic distinguishing compact objects from normal stars is their exceedingly small size. Relative to normal stars of comparable mass, compact objects have much smaller radii and hence, much stronger surface gravitational fields. A typical neutron star has a mass between 1.35 to about 2.1 solar masses ($M_\odot = 1.989 \times 10^{30}\,\mathrm{kg}$), with a corresponding radius between 20 and 10 km – 30,000 to 70,000 times smaller than the Sun ($R_\odot = 6.96 \times 10^5\,\mathrm{km}$). Thus, neutron stars have densities of $8\times10^{13}-2\times10^{15}\,\mathrm{g/cm^3}$, about the density of an atomic nucleus ($\rho_0 = 2.8\times10^{14}\,\mathrm{g/cm^3}$). By comparison, white dwarfs, which are of less than $1.44\,M_\odot$, have radii of at least several thousand kilometers, and central densities in the range of $10^5 - 10^9\,\mathrm{g/cm^3}$. If a gravitational collapse is going to occur on any star over $5\,M_\odot$, it would inevitably produce a black hole with infinite density.

Because of the enormous density range spanned by compact objects, their analysis requires a deep physical understanding of the structure of matter and the nature of interparticle forces over a vast range of parameter space. All four fundamental interactions (the strong and weak nuclear forces, electromagnetism, and gravitation) play a role in compact objects. Particularly noteworthy are the large surface potentials encountered in compact objects, which imply that general relativity is important in determining their structure.

White dwarfs can be observed directly in optical telescopes during their long cooling epoch. Neutron stars can be observed directly as pulsating radio sources (pulsars) and indirectly as gas-accreting, periodic X-ray sources (X-ray pulsars). Black holes can only be observed indirectly through the influence they exert on their environment. For example, they could be observed as gas-accreting, aperiodic X-ray sources under appropriate circumstances.

2.1 History of Discoveries

In 1932, Sir James Chadwick discovered the neutron as an elementary particle, for which he was awarded the Nobel Prize in Physics in 1935. Only a year after Chadwick's discovery of the neutron, Walter Baade and Fritz Zwicky in 1933, proposed the existence of the neutron star. In seeking an explanation for the origin of a supernova, they proposed that the neutron star is formed in a supernova. Baade and Zwicky correctly proposed at that time that the release of the gravitational binding energy GmM/R of the neutron stars powers the supernova: «*In the supernova process mass in bulk is annihilated.*»

If the central part of a massive star before its collapse contains $3\,M_\odot$, then a neutron star of $2\,M_\odot$ can be formed. The binding energy E of such a neutron star, when expressed in mass units via the mass-energy equivalence formula $E = mc^2$, is $1\,M_\odot$. It is ultimately this energy that powers the supernova.

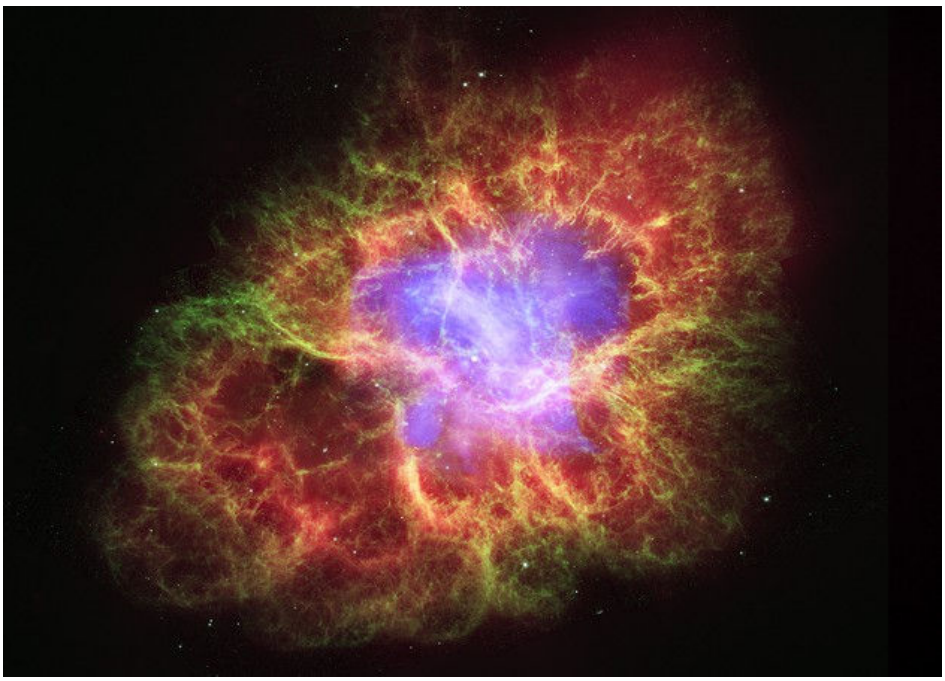

Figure 2.1: The Crab nebula is one of the most known supernova remnant in which we find the Crab pulsar, a neutron star spinning 30 times a second, is the bright spot near picture center. Credit: NASA - X-ray: CXC, J. Hester (ASU) *et al.*

First theoretical neutron star calculations were carried out by Richard Chace Tolman, Julius Robert Oppenheimer and George Michael Volkoff in 1939 and John Archibald Wheeler around 1960[2]. It was not until the discovery in 1967 by Jocelyn Bell and Antony Hewish of radio pulsars and their identification by Thomas Gold as rotating neutron stars, that the existence of neutron stars was established. The discovery of the rapidly rotating Crab pulsar (Fig. 2.1) in the remnant of the Crab supernova observed by the Chinese in 1054 A.D. confirmed the link to supernovae.

A newborn neutron star can rotate several times a second; sometimes, when they orbit a companion star and are able to accrete matter from it, they can increase this to several hundred times per second, distorting into an oblate spheroid shape despite their own immense gravity. Over time, neutron stars slow down because their rotating magnetic fields radiate energy; older neutron stars may take several seconds for each revolution. Sometimes a neutron star will spin up or undergo a glitch, a rapid and unexpected increase of its rotation speed. Glitches are thought to be the effect of a sudden coupling between the superfluid interior and the solid crust.

Neutron stars are found both in isolation and in binary star systems as well as in luminous compact X-ray binaries. About 1500 neutron stars have so far been detected in our galaxy as radio pulsars, including about 125 such pulsars with millisecond periods[3]. More than 200 accretion powered neutron stars have been detected in X-ray binary systems; about 50 are X-ray pulsars and a similar number produce intense X-ray bursts powered by thermonuclear flashes. Non-rotating and non-accreting neutron stars are virtually undetectable. With the Hubble space telescope one single thermally radiating neutron star has been found. Its distance is only 160 pc from Earth and its surface temperature reads $T \simeq 60\,\mathrm{eV}$. From its luminosity one deduces a radius of the neutron star $R \leqslant 14\,\mathrm{km}$.

The remarkable discoveries made in the past few decades will continue as numerous earth-based and satellite experiments are running at present and more will be launched. History tells us that the future will bring great surprises and discoveries in this field.

2.2 Formation of Neutron Stars

Neutron stars are formed from the collapsed remnant of a massive star, a Type II, Type Ib, or Type Ic supernova. They are cold stars supported by the Pauli exclusion principle, which produces a repulsion between neutrons. During the collapse of the core, the electrons and protons are pushed closer together, which are then combined to produce neutrons by the inverse β-decay. As the density increases, all the low energy levels available to the neutrons are filled, and hence the star becomes colder. By further gravitational collapse, the neutrons are forced into higher energy levels, filling the lowest unoccupied energy states. And so the Pauli exclusion principle takes over, creating an effective pressure which prevents further collapse. It is ultimately this degeneracy pressure that holds back the collapsed remnant so as to form a neutron star. The degeneracy pressure is caused by the close packing of the neutrons rather than by the motion of the particles. As a result, neutron stars can be stable no matter what the internal temperature is, because the pressure that supports the star is independent

of temperature.

Let us now briefly review the main stages in the evolution of a neutron star. These stages are dramatically illustrated in Fig. 2.2. Generally, stars with $M > 8\,M_\odot$ evolve in a complex fashion. In the core of the star, hydrogen is fused into helium, releasing the energy needed to support the overlaying layers against collapse. Once the hydrogen at the core becomes exhausted, the star contracts until the temperatures and pressures are high enough to allow helium fusion. As the star evolves, it undergoes repeated stages where fusion in the core stops, and the core collapses until the pressure and temperature is sufficient to begin the next stage of fusion, reigniting to halt collapse.

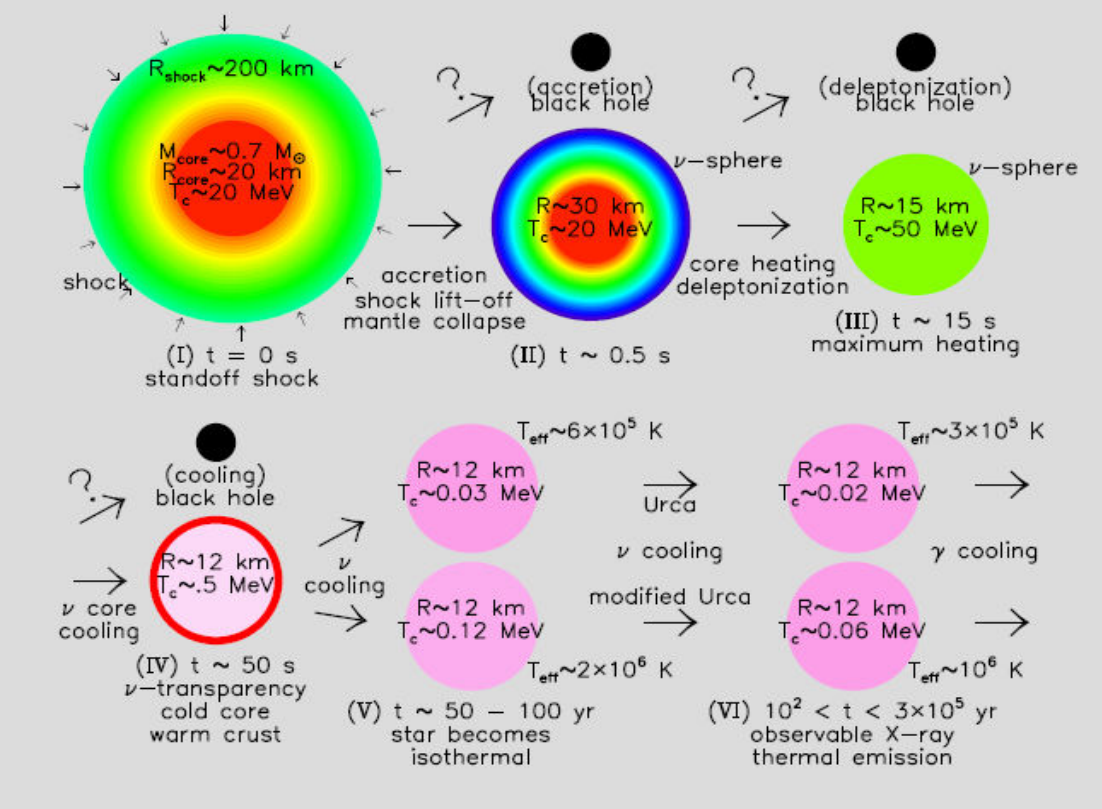

Figure 2.2: The main stages of evolution of a neutron star. The radius R and central temperatures T_c for the neutron star are indicated as it evolves in time t.

As increasingly heavier elements undergo nuclear fusion, the binding energy of the nuclei increase and progressively lower levels of energy is produced. This culminates with the production of iron, which does not produce energy through fusion. As a result, an iron core builds up that can only support the overlaying mass of the star through the degeneracy pressure of electrons. When the core's size exceeds the Chandrasekhar limit of $1.44\,M_\odot$, degeneracy pressure can no longer support it and the core undergoes a catastrophic collapse to produce a neutron star. The Chandrasekhar limit (named after Subrahmanyan Chandrasekhar) is the maximum nonrotating mass which can be supported against gravitational collapse by electron degeneracy pressure.

The core then implodes at velocities reaching $70,000\,\mathrm{km/s}$, resulting in a rapid increase in temperature and density. Through photodisintegration, gamma rays decompose the iron into helium nuclei and free neutrons. The conditions also cause electrons and protons to merge through inverse β-decay, producing neutrons and electron neutrinos. About $10^{46}\,\mathrm{J}$ of gravitational energy are converted into a ten-second burst of neutrinos. These carry away energy from the core and accelerate the collapse, while some neutrinos are absorbed by the star's outer layers and begin the supernova explosion. As the neutrinos are temporarily trapped within the star, the typical neutrino matter cross section reads $\sigma \approx 10^{-40}\,\mathrm{cm}^2$[4]. This results in a mean free path $\lambda \approx (\sigma n)^{-1} \approx 10\,\mathrm{cm}$ with the baryon number density $n \simeq 2 - 3\,n_0$ ($n_0 \simeq 0.16\,\mathrm{fm}^{-3}$). This length is much less than the proto-neutron star radius $R > 20\,\mathrm{km}$.

The inner core eventually reaches a density comparable to that of an atomic nucleus, where the collapse is halted. The infalling matter then rebounds, producing a shock wave that propagates outward. This expanding shock can stall in the outer core as energy is lost through the dissociation of heavy elements. However, through a process that is not clearly understood, the shock reabsorbs $10^{44}\,\mathrm{J}$ of energy, producing an explosion.

One speculates that the neutrinos from the core, assisted by rotation, convection and magnetic fields, resuscitate the shock, which within seconds accelerates outwards, expelling the massive stellar mantle. The proto-neutron star left behind rapidly shrinks because of pressure losses from neutrino emission in its periphery. The escape of neutrinos from the interior occurs on a diffusion time $\tau \simeq 3R^2/\lambda c \approx 10\,\mathrm{s}$.

The loss of neutrinos initially warms the stellar interior. The core temperature more than doubles, reaching $\sim 50\,\mathrm{MeV}$ ($6 \times 10^{11}\,\mathrm{K}$). After $10 - 20\,\mathrm{s}$, however, the steady emission of neutrinos begins to cool the interior. Because the cross section $\sigma \propto \lambda^{-1}$ scales as the square of the mean neutrino energy, the condition $\lambda > R$ is achieved in about $50\,\mathrm{s}$. The star becomes transparent to neutrinos, and its cooling rate accelerates.

Neutron stars rotate extremely rapidly after their creation due to the conservation of angular momentum. The slow rotation of the original star's core speeds up as it shrinks. Neutron stars may "pulse" due to particle acceleration near the magnetic poles, which are not aligned with the rotation axis of the star. Through mechanisms not yet entirely understood, these particles produce coherent beams of radio emission. The pulses come at the same rate as the rotation of the neutron star, and thus, appear periodic. The radio pulsars are rapidly rotating with periods in the range $0.033\,\mathrm{s} \leqslant P \leqslant 4.0\,\mathrm{s}$. They are believed to be powered by rotational energy loss and are rapidly spinning down with period derivatives of order $\dot{P} \sim 10^{-12} - 10^{-16}$. Their high magnetic fields are estimated to be the order of $B \sim 10^{11} - 10^{13}\,\mathrm{G}$. A distinct subclass of radio pulsars are millisecond pulsars with periods between $1.56\,\mathrm{ms} \leqslant P \leqslant 100\,\mathrm{ms}$. The period derivatives are very small corresponding to very small magnetic fields $B \sim 10^8 - 10^{10}\,\mathrm{G}$.

2.3 Structure of Neutron Stars

A neutron star has five major regions, the inner and outer cores, the crust, the envelope and the atmosphere. A scheme that visualizes these five regions is shown in Fig. 2.3. The atmosphere and envelope contain a negligible amount of mass, but the atmosphere plays an important role in shaping the emergent photon spectrum, and the envelope crucially influences the transport and release of thermal energy from the star's surface.

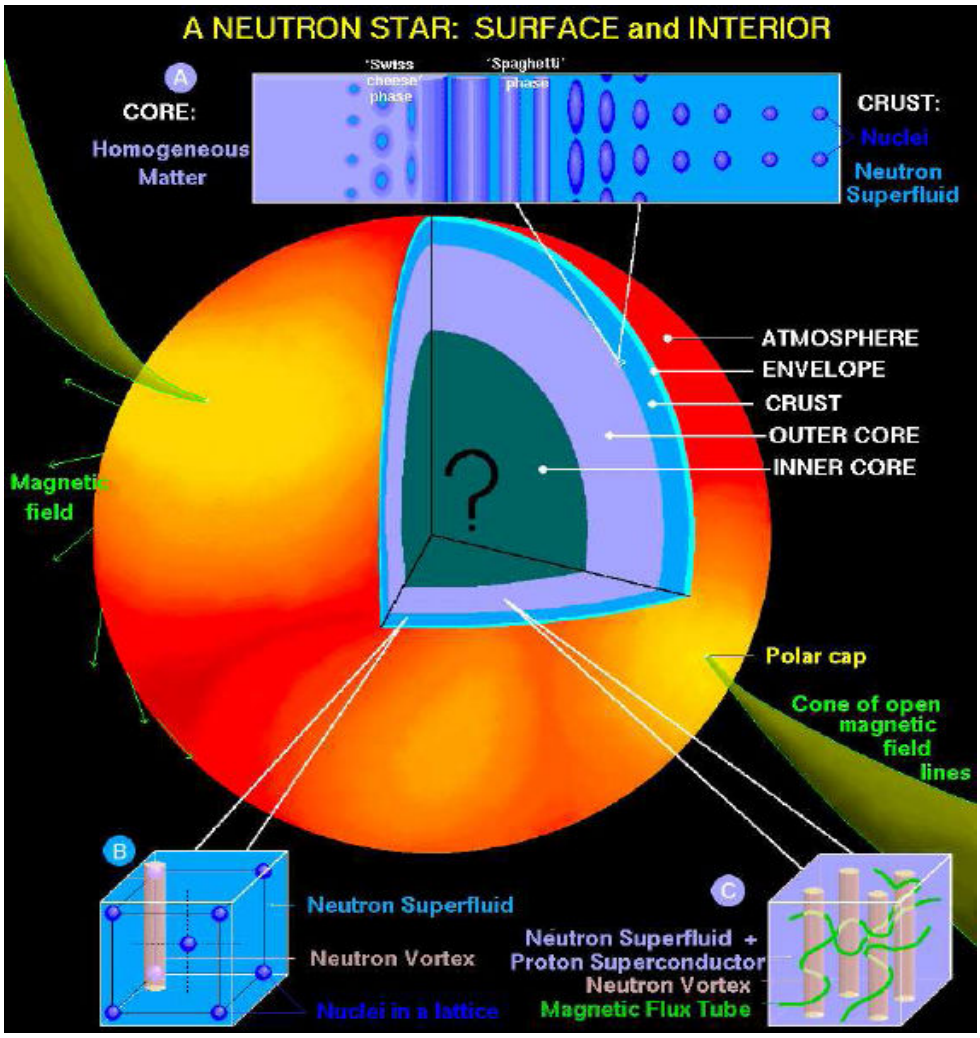

Figure 2.3: The major regions and possible composition inside a normal matter neutron star. The top bar illustrates expected geometric transitions from homogenous matter at high densities in the core to nuclei at low densities in the crust. Superfluid aspects of the crust and outer core are shown in insets.

The crust, extending about 1 to 2 km below the surface, primarily contains nuclei. The matter in the outer part of the crust is expected to be primarily ^{56}Fe, the end point of thermonuclear burning processes in stars.

With increasing depth, the electron Fermi energy rises. Beyond the density $8 \times 10^6\,\mathrm{g/cm^3}$, the Fermi energy of the electron is so high ($E_F(e) > 1\,\mathrm{MeV}$) that ^{56}Fe can capture energetic electrons. In the capture process, as occurs during the formation of the neutron star in a supernova, protons in nuclei are converted into neutrons via the inverse β-decay. The produced electron neutrinos escape the nascent neutron star, lowering the energy of the system.

The matter becomes more neutron rich and rearranges into a sequence, with increasing density. As increasingly neutron-rich nuclei emerge, one encounters nuclei such as ^{118}Kr at the neutron drip $\rho_\mathrm{d} \approx 4.3 \times 10^{11}\,\mathrm{g/cm^3}$. The nuclei present deep in the crust, cannot undergo β-decay because the electron would, by energy conservation, have to go into an already occupied state, a process forbidden by the Pauli exclusion principle. Beyond the neutron drip ρ_d, the matter becomes so neutron rich that not all the neutrons can be accommodated in the nuclei, and the matter, still solid, becomes permeated by a sea of free neutrons in addition to the sea of electrons.

As in fission, the spherical nuclei become unstable at a density $\rho \sim \rho_0/3$, and the matter proceeds through a sequence of rather unusual structures, termed "pasta nuclei". The nuclei first become rod-like and then laminar, with pure neutrons filling the space between. The pure-neutron plates become thinner; eventually the neutrons form rods, and then spheres, with the between regions containing proton-rich matter. Remarkably, over half the matter in the crust is in the form of these non-spherical configurations.

Finally, at a density of about ρ_0, the matter dissolves into a uniform liquid composed primarily of neutrons with a few percent protons and electrons and a smaller fraction of muons. The neutrons are most likely superfluid and the protons superconducting; the electrons, however, are normal. Such a superfluid may form a reservoir of angular momentum that, being loosely coupled to the crust so as to cause pulsar glitch phenomena.

The states of matter at high pressures deep in the interior are less well understood. With increasing density heavier baryons can live stably in the star. Several interesting phenomena are possible. One is that π-mesons are spontaneously produced and form a superfluid "Bose-Einstein condensed" state; such condensation would greatly enhance the cooling of neutron stars by neutrino emission. The matter may similarly undergo an analogous "kaon condensation". At ultrahigh densities, where the nucleons are strongly overlapping, matter is expected to dissolve into quark matter, in which the quarks that make up the baryons become free to run throughout. Quark matter most likely first appears as droplets in a sea of nuclear matter at densities of order several times ρ_0. A core of bulk quark matter, which would be present at higher densities, would also enhance neutron star cooling, but whether the transition to bulk quark matter is actually reached in neutron stars remains uncertain.

2.4 Cooling of Neutron Stars

As we have discussed in the introduction, a newborn neutron star looses energy by the emission of neutrinos. During the thermal evolution of the crust, the heat is transported by electron conduction into the interior. The heat is then radiated away by neutrinos, creating an isothermal structure within 10 to 100 years. The star continuously emits photons, primarily in X-rays, with an effective temperature $T_{\rm eff}$ that tracks the interior temperature by a factor of ~ 100 smaller. The energy loss from photons is swamped by neutrino emission until the star becomes about 3×10^5 years old. Besides the standard cooling scenario introduced in Chapter 1, there are also additional sources of energy loss, involving hyperons and Δ-isobars.

At densities not far above that of nuclear matter, constituent other than neutrons, protons, electrons, and muons may appear. The lightest of these are the Λ- and Σ^--hyperons, with masses of 1116 MeV and 1197 MeV, respectively. At zero temperature, it follows from the condition for chemical equilibrium that Λ-hyperons will appear when the energy of the lowest state for a Λ first lies below μ_n, while Σ^--hyperons will appear when the lowest energy state of a Σ^- first lies below $\mu_n + \mu_e$. The energy of the lowest hyperon state is the rest mass energy, plus the potential energy of interaction of the hyperon with the other constituents. As a rule, there is no kinetic-energy term, since it is expected on the basis of microscopic calculations that the lowest hyperon state will have zero momentum. The simplest weak-interaction processes in which these hyperons can participate are

$$\Lambda \longrightarrow p + e^- + \bar{\nu}_e, \qquad\qquad \Sigma^- \longrightarrow n + e^- + \bar{\nu}_e,$$

and their Urca partners that generate neutrinos. These processes are essentially the ones responsible for neutrino emission from kaon condensates. As in the case of the direct Urca process for nucleons, the processes are kinematically allowed provided the Fermi momenta satisfy the triangle inequalities. Minimum hyperon concentrations for which the Urca process can proceed may be estimated by combining two of the triangle inequalities, and this leads to the conditions

$$p_F(\Lambda) \geqslant |p_F(p) - p_F(e)|, \tag{2.1}$$
$$p_F(\Sigma) \geqslant |p_F(n) - p_F(e)|. \tag{2.2}$$

If electrons and protons were the only charged particles present, the electron and proton Fermi momenta would be equal, and Eq. (2.1) indicates that the direct Urca process could occur even for an infinitesimally small concentration of Λ-hyperons. Even if other negatively charged species were present, the threshold concentration of Λ-hyperons would be quite small, typically of the order of one part in a thousand. For the Σ^--decay to take place, the Σ^- Fermi momentum must be large enough to make up the difference between the electron and neutron momenta, which means in practice that the threshold concentration is comparable to the threshold proton concentration for the nucleon direct Urca process.

The neutrino emissivities may be estimated as in the case of nucleon direct Urca process. In hyperon Urca process there is a change of strangeness, so characteristic neutrino emission rates are proportional to $\sin^2\theta_C$ and are therefore less than one-tenth of those for the nucleon Urca process. With a greater variety of particles present, even more Urca processes could take place. For example, if both Σ^- and Λ are present, the process

$$\Sigma^- \longrightarrow \Lambda + e^- + \bar{\nu}_e,$$

is a candidate. There is no strangeness change, so the process is not Cabibbo suppressed: its matrix element squared is in fact about 20% of that for the nucleon Urca process. Threshold hyperon concentrations would not be large, since neutrons do not participate. Another particle with a mass only a little above that of the Σ^- is the Δ^-. This could participate in weak processes like

$$\Delta^- \longrightarrow n + e^- + \bar{\nu}_e.$$

Whether any of these processes can occur in neutron stars is uncertain because of our ignorance of interactions among hyperons, isobars, and nucleons at densities well above nuclear density. The important conclusion from the study of processes for hyperons and Δ-isobars is that fast cooling is possible without exotic states and without proton concentrations high enough to allow the nucleon direct Urca process.

2.5 Equations of State

The properties of neutron stars, including their radii as a function of mass, and the range of masses for which they are stable, are determined by the equation of state (EoS) of the matter they contain. From classical mechanics one has the following structure equations for stars

$$\frac{dP}{dr} = -\frac{G\rho(r)M(r)}{r^2} = -\frac{G\epsilon(r)M(r)}{c^2r^2}, \tag{2.3}$$

$$\frac{dM(r)}{dr} = 4\pi r^2\rho(r) = \frac{4\pi r^2\epsilon(r)}{c^2}, \tag{2.4}$$

$$M(r) = 4\pi\int_0^R r^2\rho(r)dr = \frac{4\pi}{c^2}\int_0^R r^2\epsilon(r)dr. \tag{2.5}$$

Here $G = 6.6742\times10^{-13}$ N cm^2/g^2 is Newton's gravitational constant, $\rho(r)$ is the mass density at distance r, and ϵ is the corresponding energy density. The quantity $M(r)$ is the total mass inside the sphere of radius r.

Note that in the second halves of Eqs. (2.3)–(2.5), we have departed slightly from Newtonian mechanics and have expressed the energy density $\epsilon(r)$ in terms of the mass density $\rho(r)$ according to the mass-energy equivalence formula, $\epsilon(r) = \rho(r)c^2$. This definition allows Eq. (2.3) to be used when we take into account contributions of the interaction energy between the particles making up the star.

To solve Eqs. (2.3)–(2.5) for $P(r)$ and $M(r)$, we can integrate from the origin, $r = 0$, to the point $r = R$ where the pressure goes to zero. This point defines R as the radius of the star. We will need an initial value of the pressure P_0 at $r = 0$, and so the total mass of the star $M(R)$ will depend on the value of P_0. To be able to perform the integration, we need to know the energy density $\epsilon(r)$ in terms of the pressure $P(r)$. This relation is the EoS for the matter making up the star.

The Newtonian formulation presented above works well in regimes where the mass of the star is not so large that it significantly warps space-time. That is, integrating Eqs. (2.3) and (2.4) will work well in cases for which general relativistic effects are not important, such as for white dwarfs. General relativistic effects become important when the ratio GM/c^2R becomes non-negligible, as is the case for typical neutron stars.

The general relativistic corrections to Eqs. (2.3)–(2.5) are attained by means of the Tolman-Oppenheimer-Volkoff equations[5], which are expressed in terms of three additional factors

$$\frac{dP}{dr} = -\frac{G\epsilon(r)M(r)}{c^2r^2}\left[1+\frac{P(r)}{\epsilon(r)}\right]\left[1+\frac{4\pi r^3P(r)}{M(r)c^2}\right]\left[1-\frac{2GM(r)}{c^2r}\right]^{-1}. \qquad (2.6)$$

The first two factors in the square brackets in Eq. (2.6) represent special relativity corrections of order v^2/c^2. These factors enter because, in the non-relativistic limit, the pressure P varies as $p_F^2/2m = mv^2/2$, while ϵ and Mc^2 vary as mc^2. These factors reduce to 1 in the non-relativistic limit. The last set of brackets in Eq. (2.6) is a general relativistic correction. Eq. (2.4) for $M(r)$ remains unchanged.

Note that the correction factors are all positive definite. It is as if Newtonian gravity becomes stronger for any value of r. That is, relativity strengthens the relentless pull of gravity. Eqs. (2.6) and (2.4) involve a balance between gravitational forces and the internal pressure. The pressure is a function of the EoS, and for certain conditions it may not be sufficient to withstand the gravitational attraction. Thus the structure equations imply there is a maximum mass that a star can have. The resultant coupled non-linear equations for $P(r)$ and $M(r)$ can be integrated from $r = 0$ to the point R where $P(R) = 0$, to determine the star mass $M(R)$ for a given value of P_0. Although a few exact solutions are known, for a realistic $P - \epsilon$ relation (EoS) these equations must be numerically solved to obtain the mass-radius relation.

A knowledge of the maximum mass $M_{\max}$ that a neutron star can have is important in distinguishing possible black holes from neutron stars by observations of their masses. There are large variations in predicted radii and maximum masses because of the uncertainties in the EoS near and above ρ_0. This seems paradoxical because the properties of matter inside laboratory nuclei are thought to be well understood. However, an important distinction between nuclear and neutron star matter is their relative proton fraction x_p. Nuclear matter has nearly equal numbers of neutrons and protons, but neutron star matter has only a few percent protons.

The properties of dense matter and the associated EoS are reasonably well understood in the density regime below the saturation density ρ_0. In the high-density range above ρ_0, the physical properties of matter are still uncertain so that the associated EoS is only very poorly known. At densities of $0.1\,\mathrm{fm}^{-3}$ and greater, one assumes a charge neutral uniform matter consisting of neutrons, protons, electrons and muons in β-equilibrium. The matter is considered to be at temperatures much lower than the typical Fermi energies. By means of the charge and chemical equilibrium, one can determine the composition of matter in the interior of the star. The equilibrium conditions are governed by the following weak processes

$$B_1 \longrightarrow B_2 + l^- + \bar{\nu}_l, \qquad\qquad B_2 + l^- \longrightarrow B_1 + \nu_l.$$

where B_1 and B_2 refer to the baryons being a neutron and a proton, respectively. l^- is either an electron or a muon and $\bar{\nu}_l$ and ν_l their respective antineutrinos and neutrinos. Muons will typically appear at a density close to the saturation density for nuclear matter. This saturation density is given by $n_0 \approx 0.16 \pm 0.02\,\mathrm{fm}^{-3}$, with a corresponding binding energy for symmetric nuclear matter of $E_0 = B/A = -15.6 \pm 0.2\,\mathrm{MeV}$. Given the energy density ϵ the pressure is defined through the relation

$$P(n, x_p) = n^2 \frac{\partial \mathscr{E}(n, x_p)}{\partial n} = n \frac{\partial \epsilon}{\partial n} - \epsilon, \tag{2.7}$$

where $\mathscr{E}(n, x_p)$ stands for the energy per baryon. Similarly, the chemical potential for each species of particle is given by

$$\mu_i = \frac{\partial \epsilon}{\partial n_i}. \tag{2.8}$$

In calculating the properties of neutron star matter in β-equilibrium, one needs to calculate the energy per baryon $\mathscr{E}(n, x_p)$ for several proton fractions x_p. The latter corresponds to the ratio of protons as compared to the total nucleon number Z/A: $x_p = n_p/n$, where $n = n_n + n_p$ is the total baryon density. In the presence of neutrons and protons only, the Fermi momenta for neutrons and protons are related to the total baryon density by

$$n = (1 - x_p)n + x_p n = \frac{p_F^3(n)}{3\pi^2\hbar^3} + \frac{p_F^3(p)}{3\pi^2\hbar^3}. \tag{2.9}$$

Since the mean free path of neutrinos is much larger than the radius of neutron stars, the neutrinos do not accumulate inside neutron stars. Accordingly, the equilibrium conditions for matter, associated with the weak processes, become

$$\mu_n = \mu_p + \mu_e, \tag{2.10}$$

$$n_p = n_e. \tag{2.11}$$

If muons are present as well, we need to modify the equation for charge conservation to read $n_p = n_e + n_\mu$, and require that $\mu_e = \mu_\mu$.

It is well known that at lower densities the properties of the EoS are primarily determined by the nuclear symmetry energy $S_v(n)$. The latter expresses the difference in energy for symmetric nuclear matter and pure neutron matter:

$$S_v(n) = \mathscr{E}(n, x_p = 0) - \mathscr{E}(n, x_p = 1/2). \tag{2.12}$$

Here $\mathscr{E}(n, x_p = 0)$ refer to the energy per baryon for pure neutron matter, while $\mathscr{E}(n, x_p = 1/2)$ is the corresponding value for symmetric nuclear matter. The symmetry energy is defined in terms of a Taylor series expansion of the energy per baryon for nuclear matter in terms of the proton fraction $x_p = Z/A$ (or equivalently the asymmetry parameter $\alpha = (N - Z)/A$),

$$\mathscr{E}(n, x_p) = \mathscr{E}(n, x_p = 1/2) + S_2(n)(x_p - 1/2)^2 + S_4(n)(x_p - 1/2)^4 + ..., \tag{2.13}$$

where $S_2(n)$ is the quadratic symmetry energy. We assume that higher-order terms in Eq. (2.13) are quite small. Near the saturation density n_0 the quadratic symmetry energy is expanded as

$$S_2(n) = \frac{1}{2}\frac{\partial^2 \mathscr{E}(n, x_p)}{\partial x_p^2}\bigg|_{x_p=1/2} = a_4 + \frac{p_0}{n_0^2}(n - n_0) + \frac{\Delta K}{18 n_0^2}(n - n_0)^2 + ... \tag{2.14}$$

The quantity a_4 corresponds to the symmetry energy at equilibrium density and the slope parameter p_0 governs the density dependence. As a result the pressure can be written as

$$P(n, x_p) = n^2 \frac{\partial \mathscr{E}(n, x_p)}{\partial n} = n^2 \left[\mathscr{E}'(n, x_p = 1/2) + S_2'(n)(1 - 2x_p)^2 + ...\right]. \tag{2.15}$$

By using β-equilibrium in a neutron star,

$$\mu_e = \mu_n - \mu_p = -\frac{\partial \mathscr{E}(n, x_p)}{\partial x_p} \sim S_2(n)(1 - 2x_p), \tag{2.16}$$

and the result for the electron chemical potential,

$$\mu_e = \frac{3}{4}\hbar c\, x_p (3\pi^2 n x_p)^{1/3}, \tag{2.17}$$

one finds the proton fraction at saturation density, to be quite small, $x_0 \sim 0.04$. Hence the pressure at saturation density can in a good approximation be expressed in terms of (the density dependence of) the symmetry energy

$$P(n_0) = n_0(1 - 2x_0)(n_0 S_2'(n_0)(1 - 2x_0) + S_2(n_0)x_0) \sim n_0^2 S_2'(n_0). \tag{2.18}$$

Thus, the symmetry energy is of paramount importance for studies of neutron star matter in β-equilibrium. One can extract information about the value of the symmetry energy at saturation density n_0 from systematic studies of the masses of atomic nuclei. However, these results are limited to densities around n_0 and for proton fractions close to 1/2. Typical values for $S_2(n)$ at n_0 are in the range $27 - 38\,\mathrm{MeV}$. For densities greater than n_0 it is more difficult to get a reliable information on the symmetry energy, and thereby the related proton fraction.

A wide range of the densities inside neutron stars can be well represented by nucleonic degrees of freedom only. This incorporate the inner part of the crust to the outer part of the core, i.e. the density range $0.5 - 2\,n_0$. Since the properties of nucleons at such densities are close to those of free nucleons, the nucleons are assumed to do not loose their individuality in the dense matter. The above density range would correspond to internucleon distances of the order of $\sim 1 - 2\,\mathrm{fm}$. At such interparticle distances there is little overlap between the various nucleons and we may therefore assume that they still behave as individual nucleons and that one can absorb the effects of overlap into the two-nucleon interaction. In the nuclear medium there are interaction mechanisms which are obviously absent in vacuum. As an example, the one-pion exchange potential is modified in nuclear matter due to softening of pion degrees of freedom in matter.

In order to illustrate how the nucleon-nucleon interaction is renormalized in a nuclear medium, one may apply the so-called Brueckner-Hartree-Fock (BHF) approach, which is the simplest possible many-body approach. The G-matrix entering the BHF approach is rather similar to the Lippmann-Schwinger equation used to construct the scattering matrix T. The difference resides in the introduction of a Pauli operator in order to prevent scattering to intermediate particle states prohibited by the Pauli exclusion principle. In addition, the single-particle energies of the interacting particle are no longer given by kinetic energies only. However, several of the features seen at the level of the scattering matrix, pertain to the G-matrix as well. Therefore, if one employs different nucleon-nucleon interactions in the calculation of the energy per baryon in pure neutron matter with the BHF G-matrix, eventual differences can be retraced at the level of the T-matrix.

For a given NN-interaction V, the R-matrix for free-space two-nucleon scattering is obtained from the Lippmann-Schwinger equation, which reads in the center-of-mass frame and in a partial-wave decomposition

$$R^{\alpha T_z}_{ll'}(kk'\omega) = V^{\alpha T_z}_{ll'}(kk') + \sum_{l''} \int \frac{d^3q}{(2\pi)^3} V^{\alpha T_z}_{ll''}(kq) \frac{1}{\omega - H_0} R^{\alpha T_z}_{l''l'}(qk'\omega), \tag{2.19}$$

with ll' and kk' the orbital angular momentum and the linear momentum of the relative motion, respectively. T_z is the total isospin projection. The angular momentum J and total spin S are represented by the variable α. The term H_0 represents the kinetic energy of the intermediate states. The phase-shifts for a given partial wave can be calculated from the on-shell matrix element of R, which is obtained by setting $q = q' = q_0$ with $\omega = q_0^2/m_N$, m_N being the mass of the nucleon.

Following the conventional many-body approach, we divide the full Hamiltonian $H = T + V$, with T being the kinetic energy and V the bare NN-interaction, into an unperturbed part $H_0 = T + U$ and an interacting part $H_I = V - U$, such that

$$H = T + V = H_0 + H_I, \tag{2.20}$$

where we have introduced an auxiliary single-particle potential U. If U is chosen such that H_I becomes small, then perturbative many-body techniques can presumably be applied. A serious obstacle to any perturbative treatment is the fact that the bare

NN-interaction V is very large at short inter-nucleonic distances, which renders a perturbative approach highly prohibitive. To overcome this problem, we introduce the reaction matrix G given by the solution of the Bethe-Goldstone equation

$$G(\omega) = V + VQ\left[1/(\omega - QH_0Q)\right]QG, \tag{2.21}$$

where ω is the unperturbed energy of the interacting nucleons and Q is the Pauli operator which prevents scattering into occupied states. In the laboratory frame, the Pauli operator is given by

$$Q(k_m\tau_m, k_n\tau_n) = \begin{cases} 1, & k_m > k_F^{\tau_m}, k_n > k_F^{\tau_n}, \\ 0 & \text{otherwise}, \end{cases} \tag{2.22}$$

where $k_F^{\tau_i}$ defines the Fermi momenta of the proton ($\tau_i = 1/2$) and neutron ($\tau_i = -1/2$). With the so-called angle-average approximation of the Pauli operator, the G-matrix reads in a partial wave representation

$$G_{ll'}^{\alpha T_z}(kk'K\omega) = V_{ll'}^{\alpha T_z}(kk') + \sum_{l''}\int \frac{d^3q}{(2\pi)^3} V_{ll''}^{\alpha T_z}(kq)\frac{Q^{T_z}(q,K)}{\omega - H_0} G_{l''l'}^{\alpha T_z}(qk'K\omega). \tag{2.23}$$

The variable K is the momentum of the center-of-mass motion. By the angular average of the Pauli operator, the G-matrix is diagonal in total angular momentum J. Further, the G-matrix is diagonal in the center-of-mass orbital momentum L and the total spin S, and so all three variables is represented by the index α. The variable α differs therefore from the definition of the R-matrix, where $K = 0$. The term H_0 is the unperturbed energy of the intermediate states and depends on k, K and the individual isospin of the interacting particles. The structure of G-matrix in Eq. (2.23) can be directly compared to the R-matrix for free NN-scattering. Therefore, eventual differences between various potentials in a finite medium should be easily retraced to the structure of the R-matrix. It is also obvious that one expects the matrix elements of G to be rather close to those of R with only small deviations. These deviations originate from two effects which reduce the contributions of second and higher order in V to the G-matrix as compared to their contributions to R. One is the Pauli quenching effect mentioned above: the Pauli operator Q in Eq. (2.23) restricts the intermediate particle states to states above the Fermi energy. The second one is the dispersive effect: the energy denominators in Eq. (2.23) are defined in terms of the single-particle energies of nucleons in the medium while the corresponding denominators of Eq. (2.19) are differences between the energies of free nucleons. As a result, the matrix elements of G tend to be less attractive than the corresponding matrix elements of R.

The continuous single-particle spectrum is defined by the self-consistent solution of the following equations

$$\varepsilon_i = t_i + u_i = \frac{k_i^2}{2m} + u_i, \tag{2.24}$$

where m is the bare nucleon mass, and

$$u_i = \sum_{h \leqslant k_F} \langle ih|G(E = \varepsilon_i + \varepsilon_h)|ih\rangle_{AS}\,. \tag{2.25}$$

In Eqs. (2.24) and (2.25), the subscripts i and h represent the quantum numbers of the single-particle states, such as isospin projections τ_i and τ_h, momenta k_i and k_h, etc. The single-particle energy is given by t_i and the corresponding potential by u_i. Finally, the non-relativistic energy per nucleon is formally given as

$$\mathscr{E} = \frac{1}{A} \sum_{h \leqslant k_F} \frac{k_h^2}{2m} + \frac{1}{2A} \sum_{\substack{h \leqslant k_F \\ h' \leqslant k_F}} \left\langle hh' | G(E = \varepsilon_h + \varepsilon_{h'}) | hh' \right\rangle_{AS} . \tag{2.26}$$

In this equation we have suppressed the isospin indices for the Fermi momenta. Eq. (2.26) is to be actually calculated for various proton fractions x_p, and is thereby a function of both density n and x_p. In the limit of pure neutron matter only those partial waves contribute where the pair of interacting nucleons is coupled to isospin $T = 1$. Due to the antisymmetry of the matrix elements this implies that only partial waves with even values for the sum $l + S$, like ${}^1S_0$, ${}^3P_0$, etc. need to be considered in this case. For proton fractions different from zero, in particular the case of symmetric nuclear matter, also the other partial waves, like ${}^3S_1 - {}^3D_1$ and ${}^1P_1$ contribute. In a BHF calculation the kinetic energy is independent of the NN-interaction chosen.

The properties of neutron stars depend on the EoS at densities up to an order of magnitude higher than those observed in ordinary nuclei. At such densities, relativistic effects certainly prevail. Among relativistic approaches to the nuclear many-body problem, the so-called Dirac-Hartree and Dirac-Hartree-Fock approaches have received much interest. One of the early successes of these approaches was the quantitative reproduction of spin observables, which are only poorly described by the non-relativistic theory. Important to these methods was the introduction of a strongly attractive scalar component and a repulsive vector component in the nucleon self-energy. Inspired by the successes of the Dirac-Hartree-Fock method, a relativistic extension of Brueckner theory was proposed by Celenza and Shakin (1986), known as the Dirac-Brueckner theory. One of the appealing features of the Dirac-Brueckner approach is the self-consistent determination of the relativistic single-particle energies and wave functions. The Dirac-Brueckner approach differs from the Dirac-Hartree-Fock one in the sense that in the former one starts from the free NN-interaction which is only constrained by a fit to the NN-data, whereas the Dirac-Hartree-Fock method pursues a line where the parameters of the theory are determined so as to reproduce the bulk properties of nuclear matter. It ought, however, to be stressed that the Dirac-Brueckner approach, which starts from NN-interactions based on meson exchange, is a non-renormalizable theory where the short-range part of the potential depends on additional parameters like vertex cut-offs, clearly minimizing the sensitivity of calculated results to short-distance inputs.

In order to introduce the relativistic nomenclature, we consider first the Dirac equation for a free nucleon, i.e.

$$(i\gamma^\mu \partial_\mu - m)\,\psi(x) = 0, \tag{2.27}$$

where m is the free nucleon mass and $\psi(x)$ is the nucleon field operator which is conventionally expanded in terms of plane wave states and the Dirac spinors $u(p,s)$, and $v(p,s)$. The positive energy Dirac spinors are

$$u(p,s) = \sqrt{E+m}\begin{pmatrix}\chi_s \\ \frac{\boldsymbol{\sigma}\cdot\mathbf{p}}{E+m}\chi_s\end{pmatrix}, \tag{2.28}$$

where χ_s is the Pauli spinor and $E = \sqrt{|\mathbf{p}|^2 + m^2}$. To account for medium modifications to the free Dirac equation, we introduce the notion of the self-energy $\Sigma(p)$. As we assume parity to be a good quantum number, the self-energy of a nucleon can be formally written as

$$\Sigma(p) = \Sigma_S(p) - \gamma_0\Sigma^0(p) + \gamma\mathbf{p}\Sigma^V(p). \tag{2.29}$$

The momentum dependence of Σ^0 and Σ_S is rather weak. Moreover, $\Sigma^V \ll 1$, such that the features of the Dirac-Brueckner-Hartree-Fock procedure can be discussed within the framework of the phenomenological Dirac-Hartree ansatz, i.e. we approximate

$$\Sigma \approx \Sigma_S\gamma_0\Sigma^0 = U_S + U_V, \tag{2.30}$$

where U_S is an attractive scalar field, and U_V is the time-like component of a repulsive vector field. The finite self-energy modifies the free Dirac spinors (2.28) as

$$\widetilde{u}(p,s) = \sqrt{\widetilde{E}+\widetilde{m}}\begin{pmatrix}\chi_s \\ \frac{\boldsymbol{\sigma}\cdot\mathbf{p}}{\widetilde{E}+\widetilde{m}}\chi_s\end{pmatrix}, \tag{2.31}$$

where we let the terms with tilde represent the medium modified quantities. Here we have defined

$$\widetilde{E} = \sqrt{|\mathbf{p}|^2 + \widetilde{m}^2}, \qquad \widetilde{m} = m + U_S. \tag{2.32}$$

The single-particle energy is now defined as

$$\widetilde{\varepsilon}_i = \widetilde{E}_i + U_V^i. \tag{2.33}$$

Correspondingly, the single-particle potential is given by the G-matrix as

$$u_i = \sum_{h\leqslant k_F} \frac{\widetilde{m}_i}{\widetilde{E}_i}\frac{\widetilde{m}_h}{\widetilde{E}_h}\left\langle ih\left|\widetilde{G}(\widetilde{E}=\widetilde{E}_i+\widetilde{E}_h)\right|ih\right\rangle_{AS}, \tag{2.34}$$

when expressed in terms of the constants U_S and U_V:

$$u_i = \frac{\widetilde{m}_i}{\widetilde{E}_i}U_S^i + U_V^i. \tag{2.35}$$

The subscripts i and h represent the quantum numbers of the single-particle states, such as isospin projections τ_i and τ_h, momenta k_i and k_h, etc. In Eq. (2.34), we have

introduced the relativistic $\widetilde{G}$-matrix. If the two interacting particles, with isospins τ_1 and τ_2, give a total isospin projection T_z, the relativistic $\widetilde{G}$-matrix in a partial wave representation is given by

$$\widetilde{G}_{ll'}^{\alpha T_z}(kk'K\widetilde{E}) = \widetilde{V}_{ll'}^{\alpha T_z}(kk') + \sum_{l''} \int \frac{d^3q}{(2\pi)^3} \widetilde{V}_{ll''}^{\alpha T_z}(kq) \frac{\widetilde{m}_1}{\widetilde{E}_1^q} \frac{\widetilde{m}_2}{\widetilde{E}_2^q} \frac{Q^{T_z}(q,K)}{(\widetilde{E} - \widetilde{E}_1^q - \widetilde{E}_2^q)} \widetilde{G}_{l''l'}^{\alpha T_z}(qk'K\widetilde{E}), \tag{2.36}$$

where the relativistic starting energy is defined according to Eq. (2.32) as

$$\widetilde{E} = \widetilde{E}(\sqrt{k^2 + K^2/4}, \tau_1) + \widetilde{E}(\sqrt{k^2 + K^2/4}, \tau_2). \tag{2.37}$$

Similarly

$$\widetilde{E}_1^q = \widetilde{E}(\sqrt{q^2 + K^2/4}, \tau_1), \qquad \widetilde{E}_2^q = \widetilde{E}(\sqrt{q^2 + K^2/4}, \tau_2). \tag{2.38}$$

Eqs. (2.33)–(2.36) are solved self-consistently, starting with adequate values for the scalar and vector components U_S and U_V. This iterative scheme is continued until these parameters show little variation. Finally, the relativistic energy per nucleon reads

$$\mathscr{E} = \frac{1}{A} \sum_{h \leqslant k_F} \frac{k_h^2 + \widetilde{m}_h m}{\widetilde{E}_h} + \frac{1}{2A} \sum_{\substack{h \leqslant k_F \\ h' \leqslant k_F}} \frac{\widetilde{m}_h}{\widetilde{E}_h} \frac{\widetilde{m}_{h'}}{\widetilde{E}_{h'}} \left\langle hh' \left| \widetilde{G}(\widetilde{E} = \widetilde{E}_h + \widetilde{E}_{h'}) \right| hh' \right\rangle_{AS} - m. \tag{2.39}$$

At nuclear matter density the electron chemical potential is $\sim 110\,\mathrm{MeV}$. Once the rest mass of the muon is exceeded, it becomes energetically favorable for an electron at the top of the Fermi surface to decay into a muon. In a similar way, as soon as the chemical potential of the neutron becomes sufficiently large, energetic neutrons can decay via weak strangeness non-conserving interactions into Λ-hyperons with $\mu_n = \mu_\Lambda$. However, if we neglect interactions, or assume that their effects are small, one would expect the Σ^- to appear via

$$n + e^- \longrightarrow \Sigma^- + \nu_e,$$

at lower densities than the Λ, even though Σ^- is more massive the reason being that the above process removes both an energetic neutron and an energetic electron, whereas the decay to a Λ, being neutral, removes only an energetic neutron. Stated differently, the negatively charged hyperons appear in the ground state of matter when their masses equal $\mu_n + \mu_e$, while the neutral hyperon Λ appears when μ_n equals its mass. Since the electron chemical potential in matter is larger than the mass difference $m_\Sigma - m_\Lambda = 81.76\,\mathrm{MeV}$, the Σ^- will appear at lower densities than the Λ.

As a next step, the G-matrix is constructed to take into account short-range correlations for all strangeness sectors and to solve the equations for the single-particle energies of the various baryons self-consistently. The G-matrix is then formally given by

$$\begin{aligned} \langle B_1 B_2 | G(\omega) | B_3 B_4 \rangle = {} & \langle B_1 B_2 | V | B_3 B_4 \rangle + \\ & + \sum_{B_5, B_6} \langle B_1 B_2 | V | B_5 B_6 \rangle \frac{1}{\omega - \varepsilon_{B_5} - \varepsilon_{B_6} + m} \langle B_5 B_6 | G(\omega) | B_3 B_4 \rangle. \end{aligned} \tag{2.40}$$

Here B_i represents all possible baryons n, p, Λ, Σ^-, Σ^0, Σ^+, Ξ^- and Ξ^0 and their quantum numbers such as spin, isospin, strangeness, linear momenta and orbital momenta. The intermediate states B_5B_6 are those which are allowed by the Pauli exclusion principle and the energy variable ω is the starting energy defined by the single-particle energies of the incoming external particles B_3B_4. The single-particle energies are given by

$$\varepsilon_{B_i} = t_{B_i} + u_{B_i} + m_{B_i}, \tag{2.41}$$

where t_{B_i} is the kinetic energy and m_{B_i} the mass of baryon B_i. The single-particle potential u_{B_i} is defined by

$$u_{B_i} = \mathrm{Re} \sum_{B_j \leqslant F_j} \langle B_i B_j | G(\omega = \varepsilon_{B_i} + \varepsilon_{B_j}) | B_i B_j \rangle. \tag{2.42}$$

The linear momentum of the intermediate single-particle state B_j is limited by the size of the Fermi surface F_j for particle species B_j.

By the way, the BHF method in its simplest form is not fully appropriate for a description of dense matter. The many-body approach outlined above is the lowest-order BHF method extended to the hyperon sector. This means also that we consider only two-body interactions. However, it is well known from studies of nuclear matter and neutron star matter with nucleonic degrees of freedom only that three-body forces are important in order to reproduce the saturation properties of nuclear matter.

Concerning the calculation of neutrino emissivities, we will employ the nuclear data from various EoS and composition of matter in the non-relativistic limit. There are primarily three EoS we will apply for the sake of many-body correlations. These involve pure nuclear matter with two-body and three-body interactions, and the hyperons in nuclear matter with two-body interactions, which we hereafter refer to as EoS I, EoS II, and EoS III, respectively. The two-body interactions for the pure nuclear matter are submitted by Eqs. (2.23)–(2.25), while the the two-body interactions for the nuclear matter with hyperons are generated by Eqs. (2.40)–(2.42). The quantities that we benefit from the nuclear data, are being the number densities, the chemical potentials and the effective masses of the interacting particles.

Chapter 3

Direct Urca Process

The simplest neutrino-emitting process one can envisage is the β-decay of the neutron,

$$n \longrightarrow p + e^- + \bar{\nu}_e,$$

and the electron capture on protons,

$$p + e^- \longrightarrow n + \nu_e.$$

These two processes were first considered by Gamow and Schoenberg (1941) as a mechanism for causing stellar collapse and supernova explosions. In their paper they state that for brevity they refer to such processes as Urca processes. As Gamow (1970) recounted, «*We called it the Urca Process, partially to commemorate the casino in which we first met, and partially because the Urca Process results in a rapid disappearance of thermal energy from the interior of a star, similar to the rapid disappearance of money from the pockets of the gamblers on the Casino da Urca.*» From now on we will refer to neutron decay and electron capture collectively as the direct Urca process.

As we have discussed at the beginning of Chapter 2, neutron stars are not made only of neutrons, but also must include a small fraction of protons and electrons. The reason is that a free neutron will undergo a weak decay or the so-called β-decay, with a lifetime of about 15 minutes. So, there must be something that prevents this decay for a star, and that is the presence of the protons and electrons. We will now briefly see how this is indeed the case.

If all the available low energy levels for the decay proton are filled by the protons already present, then the Pauli exclusion principle takes over and prevents the decay from taking place. The same might be said about the presence of the electrons, but in any case the electrons must be present within the star to cancel the positive charge of the protons. When both processes take place, a steady state can be reached if the reactions proceed at the same rate, with neutrinos and antineutrinos being emitted in equal numbers. The successive neutron decays and electron captures lead to the emission of a neutrino and an antineutrino for every cycle completed, and thereby lead to energy loss from the star.

In the following three sections we investigate the pure neutron decay, the decay of a neutron into a proton by emitting an electron and an electron antineutrino. We shall determine the emissivity associated with the neutrino emission of this process. To begin with, we calculate the β-decay matrix element. Before proceeding with these topics, we introduce natural units which considerably simplify details of the following calculations. In natural units one takes mass, action (A) and velocity (V) as fundamental dimensions and chooses $\hbar$ as unit of action and the velocity of light c as unit of velocity. As throughout the following, we put therefore $\hbar = c = 1$ in order to convert c.g.s. expressions into natural units.

3.1 Matrix Element in β-decay

We here calculate the transition matrix element for the pure neutron decay, in which the weak interaction transforms a neutron into a proton while emitting an electron and an electron antineutrino. Graphically, this process is represented by

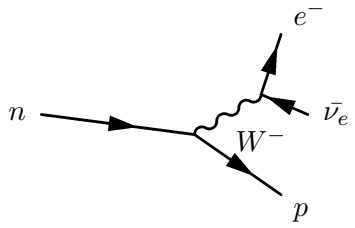

Figure 3.1: The Feynman diagram for β-decay of a neutron into a proton, electron, and electron antineutrino via an intermediate heavy W^--boson.

To describe the coupling of fermions to $W^{\pm}$-bosons, we employ the standard electroweak theory, which yields the weak vertex factor

$$\frac{-ig_W}{2\sqrt{2}}\gamma^\mu\left(1-\gamma^5\right), \tag{3.1}$$

where g_W is the weak coupling constant, expressed in terms of the electromagnetic coupling constant g_e and weak mixing angle θ_W:

$$g_W = \frac{g_e}{\sin\theta_W}. \tag{3.2}$$

The factor $(1-\gamma^5)$, however, is of profound importance, for γ^μ alone would yield a *vector* coupling, whereas $\gamma^\mu\gamma^5$ gives an *axial* vector. A theory that adds a *vector* to an *axial* vector is bound to violate the conservation of parity, and this is precisely what happens in the weak interactions.

Actually, we do not know exactly how the W couples to composite structures. But it turns out to be that the axial coupling to composite structures, such as the proton, is modified due to the strong interaction. To account for this, we make the following replacement in the vertex factor:

$$\left(1-\gamma^5\right) \longrightarrow \left(c_V - c_A\gamma^5\right),$$

where c_V is the correction to the *vector* weak-charge and c_A is the correction to the *axial* vector weak-charge. The experiments shows that

$$c_V = 1.000 \pm 0.003, \qquad c_A = 1.26 \pm 0.02.$$

As the results show, the *vector* weak-charge is not modified by the strong interactions within the nucleon. Presumably, like electric charge, it is "protected" by a conservation law; we call this the "Conserved Vector Current" (CVC) hypothesis. Even the axial term is not altered much; evidently, it is "almost" conserved. We call this the "Partially Conserved Axial Current" (PCAC) hypothesis.

Furthermore, the propagator for the exchanged W^--boson is given by

$$\frac{-i\left(g_{\mu\nu} - b_\mu b_\nu / M_W^2 c^2\right)}{b^2 - M_W^2 c^2}, \tag{3.3}$$

where $b = p_1 - p_3$ is the four-momentum transferred by the W^--boson. However, in practice, we work at energies so far below the W mass that we may safely use

$$\frac{i g_{\mu\nu}}{M_W^2}. \tag{3.4}$$

Next we turn to the Feynman diagram in Fig. 3.1 and write down the corresponding amplitude following fermion lines backwards.

$$\mathcal{M} = \bar{u}(p_4, s_4)\left[\frac{-ig_W}{2\sqrt{2}}\gamma^\mu\left(1-\gamma^5\right)\right] v(p_2, s_2)\left\{\frac{ig_{\mu\nu}}{M_W^2}\right\}\bar{u}(p_3, s_3)\left[\frac{-ig_W}{2\sqrt{2}}\gamma^\nu\left(1-c_A\gamma^5\right)\right]\times$$
$$\times\, u(p_1, s_1), \tag{3.5}$$

where we have chosen the *vector* weak-charge $c_V = 1.000$ in the first vertex and c_A remains unspecified. The Dirac spinors $u(p_1, s_1)$, $\bar{u}(p_3, s_3)$, $v(p_2, s_2)$ and $\bar{u}(p_4, s_4)$ are representing the incoming neutron, outgoing proton, outgoing electron antineutrino and outgoing electron, respectively. Combining all the constants entering into Eq. (3.5) together, we obtain

$$\mathcal{M} = -i\frac{G_F}{\sqrt{2}}\bar{u}(p_4, s_4)\gamma^\mu\left(1-\gamma^5\right) v(p_2, s_2)\bar{u}(p_3, s_3)\gamma_\mu\left(1-c_A\gamma^5\right) u(p_1, s_1), \tag{3.6}$$

where the Fermi coupling constant is defined by

$$G_F = \frac{\sqrt{2}}{8}\left(\frac{g_W}{M_W}\right)^2 = \frac{1}{\sqrt{2}}\frac{\pi\alpha}{M_W^2 \sin^2\theta_W} = 1.166 \times 10^{-5}\mathrm{GeV}^{-2}. \tag{3.7}$$

Taking the transpose conjugate of the Feynman amplitude (Eq. (3.6)) gives

$$\mathcal{M}^\dagger = i\frac{G_F}{\sqrt{2}}\bar{u}(p_1, s_1)\left(1+c_A\gamma^5\right)\gamma_\nu u(p_3, s_3)\bar{v}(p_2, s_2)\left(1+\gamma^5\right)\gamma^\nu u(p_4, s_4). \tag{3.8}$$

Let us now square the invariant Feynman amplitude. Since the interacting particles are unpolarized, we want the sum over final spins but the average over initial spins,

$$|\mathcal{M}|^2 = \frac{1}{2}\sum_{s_1}\sum_{s_2,s_3,s_4}\mathcal{M}\mathcal{M}^\dagger. \tag{3.9}$$

Writing out the summation over spin states explicitly, we can rearrange the summands in individual sums as

$$\begin{aligned}|\mathcal{M}|^2 = \frac{G_F^2}{4}\sum_{s_4}\bar{u}(p_4,s_4)\gamma^\mu\left(1-\gamma^5\right)\left(\sum_{s_2}v(p_2,s_2)\bar{v}(p_2,s_2)\right)\left(1+\gamma^5\right)\gamma^\nu u(p_4,s_4)\times\\ \times\sum_{s_3}\bar{u}(p_3,s_3)\gamma_\mu\left(1-c_A\gamma^5\right)\left(\sum_{s_1}u(p_1,s_1)\bar{u}(p_1,s_1)\right)\left(1+c_A\gamma^5\right)\gamma_\nu u(p_3,s_3).\end{aligned} \tag{3.10}$$

In describing the neutrinos in weak interactions, we are not assuming, as is sometimes done, that the neutrinos have zero mass. When doing the summation over spin states, we thus take into account both the right-handed and left-handed neutrinos. To proceed further, we have to express the summations over spins s_1 and s_2 in terms of the projection operators:

$$\sum_{s_1}u(p_1,s_1)\bar{u}(p_1,s_1) = \not{p}_1 + m_n, \tag{3.11}$$

$$\sum_{s_2}v(p_2,s_2)\bar{v}(p_2,s_2) = \not{p}_2 - m_{\bar{\nu}_e}. \tag{3.12}$$

The complete derivation of the above summations is given in Appendix A, Section A.3. By substituting these into Eq. (3.10) leads to

$$\begin{aligned}|\mathcal{M}|^2 = \frac{G_F^2}{4}\sum_{s_4}\bar{u}(p_4,s_4)\gamma^\mu\left(1-\gamma^5\right)\left(\not{p}_2 - m_{\bar{\nu}_e}\right)\left(1+\gamma^5\right)\gamma^\nu u(p_4,s_4)\sum_{s_3}\bar{u}(p_3,s_3)\gamma_\mu\times\\ \times\left(1-c_A\gamma^5\right)\left(\not{p}_1 + m_n\right)\left(1+c_A\gamma^5\right)\gamma_\nu u(p_3,s_3),\end{aligned} \tag{3.13}$$

where we recognize the summands between spinors as the product of γ-matrices and define them as follows

$$\mathcal{A} = \gamma^\mu\left(1-\gamma^5\right)\left(\not{p}_2 - m_{\bar{\nu}_e}\right)\left(1+\gamma^5\right)\gamma^\nu, \tag{3.14}$$

$$\mathcal{B} = \gamma_\mu\left(1-c_A\gamma^5\right)\left(\not{p}_1 + m_n\right)\left(1+c_A\gamma^5\right)\gamma_\nu. \tag{3.15}$$

Accordingly

$$|\mathcal{M}|^2 = \frac{G_F^2}{4}\sum_{s_4}\bar{u}(p_4,s_4)\mathcal{A}u(p_4,s_4)\sum_{s_3}\bar{u}(p_3,s_3)\mathcal{B}u(p_3,s_3), \tag{3.16}$$

The remaining two summations in Eq. (3.16) can be reduced to the traces of products of γ-matrices:

$$\begin{aligned}\mathbf{Tr}(\widetilde{\mathcal{A}}) &= \sum_{s_4} \bar{u}(p_4,s_4)\mathcal{A}u(p_4,s_4) = \mathbf{Tr}\left[(\not{p}_4 + m_e)\,\mathcal{A}\right] \\ &= \mathbf{Tr}\left[(\not{p}_4 + m_e)\,\gamma^\mu\left(1-\gamma^5\right)(\not{p}_2 - m_{\bar{\nu}_e})\left(1+\gamma^5\right)\gamma^\nu\right], \qquad (3.17)\\ \mathbf{Tr}(\widetilde{\mathcal{B}}) &= \sum_{s_3} \bar{u}(p_3,s_3)\mathcal{B}u(p_3,s_3) = \mathbf{Tr}\left[(\not{p}_3 + m_p)\,\mathcal{B}\right] \\ &= \mathbf{Tr}\left[(\not{p}_3 + m_p)\,\gamma_\mu\left(1-c_A\gamma^5\right)(\not{p}_1 + m_n)\left(1+c_A\gamma^5\right)\gamma_\nu\right]. \qquad (3.18)\end{aligned}$$

The above summations are easily evaluated in Appendix A, Section A.4. It follows that

$$\begin{aligned}|\mathcal{M}|^2 &= \frac{G_F^2}{4}\,\mathbf{Tr}(\widetilde{\mathcal{A}})\times\mathbf{Tr}(\widetilde{\mathcal{B}}) \\ &= \frac{G_F^2}{4}\,\mathbf{Tr}\left[(\not{p}_4 + m_e)\,\gamma^\mu\left(1-\gamma^5\right)(\not{p}_2 - m_{\bar{\nu}_e})\left(1+\gamma^5\right)\gamma^\nu\right]\times \\ &\quad\times\mathbf{Tr}\left[(\not{p}_3 + m_p)\,\gamma_\mu\left(1-c_A\gamma^5\right)(\not{p}_1 + m_n)\left(1+c_A\gamma^5\right)\gamma_\nu\right]. \qquad (3.19)\end{aligned}$$

The traces in Eq. (3.19) contain products of up to six γ-matrices. Their computation is much simplified by the use of the contraction identities. We illustrate the use of these tricks by computing both the traces in Appendix A, Section A.5,

$$\begin{aligned}\mathbf{Tr}(\widetilde{\mathcal{A}}) &= 8\left[p_2^\mu p_4^\nu + p_2^\nu p_4^\mu - (p_2\cdot p_4)g^{\mu\nu} + i\epsilon^{\alpha\mu\beta\nu}p_{4\alpha}p_{2\beta}\right], \qquad (3.20)\\ \mathbf{Tr}(\widetilde{\mathcal{B}}) &= 4\left(1+c_A^2\right)\left[p_{1\mu}p_{3\nu} + p_{1\nu}p_{3\mu} - (p_1\cdot p_3)g_{\mu\nu}\right] + 8c_A i\epsilon_{\rho\mu\sigma\nu}p_3^\rho p_1^\sigma + \\ &\quad + 4m_p m_n\left(1-c_A^2\right)g_{\mu\nu}. \qquad (3.21)\end{aligned}$$

On multiplying the two traces (Eqs. (3.20) and (3.21)) together, we benefit by the following contraction identity:

$$\epsilon^{\alpha\mu\beta\nu}\epsilon_{\rho\mu\sigma\nu} = -2\big(g_\rho^\alpha g_\sigma^\beta - g_\sigma^\alpha g_\rho^\beta\big). \qquad (3.22)$$

Finally, we put the result into Eq. (3.19) and obtain for the squared Feynman amplitude

$$\begin{aligned}|\mathcal{M}|^2 = 16G_F^2\Big[&\left(1+c_A\right)^2(p_1\cdot p_2)(p_3\cdot p_4) + \left(1-c_A\right)^2(p_1\cdot p_4)(p_2\cdot p_3) - \\ &- m_p m_n\left(1-c_A^2\right)(p_2\cdot p_4)\Big]. \qquad (3.23)\end{aligned}$$

If we set the *axial* vector weak-charge $c_A = 1$ in the above equation, the last two terms vanish and we recover the expression of **(author?)** [6]:

$$|\mathcal{M}|^2 = 64G_F^2(p_1\cdot p_2)(p_3\cdot p_4). \qquad (3.24)$$

3.2 Cold and Dense Matter

As already mentioned, neutron stars are born in supernova explosions and the interior temperatures initially exceed $T \sim 10^{11}\,\mathrm{K}$. As the neutron star cools down to $10^{10} - 10^{9}\,\mathrm{K}$, neutrinos begin to stream freely and essentially leave the star without further interaction. At this stage, the star as a whole is in thermal, β and charge equilibrium, and the interior matter occupies its ground state. Because of the extremely high densities and relatively low temperatures involved (in comparison with the relevant Fermi energies), the electrons, protons, and neutrons in the interior are all degenerate. This has the consequence that the interior is approximately isothermal. The electrons are also extremely relativistic, while the nucleons are approximately non-relativistic. Under these conditions, the direct Urca process can take place only near the Fermi energies of participating particles and simultaneous conservation of energy and momentum require the inequality,

$$p_F(e) + p_F(p) \geqslant p_F(n),$$

to be satisfied. This leads to the well known threshold for the proton fraction $x_p = n_p/n \geqslant 1/9 \approx 11\%$[7], where $n = n_n + n_p$ is the total baryon density. If the electron chemical potential exceeds the muon rest mass, $m_\mu = 105.658\,\mathrm{MeV/c^2}$, muons will also be present in dense matter, and this will increase the threshold proton concentration. If $\mu_e \gg m_\mu c^2$, the threshold proton concentration is ≈ 0.148; for smaller values of μ_e, the threshold concentration lies between 1/9 and this value. At densities typical of the central regions of neutron stars, the calculated proton concentration of matter is very sensitive to the choice of physical model, and in reality it might exceed the threshold value.

In the mid 1960s, when cooling of neutron stars was first studied in detail, it was argued that the direct Urca process could not occur. Since the number density of each species of particle is given by

$$n = 2\int \frac{d^3\mathbf{p}}{(2\pi\hbar)^3} = \frac{8\pi}{(2\pi\hbar)^3}\int_0^{p_F} p^2 dp = \frac{p_F^3}{3\pi^2\hbar^3}, \tag{3.25}$$

and in dense matter the proton fraction is typically of order of a few percent, it was argued that momentum could not be conserved. We now demonstrate this important result.

A neutron star is electrically neutral so that the electrons must be present within the star to cancel the positive charge of the protons. We saw above that the number density of a particle species is fixed in terms of that particle's Fermi momentum. Thus equal numbers of electrons and protons implies that

$$p_F(p) = p_F(e). \tag{3.26}$$

In addition to charge neutrality, we also require weak interaction equilibrium (β-equilibrium), that is, as many neutron decays taking place as electron captures.

This equilibrium can be expressed in terms of the chemical potentials for the three species,

$$\mu_n = \mu_p + \mu_e, \tag{3.27}$$

where to good approximation $[\mathcal{O}(k_BT/\mu_n)^2]$ the chemical potentials are just the Fermi energies[8]. Thus

$$E_F(n) = E_F(p) + E_F(e), \tag{3.28}$$

where at nuclear densities

$$E_F(n) \simeq m_n c^2 + \frac{p_F^2(n)}{2m_n}, \tag{3.29}$$

$$E_F(p) \simeq m_p c^2 + \frac{p_F^2(p)}{2m_p}, \tag{3.30}$$

$$E_F(e) \simeq p_F(e)c. \tag{3.31}$$

On combining the above relations, Eq. (3.28) becomes

$$\frac{p_F^2(n)}{2m_n} \simeq p_F(e)c\left(1 + \frac{p_F(p)}{2m_pc}\right) - Q, \tag{3.32}$$

where $Q = (m_n - m_p)c^2$ is small in comparison to the other terms in Eq. (3.32). From Eq. (3.32) we see that the neutron Fermi energy (minus rest mass) is very nearly equal to the electron Fermi energy:

$$E'_F(n) \equiv \frac{p_F^2(n)}{2m_n} \simeq p_F(e)c = E_F(e), \tag{3.33}$$

and so

$$p_F(e) = p_F(p) \ll p_F(n), \tag{3.34}$$

$$E'_F(p) \ll E'_F(n). \tag{3.35}$$

Now consider the possibility of a reaction such as neutron decay. The only neutrons capable of decaying lie within $\sim k_BT$ of the Fermi surface, $E'_F(n)$. Hence, by energy conservation, the final proton and electron must also be within $\sim k_BT$ of their Fermi surfaces; the energy of the escaping neutrino must also be $\sim k_BT$. Now, according to inequality (3.34), the proton and electron must have small momenta compared to the neutron. But this is impossible: the decay cannot conserve momentum if it conserves energy.

However, at higher densities, the proton concentrations are large enough to allow the direct Urca process to start. The reason for that the direct Urca process was neglected for so long, is that the estimates of proton fractions were based on simple models like the free-particle model, and the density was taken to be close to nuclear density. Modern estimates of proton fractions tend to be higher than the old ones because particle interactions tend to increase the proton fraction and because current estimates of central densities of neutron stars are a few times greater than nuclear density.

3.3 Neutrino Emissivities

We now turn to the study of the emissivities due to neutron decay. Physically, the emissivity represents the rate at which antineutrino energy is emitted per unit volume by the process. Before calculating the rate for neutron decay, we first write down the transition rate of the process in terms of the corresponding matrix element:

$$d\Gamma = \frac{(2\pi)^4}{2\hbar E_n}|\mathcal{M}|^2 \left(\frac{c\,d^3\mathbf{p}_p}{(2\pi\hbar)^3 2E_p}\right)\left(\frac{c\,d^3\mathbf{p}_e}{(2\pi\hbar)^3 2E_e}\right)\left(\frac{c\,d^3\mathbf{p}_{\bar{\nu}_e}}{(2\pi\hbar)^3 2E_{\bar{\nu}_e}}\right)\delta^{(4)}(p_n - p_p - p_e - p_{\bar{\nu}_e}), \tag{3.36}$$

where the Dirac delta function $\delta^{(4)}(p_n - p_p - p_e - p_{\bar{\nu}_e})$ ensures conservation of energy and momentum overall for the process. Note that factors behind the matrix element describes the phase space available for particles in the final state. The antineutrino emissivity is then obtained by integrating the transition rate (3.36) over all initial states, multiplied by $E_{\bar{\nu}_e}$:

$$\begin{aligned}\varepsilon_{\bar{\nu}} = \frac{(2\pi)^4}{\hbar}\int \frac{c\,d^3\mathbf{p}_n}{(2\pi\hbar)^3 2E_n}\int \frac{c\,d^3\mathbf{p}_p}{(2\pi\hbar)^3 2E_p}\int \frac{c\,d^3\mathbf{p}_e}{(2\pi\hbar)^3 2E_e}\int \frac{c\,d^3\mathbf{p}_{\bar{\nu}_e}}{(2\pi\hbar)^3 2E_{\bar{\nu}_e}}\times \\ \times\,\delta^{(4)}(p_n - p_p - p_e - p_{\bar{\nu}_e})|\mathcal{M}|^2 E_{\bar{\nu}_e} f(E_n)(1-f(E_p))(1-f(E_e)),\end{aligned} \tag{3.37}$$

where the Fermi-Dirac distribution functions,

$$f(E_j) = \left[\mathbf{e}^{(E_j-\mu_j)/k_B T} + 1\right]^{-1}, \tag{3.38}$$

are the fraction of phase space occupied at energy E_j. The factors $(1-f(E_j))$ are called blocking factors and express the fact that, because of the Pauli exclusion principle, the process cannot occur if the final states are occupied. Combined with the momentum-conserving delta function $\delta^{(3)}(\mathbf{p}_n - \mathbf{p}_p - \mathbf{p}_e - \mathbf{p}_{\bar{\nu}_e})$, the integral over $\mathbf{p}_e$ yields

$$\begin{aligned}\varepsilon_{\bar{\nu}} = \frac{2^4}{(4\pi)^8}\int \frac{d^3\mathbf{p}_n}{E_n}\int \frac{d^3\mathbf{p}_p}{E_p}\int \frac{d^3\mathbf{p}_{\bar{\nu}_e}}{E_e}\,\delta(E_n - E_p - E_e - E_{\bar{\nu}_e})|\mathcal{M}|^2 f(E_n)\times \\ \times\,(1-f(E_p))(1-f(E_e)).\end{aligned} \tag{3.39}$$

To carry out the $\mathbf{p}_p$ and $\mathbf{p}_{\bar{\nu}_e}$ integral, we go over to spherical coordinates,

$$d^3\mathbf{p}_p = |\mathbf{p}_p|^2 d|\mathbf{p}_p|\sin\theta_p d\theta_p\, d\phi_p = \frac{1}{c^2}|\mathbf{p}_p|\,E_p dE_p \sin\theta_p d\theta_p\, d\phi_p, \tag{3.40}$$

$$d^3\mathbf{p}_{\bar{\nu}_e} = |\mathbf{p}_{\bar{\nu}_e}|^2 d|\mathbf{p}_{\bar{\nu}_e}|\sin\theta_{\bar{\nu}_e} d\theta_{\bar{\nu}_e}\, d\phi_{\bar{\nu}_e} = \frac{2\pi}{c^2}|\mathbf{p}_{\bar{\nu}_e}|\,E_{\bar{\nu}_e} dE_{\bar{\nu}_e}\sin\theta_{\bar{\nu}_e} d\theta_{\bar{\nu}_e}, \tag{3.41}$$

and orient the coordinates so that the z-axis lies along $\mathbf{p}_n$ (which is fixed); then the $\mathbf{p}_n$ integral becomes

$$d^3\mathbf{p}_n = |\mathbf{p}_n|^2 d|\mathbf{p}_n|\sin\theta_n d\theta_n\, d\phi_n = \frac{4\pi}{c^2}|\mathbf{p}_n|\,E_n dE_n. \tag{3.42}$$

Accordingly

$$\varepsilon_{\bar{\nu}} = \frac{2^3}{(4\pi)^6}\int |\mathbf{p}_n| dE_n \int |\mathbf{p}_p| dE_p \int \sin\theta_p d\theta_p \int d\phi_p \int \frac{E_{\bar{\nu}_e}}{E_e} |\mathbf{p}_{\bar{\nu}_e}| dE_{\bar{\nu}_e} \int \sin\theta_{\bar{\nu}_e} d\theta_{\bar{\nu}_e} \times$$
$$\times \delta(E_n - E_p - E_e - E_{\bar{\nu}_e}) |\mathcal{M}|^2 f(E_n)(1 - f(E_p))(1 - f(E_e)). \tag{3.43}$$

Finally, the energy-conserving delta function $\delta(E_n - E_p - E_e - E_{\bar{\nu}_e})$ is eliminated by integrating over $E_{\bar{\nu}_e}$,

$$\varepsilon_{\bar{\nu}} = \frac{2^3}{(4\pi)^6}\int |\mathbf{p}_n| dE_n \int |\mathbf{p}_p| dE_p \int \sin\theta_p d\theta_p \int d\phi_p \int \sin\theta_{\bar{\nu}_e} d\theta_{\bar{\nu}_e} \frac{E_{\bar{\nu}_e}}{E_e} |\mathbf{p}_{\bar{\nu}_e}| |\mathcal{M}|^2 \times$$
$$\times f(E_n)(1 - f(E_p))(1 - f(E_e)). \tag{3.44}$$

To perform the remaining integrations in Eq. (3.44), we develop a numerical program, in which we implement the above expression for emissivity. Note that the underlying quark process for neutron decay is of the form,

$$d \longrightarrow u + e^- + \bar{\nu}_e,$$

and the quark vertex carries a factor of $\cos\theta_C$, where $\cos\theta_C = 13.1°$ is the Cabibbo angle. Hence, the emissivity is modified by the Cabibbo angle by $\varepsilon_{\bar{\nu}} = \cos^2\theta_C\, \varepsilon_{\bar{\nu}}$. Moreover, the electron capture gives the same energy-loss rate as neutron decay, but in neutrinos, and therefore the total emissivity of the direct Urca process is twice Eq. (3.44): $\varepsilon_{\rm Urca} = 2\,\varepsilon_{\bar{\nu}}$.

When including medium effects in the calculations, we benefit from nuclear data for various equations of state, produced by Professor Morten Hjorth-Jensen. Since the neutrons, protons, and electrons participating in the neutron decay must have energies close to their respective Fermi energies, we are just integrating around the Fermi surfaces of these particles. We use MeV as the energy and momentum units for much of the calculations here and hence Eq. (3.44) has dimensions of MeV^5. We divide Eq. (3.44) by $\hbar^4 c^3$ to convert it back to c.g.s. units of emissivity, which is $\mathrm{MeV/m^3 s}$.

We now consider the kinematics for the case at where the electron and electron antineutrino are forming a system of total rest mass M_C, total energy E_C, and total momentum $\mathbf{p}_C$. Thus, we have

$$E_C = E_e + E_{\bar{\nu}_e}, \qquad \mathbf{p}_C = \mathbf{p}_e + \mathbf{p}_{\bar{\nu}_e}, \qquad M_C^2 = E_C^2 - |\mathbf{p}_C|^2. \tag{3.45}$$

Since energy and momentum are conserved in this process, it follows that

$$E_C + E_p = E_n, \tag{3.46}$$
$$\mathbf{p}_C + \mathbf{p}_p = \mathbf{p}_n. \tag{3.47}$$

When squared, the last equation leads to the following equality,

$$|\mathbf{p}_C|^2 = |\mathbf{p}_n - \mathbf{p}_p|^2 = |\mathbf{p}_n|^2 + |\mathbf{p}_p|^2 - 2|\mathbf{p}_n||\mathbf{p}_p|\cos\theta_p. \tag{3.48}$$

From Eqs. (3.45) we find that

$$E_C - E_{\bar{\nu}_e} = E_e = \sqrt{|\mathbf{p}_e|^2 + m_e^2} = \sqrt{|\mathbf{p}_C - \mathbf{p}_{\bar{\nu}_e}|^2 + m_e^2}. \tag{3.49}$$

Squaring the above equation results in

$$\begin{aligned} E_C^2 + E_{\bar{\nu}_e}^2 - 2E_C E_{\bar{\nu}_e} &= |\mathbf{p}_C - \mathbf{p}_{\bar{\nu}_e}|^2 + m_e^2 \\ &= |\mathbf{p}_C|^2 + |\mathbf{p}_{\bar{\nu}_e}|^2 - 2|\mathbf{p}_C||\mathbf{p}_{\bar{\nu}_e}| \cos\alpha_{C\bar{\nu}_e} + m_e^2 \\ &= |\mathbf{p}_C|^2 + E_{\bar{\nu}_e}^2 - m_{\bar{\nu}_e}^2 - 2|\mathbf{p}_C|\sqrt{E_{\bar{\nu}_e}^2 - m_{\bar{\nu}_e}^2}\cos\alpha_{C\bar{\nu}_e} + m_e^2. \end{aligned} \tag{3.50}$$

In order to solve Eq. (3.50) for $E_{\bar{\nu}_e}$, we square it again,

$$\left[E_C^2 - |\mathbf{p}_C|^2 + m_{\bar{\nu}_e}^2 - m_e^2 - 2E_C E_{\bar{\nu}_e}\right]^2 = \left[-2|\mathbf{p}_C|\sqrt{E_{\bar{\nu}_e}^2 - m_{\bar{\nu}_e}^2}\cos\alpha_{C\bar{\nu}_e}\right]^2. \tag{3.51}$$

By introducing new variables,

$$\begin{aligned} K &= E_C^2 - |\mathbf{p}_C|^2 + m_{\bar{\nu}_e}^2 - m_e^2 \\ &= E_n^2 + E_p^2 - 2E_nE_p - |\mathbf{p}_n|^2 - |\mathbf{p}_p|^2 + 2|\mathbf{p}_n||\mathbf{p}_p|\cos\theta_p + m_{\bar{\nu}_e}^2 - m_e^2 \\ &= m_n^2 + m_p^2 - 2E_nE_p + 2|\mathbf{p}_n||\mathbf{p}_p|\cos\theta_p + m_{\bar{\nu}_e}^2 - m_e^2, \end{aligned} \tag{3.52}$$

and

$$L = |\mathbf{p}_C|\cos\alpha_{C\bar{\nu}_e} = \frac{\mathbf{p}_C \cdot \mathbf{p}_{\bar{\nu}_e}}{|\mathbf{p}_{\bar{\nu}_e}|}, \tag{3.53}$$

Eq. (3.51) becomes

$$\left(E_C^2 - L^2\right) E_{\bar{\nu}_e}^2 - KE_C E_{\bar{\nu}_e} + \left(K^2/4 + L^2 m_{\bar{\nu}_e}^2\right) = 0. \tag{3.54}$$

Note that this is a second-order equation in $E_{\bar{\nu}_e}$ and may be solved for $E_{\bar{\nu}_e}$ to give

$$E_{\bar{\nu}_e} = \frac{KE_C + \sqrt{\left(KE_C\right)^2 - 4\left(E_C^2 - L^2\right)\left(K^2/4 + L^2 m_{\bar{\nu}_e}^2\right)}}{2\left(E_C^2 - L^2\right)}. \tag{3.55}$$

Whether or not the direct Urca process occurs in reality, the above calculation is an instructive one, since neutrino emissivities from other neutrino emission processes may be understood in terms of it.

Until 1990, it was tacitly assumed by most people that proton concentrations in dense matter lie below the threshold value for the direct Urca process. In this case, the simplest allowed weak-interaction processes for nucleons are the modified Urca process:

$$\begin{aligned} n + n &\longrightarrow n + p + e^- + \bar{\nu}_e, \\ n + p + e^- &\longrightarrow n + n + \nu_e. \end{aligned}$$

which for the past quarter of a century has been regarded as the standard process for neutron star cooling. They differ from the direct Urca process by the presence in the initial and final states of a bystander particle whose sole purpose is to make possible conservation of momentum for particles close to the Fermi surfaces. They were first

discussed by Chiu and Salpeter (1964), and detailed estimates of their rates were made by Finzi (1964), Bahcall and Wolf (1965), and Friman and Maxwell (1979)[7]. The process is basically the direct Urca process, with the modification that a nucleon in an initial or final state interacts, via the nucleon-nucleon strong interaction, with a bystander nucleon.

Chapter 4

Neutrino Pair Bremsstrahlung

The discovery of weak neutral currents suggested two other processes that might be important for the cooling of neutron stars: neutrino pair bremsstrahlung from neutron-neutron and neutron-proton scattering,

$$n + n \longrightarrow n + n + \nu + \bar{\nu},$$
$$n + p \longrightarrow n + p + \nu + \bar{\nu},$$

which we hereafter refer to as the $nn\nu\bar{\nu}$ and $np\nu\bar{\nu}$ processes, respectively. Both processes may involve either electron-type neutrinos or muon-type neutrinos. They have been first studied by Flowers, Sutherland and Bond (1975), and later by **(author?)** [1], who found that while the energy loss rate varies as T^8, it is smaller than the modified Urca rate by a factor of 30. This is the same temperature dependence as that found for the modified Urca process. For neutron-neutron scattering the coefficient of T^8 (determined by densities of states and an averaged neutron-neutron cross section) is much smaller than that for modified Urca process, but for neutron-proton scattering the coefficient of T^8 is comparable to that for modified Urca process. However, a proper evaluation of these processes based on an more realistic effective-interaction has not been done since the classical approach by Friman *et al.* (1979).

If the direct Urca process is allowed, it would lead to more rapid cooling than any other process. On the other hand, processes like the neutrino pair bremsstrahlung and modified Urca process would proceed slowly as the star cools. One possible explanation is that neutrons and protons turn superfluid. The rates of neutrino emission are then suppressed by the presence of energy gaps (above the Fermi energies) in the energy spectrum of the particles. If exceptionally slow cooling is observed for a neutron star, this may indicate the presence of superfluidity.

In this chapter we study the neutrino pair bremsstrahlung in more detail, starting by drawing Feynman diagrams for the processes. We here evaluate analytical expressions for the Feynman amplitude and develop a generic code for calculating the amplitude for any process. Afterwards, we construct a numerical program for determining neutrino emissivities due to the neutron-neutron and neutron-proton scattering.

4.1 Feynman Diagrams

The direct diagrams contributing to the $nn\nu\bar{\nu}$ and $np\nu\bar{\nu}$ processes are illustrated in Fig. 4.1 and Fig. 4.2. Here time is flowing upwards and space axis points to the right. In each of these diagrams, the four-momentum imparted to the neutrino pair is denoted b, and the momentum transferred between the nucleons either $\mathbf{k}$ or $\mathbf{k}'$. Momentum conservation requires that

$$\mathbf{k}' = \mathbf{k} + \mathbf{b}, \tag{4.1}$$

so that $\mathbf{k}$ and $\mathbf{k}'$ are not exactly equal. However, for both processes $|\mathbf{k}|$ and $|\mathbf{k}'|$ are large compared with $|\mathbf{b}|$ over most of the allowed phase space; thus $\mathbf{k}$ and $\mathbf{k}'$ can be equated without introducing significant errors into the emissivities.

In Fig. 4.2, the first four diagrams involve a different final state from the last four diagrams so that the matrix element contributions from the two groups of diagrams must be added incoherently. In order to distinguish the two matrix element contributions, we will hereafter denote the first set of diagrams (A-D) group I diagrams and the second set (E-H) group II diagrams.

4.1.1 Diagrams for the $nn\nu\bar{\nu}$ process

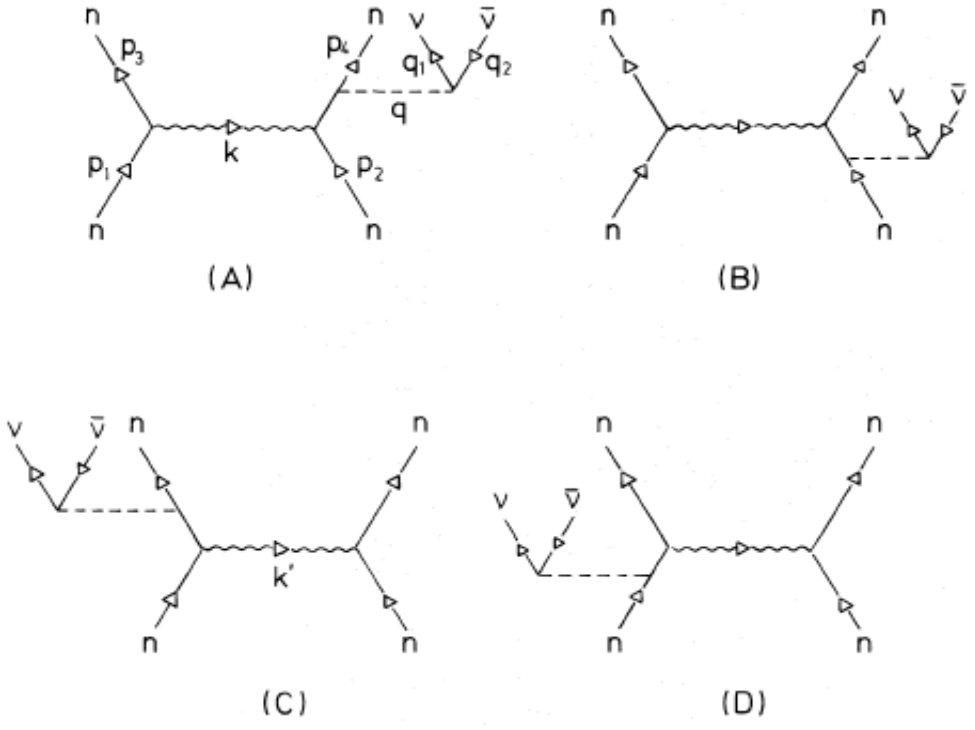

Figure 4.1: The directed solid lines indicate neutrons or neutrinos as indicated.

4.1.2 Diagrams for the $np\nu\bar{\nu}$ process

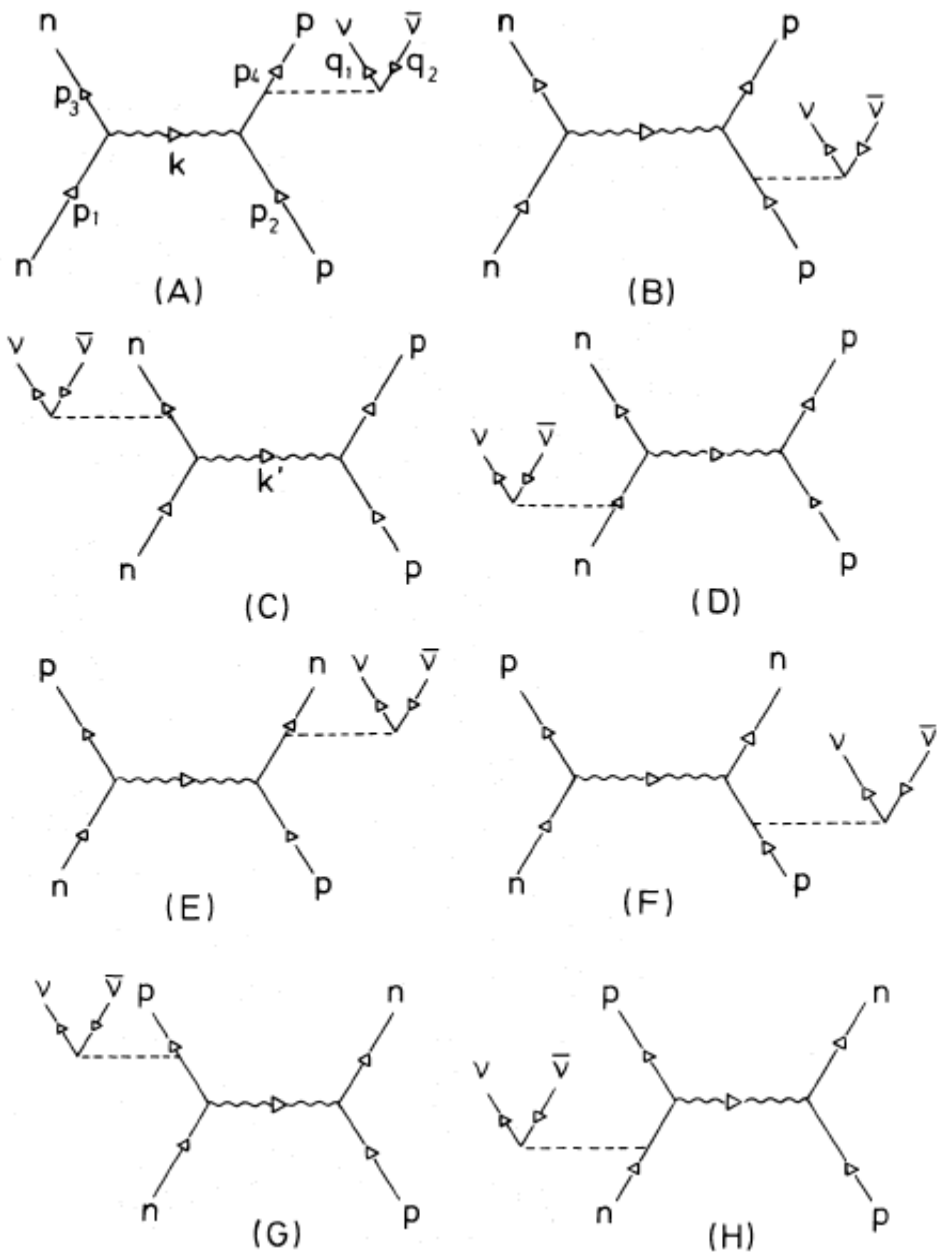

Figure 4.2: The directed wavy line indicates the nucleon-nucleon interaction involving exchange of momentum k or k', and the dashed line indicates the weak interaction involving exchange of momentum b.

4.2 The Nucleon-Nucleon Interaction

Both the $nn\nu\bar{\nu}$ and $np\nu\bar{\nu}$ processes described above, involve a strong nucleon-nucleon (NN) interaction as well as the weak interaction responsible for the neutrino production. Let us now briefly review the empirically known features of the strong interactions. Strong interactions are in principle explained by quantum chromodynamics (QCD), which is founded on a non-Abelian gauge group. It was first introduced by Yang and Mills, where the main idea is the principle of local gauge invariance. The symmetry group of QCD is $\mathrm{SU}(3)_c$ because the quarks may have one of the three colours as the quantum number, while the gluons come in eight colours.

The QCD Lagrangian density, which is believed to govern all hadronic processes is written as

$$\mathscr{L}_{QCD} = -\frac{1}{4} G^a_{\mu\nu} G^{\mu\nu}_a + \sum_q \bar{q}\big(i\gamma^\mu D_\mu - m_q\big)q, \tag{4.2}$$

where $D_\mu = \partial_\mu - i g_c \lambda_a / 2 A^a_\mu$ is the covariant derivative with λ_a, the Gell-Mann matrices and $g_c = \sqrt{4\pi\alpha_s}$, the quark-gluon coupling constant. Quarks come in six flavours: up, down, strange, charm, bottom, and top and are represented by the quark fields q. The field strength tensor $G^a_{\mu\nu}$ is expressed in terms of potentials A^μ as

$$G^a_{\mu\nu} = \partial_\mu A^a_\nu - \partial_\nu A^a_\mu + g_c f^{abc} A^b_\mu A^c_\nu, \tag{4.3}$$

where f^{abc} are the structure constants of the group and a represents the 8 generators of the $\mathrm{SU}(3)_c$ rotations. One of the properties of QCD is the asymptotic freedom due to the non-Abelian nature of the gauge theory. The strong coupling constant scales with momentum p as

$$\alpha_s(p^2) = \frac{12\pi}{\big(33 - 2N_f\big)\ln\big(p^2/\Lambda^2_{QCD}\big)} \left[1 - \frac{6\big(153 - 19N_f\big)}{\big(33 - 2N_f\big)^2} \frac{\ln\big[\ln\big(p^2/\Lambda^2_{QCD}\big)\big]}{\ln\big(p^2/\Lambda^2_{QCD}\big)}\right], \tag{4.4}$$

where N_f is the number of quark flavours. We see that, at large momentum or at small distances, the strong coupling constant vanishes so that one can make perturbative calculations. However, due to the non-perturbative character of QCD at low energies, we do not have a quantitative understanding of the nuclear force from this point of view. Asymptotic freedom is one of the strongest reasons why we believe that QCD is the correct theory of strong interactions. The parametrization in Eq. (4.4) includes the QCD scaling parameter $\Lambda_{QCD} \sim 0.1 - 0.2\,\mathrm{GeV}$, which fixes the scale of strong interactions.

The gauge fields of QCD, gluons, can interact with each other because they carry colour charge. Since quarks, as well as gluons, are not colour-neutral, they cannot be observed as physical states but as confined with other quarks and gluons. The hadrons are colour singlet combinations of quarks, antiquarks and gluons. This mechanism is known as colour confinement which is one of the most non-trivial features of QCD that has remained unsolved up to now. Colour confinement limits the direct use of the QCD Lagrangian (4.2) since one needs highly virtual quarks and gluons that can be treated as free so that perturbative expansions are applicable.

In the regime where perturbation theory fails, one should use some non-perturbative methods. Among non-perturbative approaches to QCD, the most well established one is lattice QCD. This approach uses a discrete set of space-time points (called the lattice) to reduce the analytically intractable path integrals of the continuum theory to a very difficult numerical computation which is then carried out on supercomputers. While it is a slow and resource-intensive approach, it has wide applicability, giving insight into parts of the theory inaccessible by other means.

There are very successful approaches in explaining the nucleon-nucleon (NN), hyperon-nucleon (YN) and hyperon-hyperon (YY) interactions in terms of one-boson-exchange (OBE) models, based on Regge-pole theory. The main idea is that the interaction of two baryons can be completely explained with one meson exchanges. The interaction mechanism can be extended beyond one-meson exchanges to e.g. two-meson exchanges, however OBE has been reasonably successful in describing the complete interaction. In these models, the values of the meson-baryon coupling constants are empirically determined so as to reproduce the NN and YN interactions.

The OBE models include the following meson exchanges:

a) The pseudoscalar mesons (π, η),

b) The scalar mesons (σ, δ),

c) The vector mesons (ρ, ω).

The interaction Lagrangians that couple these mesons to the nucleons are

$$\mathscr{L}_{NNps} = -g_{NNps}\,\bar{\psi} i\gamma_5 \psi\,\varphi^{(ps)}, \tag{4.5}$$

$$\mathscr{L}_{NNs} = g_{NNs}\,\bar{\psi}\psi\,\varphi^{(s)}, \tag{4.6}$$

$$\mathscr{L}_{NNv} = -g_{NNv}\,\bar{\psi}\gamma^{\mu}\psi\,\varphi^{(v)}_{\mu} - \frac{f_v}{4M}\,\bar{\psi}\sigma^{\mu\nu}\psi\big(\partial_\mu\varphi^{(v)}_{\nu} - \partial_\nu\varphi^{(v)}_{\mu}\big), \tag{4.7}$$

where ψ denotes the nucleon Dirac spinor field, while $\varphi^{(ps)}$, $\varphi^{(s)}$, and $\varphi^{(v)}_{\mu}$ are the pseudoscalar, scalar, and vector boson fields, respectively. M is the nucleon mass. In Eq. (4.7) the first term on the right-hand side is called the vector and the second term the tensor coupling. These two couplings are similar to the interaction of a photon with a nucleon.

Alternatively, for the pseudoscalar field there is also the so-called pseudovector or gradient coupling to the nucleon, which is suggested as an effective coupling by chiral symmetry,

$$\mathscr{L}_{NNpv} = -\frac{f_{ps}}{m_{ps}}\,\bar{\psi}\gamma^5\gamma^{\mu}\psi\,\partial_\mu\varphi^{(ps)}. \tag{4.8}$$

The pseudoscalar and the pseudovector coupling are equivalent for on-mass-shell nucleons if the coupling constants are related by $f_{ps} = (m_{ps}/2M)g_{NNps}$. However, off shell the predictions are rather different. Antiparticle contributions turn out to be huge when using the pseudoscalar coupling, whereas they are suppressed by the gradient coupling.

Naturally, the nuclear force may be subdivided into three regions:

1. The "classical" or long-range part with a range, $R \gtrsim 2\,\mathrm{fm}$,
2. The "dynamical" or intermediate part with a range, $1\,\mathrm{fm} \lesssim R \lesssim 2\,\mathrm{fm}$,
3. The "phenomenological" or short-range part with a range, $R \lesssim 1\,\mathrm{fm}$.

The long-range part is dominated by the pion (π) as a one-pion exchange. A much smaller contribution in the classical region comes from another pseudoscalar, namely the eta (η) meson. In the intermediate region, the two-pion exchange is the dominant one. This is a difficult interaction to include. It gives a loop diagram, which for a realistic pseudovector coupling is not renormalizable. Finally, in the short-range part, many different processes play a part. There are many-pion exchanges, heavy meson exchanges, and not least gluon exchanges among the quarks. For the multi-pion resonances and heavy meson exchanges we include the rho (ρ) meson and the omega (ω) meson. The other processes will be taken into account by the form factors. However, the average interparticle separation in neutron matter at nuclear density is 2.2 fm, which is large enough that the long-range part of the NN interaction should dominate.

4.3 Feynman Amplitudes

Physically, the Feynman amplitude $\mathcal{M}$ contains all the dynamical information of the process under consideration. And it is obtained by evaluating the relevant Feynman diagrams, using the Feynman rules appropriate to the interaction in question. More concretely, we write down all diagrams contributing to the process, calculate the amplitude $\mathcal{M}$ for each one, and add them up to get the total amplitude. Consequently, the square of the entire Feynman amplitude is imposed to include every possible combination as follows,

$$|\mathcal{M}|^2 = \left| \sum_{i=1}^{n} \mathcal{M}_i \right|^2 = \sum_{i=1}^{n} \sum_{j=1}^{n} \mathcal{M}_i \mathcal{M}_j^\dagger. \tag{4.9}$$

It turns out that all terms of the form $\mathcal{M}_i \mathcal{M}_j^\dagger$ are all hermitian; that is,

$$\mathcal{M}_i \mathcal{M}_j^\dagger = \mathcal{M}_j \mathcal{M}_i^\dagger. \tag{4.10}$$

This means that we only need to calculate terms in the sum

$$|\mathcal{M}|^2 = \sum_{i \leqslant j} \mathcal{M}_i \mathcal{M}_j^\dagger. \tag{4.11}$$

In addition, the Pauli exclusion principle demands that for two identical fermions, the total wavefunction is antisymmetric. This means that we have to insert a minus sign in combining amplitudes that differ only in the interchange of two identical external fermions. It doesn't matter which diagram we associate the minus sign with, since the total will be squared eventually anyway; but there must be a relative minus sign between them.

In some processes the initial and final states are completely specified, including the polarization states of the particles present initially and finally. If so, the next step is to insert the appropriate spinors and polarization vectors into the expression for $\mathcal{M}$, and compute $|\mathcal{M}|^2$, the quantity we actually need to determine emissivities. More often, the interacting particles are unpolarized, i.e. the initial and final spin orientations are random. To obtain the corresponding unpolarized amplitudes, we have to average $|\mathcal{M}|^2$ over all initial spin configurations and sum it over all final spin configurations. In principle, we could compute $|\mathcal{M}|^2$ for every possible spin configuration, and then do the summing and averaging. Usually, it is much easier to compute $|\mathcal{M}|^2$ directly, without ever evaluating the individual amplitudes.

By the way, the amplitude $\mathcal{M}$ has units which depend on the number of particles involved. If there are n external lines (both incoming and outgoing), the dimensions of $\mathcal{M}$ are those of momentum raised to the power $4-n$: $[\mathcal{M}] = (\mathrm{eV/c})^{4-n}$. For example, in a three-body process ($A \longrightarrow B + C$), $\mathcal{M}$ has dimensions of momentum; in a four-body process ($A \longrightarrow B + C + D$, or $A + B \longrightarrow C + D$), $\mathcal{M}$ is dimensionless.

Now, we are going to evaluate the Feynman amplitudes analytically for the $nn\nu\bar{\nu}$ and $np\nu\bar{\nu}$ processes in which the exchange of pseudoscalar and scalar mesons are involved.

4.3.1 Exchange of pseudoscalar mesons

Let us now calculate the Feynman amplitude for the one-pion exchange contribution to the first diagram in Fig. 4.1. The four-momentum transfers which are carried by the π^0-meson and neutron, are defined by

$$k = p_1 - p_3 \tag{4.12}$$

$$q = p_1 + p_2 - p_3 \tag{4.13}$$

According to the Glashow-Weinberg-Salam model [9], the four-fermion coupling of Z^0-boson or the so-called Z^0 vertex factor is given by

$$\frac{-ig_Z}{2}\gamma^\mu \left(c_V^f - c_A^f \gamma^5\right) \tag{4.14}$$

where g_Z is the neutral coupling constant, and the coefficients c_V^f and c_A^f are representing the vector- and axial-current couplings to fermions. Moreover, the neutral coupling constant g_Z is related to the basic unit of electric charge by

$$g_Z = \frac{g_e}{\sin\theta_W \cos\theta_W} \tag{4.15}$$

where g_e is the electromagnetic coupling constant (in appropriate units, the charge of the positron) and θ_W is the weak mixing angle (or Weinberg angle).

The probability amplitude for Z^0-boson to travel with a certain energy and momentum, is given by the Z^0 propagator:

$$\frac{-i\left(g_{\mu\nu} - b_\mu b_\nu / M_Z^2 c^2\right)}{b^2 - M_Z^2 c^2} \tag{4.16}$$

where $b = q - p_4$ is the four-momentum transferred by the Z^0-boson. Since the processes we are considering, take place at very low energies compared with the Z^0 mass; that is $b^2 \ll M_Z^2 c^2$, the Z^0 propagator reduces to

$$\frac{i g_{\mu\nu}}{M_Z^2} \tag{4.17}$$

Similarly, the propagator corresponding to the neutron is given by

$$\frac{i\left(\not{q} + m_n c\right)}{q^2 - m_n^2 c^2} \tag{4.18}$$

Since the π^0-meson has spin 0, the π^0 propagator takes the following form

$$\frac{i}{k^2 - m_\pi^2 c^2} \tag{4.19}$$

The effective coupling of π^0-meson to fermions is given by

$$-i g_{NN\pi} \gamma^5 \tag{4.20}$$

We are now equipped to write down the Feynman amplitude for the first diagram to the $nn\nu\bar{\nu}$ process

$$\begin{aligned}\mathcal{M}_1 = \bar{u}(q_2, r_2)\left[\frac{-ig_Z}{2}\gamma^\mu\left(c_V^\nu - c_A^\nu\gamma^5\right)\right] v(q_1, r_1)\left\{\frac{ig_{\mu\nu}}{M_Z^2}\right\}\bar{u}(p_4, s_4)\times \\ \times\left[\frac{-ig_Z}{2}\gamma^\nu\left(c_V^n - c_A^n\gamma^5\right)\right]\left\{\frac{i\left(\not{q} + m_n\right)}{q^2 - m_n^2}\right\}\left[-ig_{NN\pi}\gamma^5\right] u(p_2, s_2)\times \\ \times\left\{\frac{i}{k^2 - m_\pi^2}\right\}\bar{u}(p_3, s_3)\left[-ig_{NN\pi}\gamma^5\right] u(p_1, s_1)\end{aligned} \tag{4.21}$$

where $u(p_1, s_1)$, $\bar{u}(p_3, s_3)$, $u(p_2, s_2)$ and $\bar{u}(p_4, s_4)$ are Dirac spinors representing the incoming and outgoing neutrons respectively. Similarly, $v(q_1, r_1)$ and $\bar{u}(q_2, r_2)$ denotes the outgoing antineutrino and the outgoing neutrino. By substituting the neutral weak couplings for the neutrino; $c_V^\nu = c_A^\nu = 1/2$, in Eq. (4.21), we get

$$\begin{aligned}\mathcal{M}_1 = -i\frac{G_F}{\sqrt{2}}\frac{g_{NN\pi}^2}{\left(k^2 - m_\pi^2\right)\left(q^2 - m_n^2\right)}\bar{u}(q_2, r_2)\gamma^\mu\left(1 - \gamma^5\right) v(q_1, r_1)\bar{u}(p_4, s_4)\gamma_\mu\times \\ \times\left(c_V^n - c_A^n\gamma^5\right)\left(\not{q} + m_n\right)\gamma^5 u(p_2, s_2)\bar{u}(p_3, s_3)\gamma^5 u(p_1, s_1)\end{aligned} \tag{4.22}$$

where the Fermi coupling constant is defined by

$$G_F = \frac{\sqrt{2}}{8}\left(\frac{g_Z}{M_Z}\right)^2 = \frac{1}{\sqrt{2}}\frac{\pi\alpha}{M_Z^2 \sin^2\theta_W \cos^2\theta_W} = 1.166 \times 10^{-5}\mathrm{GeV}^{-2} \tag{4.23}$$

Taking the hermitian conjugate of the Feynman amplitude (4.22) gives

$$\mathcal{M}_1^\dagger = i\frac{G_F}{\sqrt{2}}\frac{g_{NN\pi}^2}{(k^2-m_\pi^2)(q^2-m_n^2)}\bar{u}(p_1,s_1)\gamma^5 u(p_3,s_3)\bar{u}(p_2,s_2)\gamma^5(\not{q}+m_n)\times \\ \times\left(c_V^n+c_A^n\gamma^5\right)\gamma_\nu u(p_4,s_4)\bar{v}(q_1,r_1)\left(1+\gamma^5\right)\gamma^\nu u(q_2,r_2) \tag{4.24}$$

We perform the by now very familiar calculation of squaring the invariant Feynman amplitude:

$$|\mathcal{M}_1|^2 = \frac{1}{4}\sum_{s_1,s_2}\sum_{\substack{s_3,s_4\\r_1,r_2}}\mathcal{M}_1\mathcal{M}_1^\dagger \tag{4.25}$$

where we sum over final spins and average over initial spins by the fact that the polarizations of the initial-state and final-state particles are unknown. By expanding the summation over spin states, we achieve

$$|\mathcal{M}_1|^2 = \frac{G_F^2}{8}\frac{g_{NN\pi}^4}{(k^2-m_\pi^2)^2(q^2-m_n^2)^2}\sum_{r_2}\bar{u}(q_2,r_2)\gamma^\mu\left(1-\gamma^5\right)\left(\sum_{r_1}v(q_1,r_1)\bar{v}(q_1,r_1)\right)\times \\ \times\left(1+\gamma^5\right)\gamma^\nu u(q_2,r_2)\sum_{s_4}\bar{u}(p_4,s_4)\gamma_\mu\left(c_V^n-c_A^n\gamma^5\right)(\not{q}+m_n)\gamma^5\times \\ \times\left(\sum_{s_2}u(p_2,s_2)\bar{u}(p_2,s_2)\right)\gamma^5(\not{q}+m_n)\left(c_V^n+c_A^n\gamma^5\right)\gamma_\nu u(p_4,s_4)\sum_{s_3}\bar{u}(p_3,s_3)\gamma^5\times \\ \times\left(\sum_{s_1}u(p_1,s_1)\bar{u}(p_1,s_1)\right)\gamma^5 u(p_3,s_3) \tag{4.26}$$

The summations over spins r_1, s_2 and s_1 can be expressed in terms of the projection operators:

$$\sum_{r_1}v(q_1,r_1)\bar{v}(q_1,r_1) = \not{q}_1 - m_\nu \tag{4.27}$$

$$\sum_{s_2}u(p_2,s_2)\bar{u}(p_2,s_2) = \not{p}_2 + m_n \tag{4.28}$$

$$\sum_{s_1}u(p_1,s_1)\bar{u}(p_1,s_1) = \not{p}_1 + m_n \tag{4.29}$$

See Appendix A, Section A.3 for the detailed calculation of the above summations. Feeding these into Eq. (4.26) leads to

$$|\mathcal{M}_1|^2 = \frac{G_F^2}{8}\frac{g_{NN\pi}^4}{(k^2-m_\pi^2)^2(q^2-m_n^2)^2}\sum_{r_2}\bar{u}(q_2,r_2)\gamma^\mu\left(1-\gamma^5\right)(\not{q}_1-m_\nu)\times \\ \times\left(1+\gamma^5\right)\gamma^\nu u(q_2,r_2)\sum_{s_4}\bar{u}(p_4,s_4)\gamma_\mu\left(c_V^n-c_A^n\gamma^5\right)(\not{q}+m_n)\gamma^5\times \\ \times(\not{p}_2+m_n)\gamma^5(\not{q}+m_n)\left(c_V^n+c_A^n\gamma^5\right)\gamma_\nu u(p_4,s_4)\sum_{s_3}\bar{u}(p_3,s_3)\gamma^5\times \\ \times(\not{p}_1+m_n)\gamma^5 u(p_3,s_3) \tag{4.30}$$

Before going on to the remaining summations in Eq. (4.30), we associate the summands between spinors with the product of γ-matrices and rewrite them in the following way

$$|\mathcal{M}_1|^2 = \frac{G_F^2}{8}\frac{g_{NN\pi}^4}{\left(k^2-m_\pi^2\right)^2\left(q^2-m_n^2\right)^2}\sum_{r_2}\bar{u}(q_2,r_2)\mathcal{A}u(q_2,r_2)\sum_{s_4}\bar{u}(p_4,s_4)\mathcal{B}u(p_4,s_4)\times \\ \times\sum_{s_3}\bar{u}(p_3,s_3)\mathcal{C}u(p_3,s_3) \tag{4.31}$$

where the matrices $\mathcal{A}$, $\mathcal{B}$ and $\mathcal{C}$ are defined by

$$\mathcal{A} = \gamma^\mu\left(1-\gamma^5\right)\left(\not{q}_1 - m_\nu\right)\left(1+\gamma^5\right)\gamma^\nu \tag{4.32}$$

$$\mathcal{B} = \gamma_\mu\left(c_V^n - c_A^n\gamma^5\right)\left(\not{q}+m_n\right)\gamma^5\left(\not{p}_2+m_n\right)\gamma^5\left(\not{q}+m_n\right)\left(c_V^n+c_A^n\gamma^5\right)\gamma_\nu \tag{4.33}$$

$$\mathcal{C} = \gamma^5\left(\not{p}_1+m_n\right)\gamma^5 \tag{4.34}$$

The summations in the squared Feynman amplitude (4.31) can be expressed in terms of the traces:

$$\begin{aligned}\mathbf{Tr}(\widetilde{\mathcal{A}}) &= \sum_{r_2}\bar{u}(q_2,r_2)\mathcal{A}u(q_2,r_2) = \mathbf{Tr}\left[\left(\not{q}_2+m_\nu\right)\mathcal{A}\right] \\ &= \mathbf{Tr}\left[\left(\not{q}_2+m_\nu\right)\gamma^\mu\left(1-\gamma^5\right)\left(\not{q}_1-m_\nu\right)\left(1+\gamma^5\right)\gamma^\nu\right] \qquad (4.35)\\ \mathbf{Tr}(\widetilde{\mathcal{B}}) &= \sum_{s_4}\bar{u}(p_4,s_4)\mathcal{B}u(p_4,s_4) = \mathbf{Tr}\left[\left(\not{p}_4+m_n\right)\mathcal{B}\right] \\ &= \mathbf{Tr}\Big[\left(\not{p}_4+m_n\right)\gamma_\mu\left(c_V^n-c_A^n\gamma^5\right)\left(\not{q}+m_n\right)\gamma^5\left(\not{p}_2+m_n\right)\gamma^5\left(\not{q}+m_n\right)\cdot \\ &\quad\cdot\left(c_V^n+c_A^n\gamma^5\right)\gamma_\nu\Big] \qquad (4.36)\\ \mathbf{Tr}(\widetilde{\mathcal{C}}) &= \sum_{s_3}\bar{u}(p_3,s_3)\mathcal{C}u(p_3,s_3) = \mathbf{Tr}\left[\left(\not{p}_3+m_n\right)\mathcal{C}\right] \\ &= \mathbf{Tr}\left[\left(\not{p}_3+m_n\right)\gamma^5\left(\not{p}_1+m_n\right)\gamma^5\right] \qquad (4.37)\end{aligned}$$

In Appendix A, Section A.4, we show how this kind of summations can be executed in order to reduce these down to the traces of products of γ-matrices. By combining these results we arrive at

$$\begin{aligned}|\mathcal{M}_1|^2 &= \frac{G_F^2}{8}\frac{g_{NN\pi}^4}{\left(k^2-m_\pi^2\right)^2\left(q^2-m_n^2\right)^2}\;\mathbf{Tr}(\widetilde{\mathcal{A}})\times\mathbf{Tr}(\widetilde{\mathcal{B}})\times\mathbf{Tr}(\widetilde{\mathcal{C}}) \\ &= \frac{G_F^2}{8}\frac{g_{NN\pi}^4}{\left(k^2-m_\pi^2\right)^2\left(q^2-m_n^2\right)^2}\;\mathbf{Tr}\Big[\left(\not{q}_2+m_\nu\right)\gamma^\mu\left(1-\gamma^5\right)\left(\not{q}_1-m_\nu\right)\cdot \\ &\quad\cdot\left(1+\gamma^5\right)\gamma^\nu\Big]\times\mathbf{Tr}\Big[\left(\not{p}_4+m_n\right)\gamma_\mu\left(c_V^n-c_A^n\gamma^5\right)\left(\not{q}+m_n\right)\gamma^5\left(\not{p}_2+m_n\right)\cdot \\ &\quad\cdot\gamma^5\left(\not{q}+m_n\right)\left(c_V^n+c_A^n\gamma^5\right)\gamma_\nu\Big]\times\mathbf{Tr}\left[\left(\not{p}_3+m_n\right)\gamma^5\left(\not{p}_1+m_n\right)\gamma^5\right] \qquad (4.38)\end{aligned}$$

In order to complete the calculation of Feynman amplitude, we have to compute the traces of products of γ-matrices. In particular, the second trace in Eq. (4.38) involves product of up to ten γ-matrices. Of course, in principle, these can all be done by hand. However, we employ an algebraic manipulation program `FORM`, which is written by Jos Vermaseren in 1989 for fast handling of very large-scale symbolic mathematics

problems. By means of this package, we obtain for the first trace

$$\mathbf{Tr}(\widetilde{\mathcal{A}}) = 8\left[q_1^\mu q_2^\nu + q_1^\nu q_2^\mu - (q_1\cdot q_2)g^{\mu\nu} + i\epsilon^{\eta\mu\delta\nu}q_{2\eta}q_{1\delta}\right] \tag{4.39}$$

Furthermore, the second and third traces are computed to be

$$\begin{aligned}
\mathbf{Tr}(\widetilde{\mathcal{B}}) = {} & 4\left(c_V^{n^2} + c_A^{n^2}\right)\Big[p_{2\mu}p_{4\nu}(q\cdot q) + p_{2\nu}p_{4\mu}(q\cdot q) - 2p_{4\mu}q_\nu(p_2\cdot q) - \\
& - 2p_{4\nu}q_\mu(p_2\cdot q) - (p_2\cdot p_4)(q\cdot q)g_{\mu\nu} + 2(p_2\cdot q)(p_4\cdot q)g_{\mu\nu}\Big] + \\
& + 4m_n^2\left(c_V^{n^2} + c_A^{n^2}\right)\Big[2p_{4\mu}q_\nu + 2p_{4\nu}q_\mu - p_{2\mu}p_{4\nu} - p_{2\nu}p_{4\mu} + \\
& + (p_2\cdot p_4)g_{\mu\nu} - 2(p_4\cdot q)g_{\mu\nu}\Big] + \\
& + 4m_n^2\left(c_V^{n^2} - c_A^{n^2}\right)\Big[(q\cdot q)g_{\mu\nu} - 2(p_2\cdot q)g_{\mu\nu} + m_n^2 g_{\mu\nu}\Big] + \\
& + 8c_V^n c_A^n\Big[i\epsilon_{\alpha\mu\beta\nu}p_4^\alpha p_2^\beta(q\cdot q) - 2i\epsilon_{\alpha\mu\sigma\nu}p_4^\alpha q^\sigma(p_2\cdot q)\Big] - \\
& - 8m_n^2 c_V^n c_A^n\Big[i\epsilon_{\alpha\mu\beta\nu}p_4^\alpha p_2^\beta - 2i\epsilon_{\alpha\mu\sigma\nu}p_4^\alpha q^\sigma\Big]
\end{aligned} \tag{4.40}$$

$$\mathbf{Tr}(\widetilde{\mathcal{C}}) = 4\left[m_n^2 - (p_1\cdot p_3)\right] \tag{4.41}$$

In multiplying the three traces (4.39), (4.40), and (4.41) together, we make use of the following contraction identity:

$$\epsilon^{\eta\mu\delta\nu}\epsilon_{\alpha\mu\beta\nu} = -2\big(g_\alpha^\eta g_\beta^\delta - g_\beta^\eta g_\alpha^\delta\big) \tag{4.42}$$

Finally, the squared Feynman amplitude for the one-pion exchange contribution to $nn\nu\bar{\nu}$ process becomes

$$
\begin{aligned}
|\mathcal{M}_1|^2 = \frac{32G_F^2 g_{NN\pi}^4}{\left(k^2-m_\pi^2\right)^2\left(q^2-m_n^2\right)^2}\Bigg\{ & \left(c_V^{n^2}+c_A^{n^2}\right)\Big[2(p_1\cdot p_3)(p_2\cdot q)(p_4\cdot q_1)(q_2\cdot q)+ \\
& +2(p_1\cdot p_3)(p_2\cdot q)(p_4\cdot q_2)(q_1\cdot q)-(p_1\cdot p_3)(p_2\cdot q_1)(p_4\cdot q_2)(q\cdot q)- \\
& -(p_1\cdot p_3)(p_2\cdot q_2)(p_4\cdot q_1)(q\cdot q)\Big]+m_n^2\left(c_V^{n^2}+c_A^{n^2}\right)\Big[2m_n^2(p_4\cdot q_1)(q_2\cdot q)+ \\
& +2m_n^2(p_4\cdot q_2)(q_1\cdot q)-m_n^2(p_2\cdot q_1)(p_4\cdot q_2)-m_n^2(p_2\cdot q_2)(p_4\cdot q_1)- \\
& -2(p_2\cdot q)(p_4\cdot q_1)(q_2\cdot q)-2(p_2\cdot q)(p_4\cdot q_2)(q_1\cdot q)+(p_2\cdot q_1)(p_4\cdot q_2)(q\cdot q)+ \\
& +(p_2\cdot q_2)(p_4\cdot q_1)(q\cdot q)-2(p_1\cdot p_3)(p_4\cdot q_1)(q_2\cdot q)-2(p_1\cdot p_3)(p_4\cdot q_2)(q_1\cdot q)+ \\
& +(p_1\cdot p_3)(p_2\cdot q_1)(p_4\cdot q_2)+(p_1\cdot p_3)(p_2\cdot q_2)(p_4\cdot q_1)\Big]- \\
& -m_n^2\left(c_V^{n^2}-c_A^{n^2}\right)\Big[2(p_1\cdot p_3)(p_2\cdot q)(q_1\cdot q_2)-(p_1\cdot p_3)(q_1\cdot q_2)(q\cdot q)- \\
& -2m_n^2(p_2\cdot q)(q_1\cdot q_2)-m_n^2(p_1\cdot p_3)(q_1\cdot q_2)+m_n^2(q_1\cdot q_2)(q\cdot q)+ \\
& +m_n^4(q_1\cdot q_2)\Big]-2c_V^n c_A^n\Big[2(p_1\cdot p_3)(p_2\cdot q)(p_4\cdot q_1)(q_2\cdot q)- \\
& -2(p_1\cdot p_3)(p_2\cdot q)(p_4\cdot q_2)(q_1\cdot q)+(p_1\cdot p_3)(p_2\cdot q_1)(p_4\cdot q_2)(q\cdot q)- \\
& -(p_1\cdot p_3)(p_2\cdot q_2)(p_4\cdot q_1)(q\cdot q)\Big]-2m_n^2c_V^n c_A^n\Big[2m_n^2(p_4\cdot q_1)(q_2\cdot q)- \\
& -2m_n^2(p_4\cdot q_2)(q_1\cdot q)+m_n^2(p_2\cdot q_1)(p_4\cdot q_2)-m_n^2(p_2\cdot q_2)(p_4\cdot q_1)- \\
& -2(p_2\cdot q)(p_4\cdot q_1)(q_2\cdot q)+2(p_2\cdot q)(p_4\cdot q_2)(q_1\cdot q)-(p_2\cdot q_1)(p_4\cdot q_2)(q\cdot q)+ \\
& +(p_2\cdot q_2)(p_4\cdot q_1)(q\cdot q)-2(p_1\cdot p_3)(p_4\cdot q_1)(q_2\cdot q)+2(p_1\cdot p_3)(p_4\cdot q_2)(q_1\cdot q)- \\
& -(p_1\cdot p_3)(p_2\cdot q_1)(p_4\cdot q_2)+(p_1\cdot p_3)(p_2\cdot q_2)(p_4\cdot q_1)\Big]\Bigg\}
\end{aligned}
\tag{4.43}
$$

Note that the four diagrams contributing to the $nn\nu\bar{\nu}$ process are all topologically equivalent. In this regard, they are described by the same Feynman amplitude, and hence the square of the total Feynman amplitude becomes

$$
|\mathcal{M}|^2 = \left|\sum_{i=1}^{4}\mathcal{M}_i\right|^2 = |4\mathcal{M}_1|^2 = 16|\mathcal{M}_1|^2 \tag{4.44}
$$

In the next section, we proceed along the same lines to calculate the Feynman amplitude for the $np\nu\bar{\nu}$ process with the scalar meson exchanges.

4.3.2 Exchange of scalar mesons

We now consider the $np\nu\bar{\nu}$ process and calculate the Feynman amplitude for the σ exchange contribution to the first diagram in Fig. 4.2. As before, the four-momentum transfers which are carried by the σ-meson and proton, are defined by

$$
k = p_1 - p_3 \tag{4.45}
$$

$$
q = p_1 + p_2 - p_3 \tag{4.46}
$$

Applying the Feynman rules to the first diagram in Fig. 4.2, we attain the following Feynman amplitude

$$\begin{aligned}\mathcal{M}_1 = \bar{u}(q_2, r_2)\left[\frac{-ig_Z}{2}\gamma^\mu\left(c_V^\nu - c_A^\nu\gamma^5\right)\right]v(q_1, r_1)\left\{\frac{ig_{\mu\nu}}{M_Z^2}\right\}\bar{u}(p_4, s_4)\times \\ \times\left[\frac{-ig_Z}{2}\gamma^\nu\left(c_V^p - c_A^p\gamma^5\right)\right]\left\{\frac{i\left(\not{q}+m_p\right)}{q^2-m_p^2}\right\}\left[g_{NN\sigma}\right]u(p_2, s_2)\times \\ \times\left\{\frac{i}{k^2-m_\sigma^2}\right\}\bar{u}(p_3, s_3)\left[g_{NN\sigma}\right]u(p_1, s_1)\end{aligned} \tag{4.47}$$

where $u(p_1, s_1)$ and $\bar{u}(p_3, s_3)$ are Dirac spinors representing the incoming and outgoing neutrons, while $u(p_2, s_2)$ and $\bar{u}(p_4, s_4)$ stands for the incoming and outgoing protons. Similarly, $v(q_1, r_1)$ and $\bar{u}(q_2, r_2)$ denotes the outgoing antineutrino and the outgoing neutrino. Putting the neutral weak couplings for the neutrino; $c_V^\nu = c_A^\nu = 1/2$, into Eq. (4.47), we obtain

$$\begin{aligned}\mathcal{M}_1 = i\frac{G_F}{\sqrt{2}}\frac{g_{NN\sigma}^2}{\left(k^2-m_\sigma^2\right)\left(q^2-m_p^2\right)}\bar{u}(q_2, r_2)\gamma^\mu\left(1-\gamma^5\right)v(q_1, r_1)\bar{u}(p_4, s_4)\gamma_\mu\times \\ \times\left(c_V^p - c_A^p\gamma^5\right)\left(\not{q}+m_p\right)u(p_2, s_2)\bar{u}(p_3, s_3)u(p_1, s_1)\end{aligned} \tag{4.48}$$

where G_F is the Fermi coupling constant, defined in Eq. (4.23). Taking the adjoint of the Feynman amplitude (Eq. (4.48)) yields

$$\begin{aligned}\mathcal{M}_1^\dagger = -i\frac{G_F}{\sqrt{2}}\frac{g_{NN\sigma}^2}{\left(k^2-m_\sigma^2\right)\left(q^2-m_p^2\right)}\bar{u}(p_1, s_1)u(p_3, s_3)\bar{u}(p_2, s_2)\left(\not{q}+m_p\right)\times \\ \times\left(c_V^p + c_A^p\gamma^5\right)\gamma_\nu u(p_4, s_4)\bar{v}(q_1, r_1)\left(1+\gamma^5\right)\gamma^\nu u(q_2, r_2)\end{aligned} \tag{4.49}$$

In squaring the invariant Feynman amplitude, we average it over spins in the initial state and sum it over spins in the final state:

$$|\mathcal{M}_1|^2 = \frac{1}{4}\sum_{s_1,s_2}\sum_{\substack{s_3,s_4\\r_1,r_2}}\mathcal{M}_1\mathcal{M}_1^\dagger \tag{4.50}$$

By splitting the summation over the spin states into individual sums, we achieve

$$\begin{aligned}|\mathcal{M}_1|^2 = \frac{G_F^2}{8}\frac{g_{NN\sigma}^4}{\left(k^2-m_\sigma^2\right)^2\left(q^2-m_p^2\right)^2}\sum_{r_2}\bar{u}(q_2, r_2)\gamma^\mu\left(1-\gamma^5\right)\left(\sum_{r_1}v(q_1, r_1)\bar{v}(q_1, r_1)\right)\times \\ \times\left(1+\gamma^5\right)\gamma^\nu u(q_2, r_2)\sum_{s_4}\bar{u}(p_4, s_4)\gamma_\mu\left(c_V^p - c_A^p\gamma^5\right)\left(\not{q}+m_p\right)\times \\ \times\left(\sum_{s_2}u(p_2, s_2)\bar{u}(p_2, s_2)\right)\left(\not{q}+m_p\right)\left(c_V^p + c_A^p\gamma^5\right)\gamma_\nu u(p_4, s_4)\sum_{s_3}\bar{u}(p_3, s_3)\times \\ \times\left(\sum_{s_1}u(p_1, s_1)\bar{u}(p_1, s_1)\right)u(p_3, s_3)\end{aligned} \tag{4.51}$$

We next perform the summations in the round brackets in Eq. (4.51), which results in the projection operators (Appendix A, Section A.3). It then follows that

$$
\begin{aligned}
|\mathcal{M}_1|^2 = \frac{G_F^2}{8}\frac{g_{NN\sigma}^4}{\left(k^2-m_\sigma^2\right)^2\left(q^2-m_p^2\right)^2}\sum_{r_2}\bar{u}(q_2,r_2)\gamma^\mu\left(1-\gamma^5\right)\left(\not{q}_1-m_\nu\right)\times \\
\times\left(1+\gamma^5\right)\gamma^\nu u(q_2,r_2)\sum_{s_4}\bar{u}(p_4,s_4)\gamma_\mu\left(c_V^p-c_A^p\gamma^5\right)\left(\not{q}+m_p\right)\times \\
\times\left(\not{p}_2+m_p\right)\left(\not{q}+m_p\right)\left(c_V^p+c_A^p\gamma^5\right)\gamma_\nu u(p_4,s_4)\sum_{s_3}\bar{u}(p_3,s_3)\times \\
\times\left(\not{p}_1+m_n\right)u(p_3,s_3) \qquad (4.52)
\end{aligned}
$$

In the remaining three summations in Eq. (4.52), we identify the summands between spinors as the product of γ-matrices and define them as follows

$$\mathcal{A} = \gamma^\mu\left(1-\gamma^5\right)\left(\not{q}_1-m_\nu\right)\left(1+\gamma^5\right)\gamma^\nu \qquad (4.53)$$

$$\mathcal{B} = \gamma_\mu\left(c_V^p-c_A^p\gamma^5\right)\left(\not{q}+m_p\right)\left(\not{p}_2+m_p\right)\left(\not{q}+m_p\right)\left(c_V^p+c_A^p\gamma^5\right)\gamma_\nu \qquad (4.54)$$

$$\mathcal{C} = \left(\not{p}_1+m_n\right) \qquad (4.55)$$

which is leading to

$$
\begin{aligned}
|\mathcal{M}_1|^2 = \frac{G_F^2}{8}\frac{g_{NN\sigma}^4}{\left(k^2-m_\sigma^2\right)^2\left(q^2-m_p^2\right)^2}\sum_{r_2}\bar{u}(q_2,r_2)\mathcal{A}u(q_2,r_2)\sum_{s_4}\bar{u}(p_4,s_4)\mathcal{B}u(p_4,s_4)\times \\
\times\sum_{s_3}\bar{u}(p_3,s_3)\mathcal{C}u(p_3,s_3) \qquad (4.56)
\end{aligned}
$$

As we have shown in Appendix A, Section A.4, we express the summations in the above equation in terms of the traces:

$$
\begin{aligned}
\mathbf{Tr}(\widetilde{\mathcal{A}}) &= \sum_{r_2}\bar{u}(q_2,r_2)\mathcal{A}u(q_2,r_2) = \mathbf{Tr}\left[\left(\not{q}_2+m_\nu\right)\mathcal{A}\right] \\
&= \mathbf{Tr}\left[\left(\not{q}_2+m_\nu\right)\gamma^\mu\left(1-\gamma^5\right)\left(\not{q}_1-m_\nu\right)\left(1+\gamma^5\right)\gamma^\nu\right] \qquad (4.57) \\
\mathbf{Tr}(\widetilde{\mathcal{B}}) &= \sum_{s_4}\bar{u}(p_4,s_4)\mathcal{B}u(p_4,s_4) = \mathbf{Tr}\left[\left(\not{p}_4+m_p\right)\mathcal{B}\right] \\
&= \mathbf{Tr}\big[\left(\not{p}_4+m_p\right)\gamma_\mu\left(c_V^p-c_A^p\gamma^5\right)\left(\not{q}+m_p\right)\left(\not{p}_2+m_p\right)\left(\not{q}+m_p\right)\cdot \\
&\quad\cdot\left(c_V^p+c_A^p\gamma^5\right)\gamma_\nu\big] \qquad (4.58) \\
\mathbf{Tr}(\widetilde{\mathcal{C}}) &= \sum_{s_3}\bar{u}(p_3,s_3)\mathcal{C}u(p_3,s_3) = \mathbf{Tr}\left[\left(\not{p}_3+m_n\right)\mathcal{C}\right] \\
&= \mathbf{Tr}\left[\left(\not{p}_3+m_n\right)\left(\not{p}_1+m_n\right)\right] \qquad (4.59)
\end{aligned}
$$

By combining these results we arrive at

$$
\begin{aligned}
|\mathcal{M}_1|^2 &= \frac{G_F^2}{8}\frac{g_{NN\sigma}^4}{\left(k^2-m_\sigma^2\right)^2\left(q^2-m_p^2\right)^2}\;\mathbf{Tr}(\widetilde{\mathcal{A}})\times\mathbf{Tr}(\widetilde{\mathcal{B}})\times\mathbf{Tr}(\widetilde{\mathcal{C}}) \\
&= \frac{G_F^2}{8}\frac{g_{NN\sigma}^4}{\left(k^2-m_\sigma^2\right)^2\left(q^2-m_p^2\right)^2}\;\mathbf{Tr}\big[\left(\not{q}_2+m_\nu\right)\gamma^\mu\left(1-\gamma^5\right)\left(\not{q}_1-m_\nu\right)\cdot \\
&\quad\cdot\left(1+\gamma^5\right)\gamma^\nu\big]\times\mathbf{Tr}\big[\left(\not{p}_4+m_p\right)\gamma_\mu\left(c_V^p-c_A^p\gamma^5\right)\left(\not{q}+m_p\right)\left(\not{p}_2+m_p\right)\cdot \\
&\quad\cdot\left(\not{q}+m_p\right)\left(c_V^p+c_A^p\gamma^5\right)\gamma_\nu\big]\times\mathbf{Tr}\left[\left(\not{p}_3+m_n\right)\left(\not{p}_1+m_n\right)\right] \qquad (4.60)
\end{aligned}
$$

In order to calculate the traces in Eq. (4.60), we again employ the algebraic manipulator `FORM`, which is been introduced in Section 4.3.1. By use of this package, we obtain for the three traces

$$
\begin{aligned}
\mathbf{Tr}(\widetilde{\mathcal{A}}) &= 8\left[q_1^\mu q_2^\nu+q_1^\nu q_2^\mu-(q_1\cdot q_2)g^{\mu\nu}+i\epsilon^{\eta\mu\delta\nu}q_{2\eta}q_{1\delta}\right] \qquad (4.61)\\
\mathbf{Tr}(\widetilde{\mathcal{B}}) &= 4\left(c_V^{p^2}+c_A^{p^2}\right)\Big[2p_{4\mu}q_\nu(p_2\cdot q)+2p_{4\nu}q_\mu(p_2\cdot q)-p_{2\mu}p_{4\nu}(q\cdot q)- \\
&\quad-p_{2\nu}p_{4\mu}(q\cdot q)+(p_2\cdot p_4)(q\cdot q)g_{\mu\nu}-2(p_2\cdot q)(p_4\cdot q)g_{\mu\nu}\Big]+ \\
&\quad+4m_p^2\left(c_V^{p^2}+c_A^{p^2}\right)\Big[p_{2\mu}p_{4\nu}+p_{2\nu}p_{4\mu}+2p_{4\mu}q_\nu+2p_{4\nu}q_\mu- \\
&\quad-(p_2\cdot p_4)g_{\mu\nu}-2(p_4\cdot q)g_{\mu\nu}\Big]+ \\
&\quad+4m_p^2\left(c_V^{p^2}-c_A^{p^2}\right)\Big[(q\cdot q)g_{\mu\nu}+2(p_2\cdot q)g_{\mu\nu}+m_p^2g_{\mu\nu}\Big]- \\
&\quad-8c_V^pc_A^p\Big[i\epsilon_{\alpha\mu\beta\nu}p_4^\alpha p_2^\beta(q\cdot q)-2i\epsilon_{\alpha\mu\sigma\nu}p_4^\alpha q^\sigma(p_2\cdot q)\Big]+ \\
&\quad+8m_p^2c_V^pc_A^p\Big[i\epsilon_{\alpha\mu\beta\nu}p_4^\alpha p_2^\beta+2i\epsilon_{\alpha\mu\sigma\nu}p_4^\alpha q^\sigma\Big] \qquad (4.62)\\
\mathbf{Tr}(\widetilde{\mathcal{C}}) &= 4\left[m_n^2+(p_1\cdot p_3)\right] \qquad (4.63)
\end{aligned}
$$

The next step is to multiply the three traces (4.61), (4.62), and (4.63) together, for which we apply the following contraction identity:

$$
\epsilon^{\eta\mu\delta\nu}\epsilon_{\alpha\mu\sigma\nu}=-2\big(g_\alpha^\eta g_\sigma^\delta-g_\sigma^\eta g_\alpha^\delta\big) \qquad (4.64)
$$

Finally, the squared Feynman amplitude for the σ exchange contribution to $np\nu\bar{\nu}$ process becomes

$$
\begin{aligned}
|\mathcal{M}_1|^2 = \frac{32G_F^2 g_{NN\sigma}^4}{\left(k^2-m_\sigma^2\right)^2\left(q^2-m_p^2\right)^2}\Bigg\{ & \left(c_V^{p^2}+c_A^{p^2}\right)\Big[2(p_1\cdot p_3)(p_2\cdot q)(p_4\cdot q_1)(q_2\cdot q)+ \\
& +2(p_1\cdot p_3)(p_2\cdot q)(p_4\cdot q_2)(q_1\cdot q)-(p_1\cdot p_3)(p_2\cdot q_1)(p_4\cdot q_2)(q\cdot q)- \\
& -(p_1\cdot p_3)(p_2\cdot q_2)(p_4\cdot q_1)(q\cdot q)+2m_n^2m_p^2(p_4\cdot q_1)(q_2\cdot q)+ \\
& +2m_n^2m_p^2(p_4\cdot q_2)(q_1\cdot q)+m_n^2m_p^2(p_2\cdot q_1)(p_4\cdot q_2)+ \\
& +m_n^2m_p^2(p_2\cdot q_2)(p_4\cdot q_1)+2m_n^2(p_2\cdot q)(p_4\cdot q_1)(q_2\cdot q)+ \\
& +2m_n^2(p_2\cdot q)(p_4\cdot q_2)(q_1\cdot q)-m_n^2(p_2\cdot q_1)(p_4\cdot q_2)(q\cdot q)- \\
& -m_n^2(p_2\cdot q_2)(p_4\cdot q_1)(q\cdot q)+2m_p^2(p_1\cdot p_3)(p_4\cdot q_1)(q_2\cdot q)+ \\
& +2m_p^2(p_1\cdot p_3)(p_4\cdot q_2)(q_1\cdot q)+m_p^2(p_1\cdot p_3)(p_2\cdot q_1)(p_4\cdot q_2)+ \\
& +m_p^2(p_1\cdot p_3)(p_2\cdot q_2)(p_4\cdot q_1)\Big]-\left(c_V^{p^2}-c_A^{p^2}\right)\Big[2m_n^2m_p^2(p_2\cdot q)(q_1\cdot q_2)+ \\
& +m_n^2m_p^2(q_1\cdot q_2)(q\cdot q)+m_n^2m_p^4(q_1\cdot q_2)+2m_p^2(p_1\cdot p_3)(p_2\cdot q)(q_1\cdot q_2)+ \\
& +m_p^2(p_1\cdot p_3)(q_1\cdot q_2)(q\cdot q)+m_p^4(p_1\cdot p_3)(q_1\cdot q_2)\Big]- \\
& -2c_V^pc_A^p\Big[2(p_1\cdot p_3)(p_2\cdot q)(p_4\cdot q_1)(q_2\cdot q)-2(p_1\cdot p_3)(p_2\cdot q)(p_4\cdot q_2)(q_1\cdot q)+ \\
& +(p_1\cdot p_3)(p_2\cdot q_1)(p_4\cdot q_2)(q\cdot q)-(p_1\cdot p_3)(p_2\cdot q_2)(p_4\cdot q_1)(q\cdot q)+ \\
& +2m_n^2m_p^2(p_4\cdot q_1)(q_2\cdot q)-2m_n^2m_p^2(p_4\cdot q_2)(q_1\cdot q)- \\
& -m_n^2m_p^2(p_2\cdot q_1)(p_4\cdot q_2)+m_n^2m_p^2(p_2\cdot q_2)(p_4\cdot q_1)+ \\
& +2m_n^2(p_2\cdot q)(p_4\cdot q_1)(q_2\cdot q)-2m_n^2(p_2\cdot q)(p_4\cdot q_2)(q_1\cdot q)+ \\
& +m_n^2(p_2\cdot q_1)(p_4\cdot q_2)(q\cdot q)-m_n^2(p_2\cdot q_2)(p_4\cdot q_1)(q\cdot q)+ \\
& +2m_p^2(p_1\cdot p_3)(p_4\cdot q_1)(q_2\cdot q)-2m_p^2(p_1\cdot p_3)(p_4\cdot q_2)(q_1\cdot q)- \\
& -m_p^2(p_1\cdot p_3)(p_2\cdot q_1)(p_4\cdot q_2)+m_p^2(p_1\cdot p_3)(p_2\cdot q_2)(p_4\cdot q_1)\Big]\Bigg\}
\end{aligned}
\tag{4.65}
$$

The procedure we have outlined in the last two sections, can be carried out for all the diagrams of the $nn\nu\bar{\nu}$ and $np\nu\bar{\nu}$ processes. Note that the group I diagrams are topologically different from the group II diagrams so that the matrix element contributions from the two groups of diagrams must be added incoherently. It then follows that

$$
|\mathcal{M}|^2 = \left|\sum_{i=1}^{8}\mathcal{M}_i\right|^2 = |4\mathcal{M}_1+4\mathcal{M}_5|^2 = 16\left(|\mathcal{M}_1|^2+|\mathcal{M}_5|^2+2\mathcal{M}_1\mathcal{M}_5^\dagger\right) \tag{4.66}
$$

4.4 Neutrino Emissivities

We now go for estimates of the energy loss rate from $nn\nu\bar{\nu}$ and $np\nu\bar{\nu}$ processes. Concerning the neutrino emission from neutrino pair bremsstrahlung, the rate of energy loss is obtained by integrating the total phase space available to the participating particles, multiplied by the corresponding Feynman amplitude and total neutrino energy:

$$\varepsilon_{\nu\bar{\nu}} = \frac{(2\pi)^4}{\hbar}\left[\prod_{i=1}^{4}\int \frac{c\,d^3\mathbf{p}_i}{(2\pi\hbar)^3 2E_i}\right]\int \frac{c\,d^3\mathbf{q}_\nu}{(2\pi\hbar)^3 2E_\nu}\int \frac{c\,d^3\mathbf{q}_{\bar{\nu}}}{(2\pi\hbar)^3 2E_{\bar{\nu}}}\times$$
$$\times\,\delta^{(4)}(p_1+p_2-p_3-p_4-q_\nu-q_{\bar{\nu}})|\mathcal{M}|^2(E_\nu+E_{\bar{\nu}})\mathcal{F}(E_i) \tag{4.67}$$

where $\mathbf{p}_i$ denote the momenta of the incoming and outgoing nucleons, and $(E_\nu + E_{\bar{\nu}})$ is the total neutrino energy. The Dirac delta function $\delta^{(4)}(p_1 + p_2 - p_3 - p_4 - q_\nu - q_{\bar{\nu}})$ accounts for energy and momentum conservation, and the function $\mathcal{F}(E_i) = f(E_1)f(E_2)\,(1-f(E_3))\,(1-f(E_4))$ is the appropriate product of Fermi-Dirac distribution functions, defined in Eq. (3.38).

The emissivity due to the $nn\nu\bar{\nu}$ process takes the following form

$$\varepsilon_{\nu\bar{\nu}} = \frac{2^8}{(4\pi)^{14}}\int\frac{d^3\mathbf{p}_1}{E_1}\int\frac{d^3\mathbf{p}_2}{E_2}\int\frac{d^3\mathbf{p}_3}{E_3}\int\frac{d^3\mathbf{p}_4}{E_4}\int\frac{d^3\mathbf{q}_\nu}{E_\nu}\int\frac{d^3\mathbf{q}_{\bar{\nu}}}{E_{\bar{\nu}}}\times$$
$$\times\,\delta^{(4)}(p_1+p_2-p_3-p_4-q_\nu-q_{\bar{\nu}})|\mathcal{M}|^2(E_\nu+E_{\bar{\nu}})f(E_1)\times$$
$$\times\, f(E_2)(1-f(E_3))(1-f(E_4)) \tag{4.68}$$

Final nucleon states must be vacant if the process is to proceed, and this accounts for the blocking factors $(1-f(E_3))$ and $(1-f(E_4))$. The momentum-conserving delta function $\delta^{(3)}(\mathbf{p}_1+\mathbf{p}_2-\mathbf{p}_3-\mathbf{p}_4-\mathbf{q}_\nu-\mathbf{q}_{\bar{\nu}})$ is absorbed into the integration of $\mathbf{p}_4$:

$$\varepsilon_{\nu\bar{\nu}} = \frac{2^8}{(4\pi)^{14}}\int\frac{d^3\mathbf{p}_1}{E_1}\int\frac{d^3\mathbf{p}_2}{E_2}\int\frac{d^3\mathbf{p}_3}{E_3E_4}\int\frac{d^3\mathbf{q}_\nu}{E_\nu}\int\frac{d^3\mathbf{q}_{\bar{\nu}}}{E_{\bar{\nu}}}\times$$
$$\times\,\delta(E_1+E_2-E_3-E_4-E_\nu-E_{\bar{\nu}})|\mathcal{M}|^2(E_\nu+E_{\bar{\nu}})\times$$
$$\times\, f(E_1)f(E_2)(1-f(E_3))(1-f(E_4)) \tag{4.69}$$

By transforming the integrands to spherical coordinates, the integrals over $\mathbf{p}_3$ and $\mathbf{q}_\nu$ yield

$$d^3\mathbf{p}_3 = |\mathbf{p}_3|^2 d|\mathbf{p}_3|\sin\theta_3 d\theta_3\,d\phi_3 = \frac{1}{c^2}\,|\mathbf{p}_3|\,E_3 dE_3\sin\theta_3 d\theta_3\,d\phi_3 \tag{4.70}$$

$$d^3\mathbf{q}_\nu = |\mathbf{q}_\nu|^2 d|\mathbf{q}_\nu|\sin\theta_\nu d\theta_\nu\,d\phi_\nu = \frac{2\pi}{c^2}\,|\mathbf{q}_\nu|\,E_\nu dE_\nu\sin\theta_\nu d\theta_\nu \tag{4.71}$$

Next we fix the direction of $\mathbf{p}_1$ to lie in the z-axis, which is leading to

$$d^3\mathbf{p}_1 = |\mathbf{p}_1|^2 d|\mathbf{p}_1|\sin\theta_1 d\theta_1\,d\phi_1 = \frac{4\pi}{c^2}\,|\mathbf{p}_1|\,E_1 dE_1 \tag{4.72}$$

It follows that

$$\varepsilon_{\nu\bar{\nu}} = \frac{2^7}{(4\pi)^{12}} \int |\mathbf{p}_1| dE_1 \int \frac{d^3\mathbf{p}_2}{E_2} \int \frac{|\mathbf{p}_3|}{E_4}\, dE_3 \int \sin\theta_3 d\theta_3 \int d\phi_3 \int |\mathbf{q}_\nu| dE_\nu \times$$
$$\times \int \sin\theta_\nu d\theta_\nu \int \frac{d^3\mathbf{q}_{\bar{\nu}}}{E_{\bar{\nu}}}\, \delta(E_1 + E_2 - E_3 - E_4 - E_\nu - E_{\bar{\nu}}) |\mathcal{M}|^2 \times$$
$$\times (E_\nu + E_{\bar{\nu}}) f(E_1) f(E_2) (1 - f(E_3))(1 - f(E_4)) \tag{4.73}$$

It becomes much simpler if we work in the center-of-mass frame and restrict the neutrino-antineutrino pairs to come out back-to-back. In particular, we make the following four-vector assignments:

$$p_1 = (E_1, 0, 0, |\mathbf{p}_1|) \tag{4.74}$$
$$p_2 = (E_1, 0, 0, -|\mathbf{p}_1|) \tag{4.75}$$
$$p_3 = (E_3, |\mathbf{p}_3| \sin\theta_3 \cos\phi_3, |\mathbf{p}_3| \sin\theta_3 \sin\phi_3, |\mathbf{p}_3| \cos\theta_3) \tag{4.76}$$
$$p_4 = (E_3, -|\mathbf{p}_3| \sin\theta_3 \cos\phi_3, -|\mathbf{p}_3| \sin\theta_3 \sin\phi_3, -|\mathbf{p}_3| \cos\theta_3) \tag{4.77}$$
$$q_\nu = (E_\nu, |\mathbf{q}_\nu| \sin\theta_\nu, 0, |\mathbf{q}_\nu| \sin\theta_\nu) \tag{4.78}$$
$$q_{\bar{\nu}} = (E_\nu, -|\mathbf{q}_\nu| \sin\theta_\nu, 0, -|\mathbf{q}_\nu| \sin\theta_\nu) \tag{4.79}$$

Consequently

$$\varepsilon_{\nu\bar{\nu}} = \frac{2^6}{(4\pi)^{10}} \int |\mathbf{p}_1| dE_1 \int |\mathbf{p}_2| dE_2 \int \frac{|\mathbf{p}_3|}{E_4}\, dE_3 \int \sin\theta_3 d\theta_3 \int d\phi_3 \int |\mathbf{q}_\nu| dE_\nu \times$$
$$\times \int \sin\theta_\nu d\theta_\nu \int |\mathbf{q}_{\bar{\nu}}| dE_{\bar{\nu}} \int \sin\theta_{\bar{\nu}} d\theta_{\bar{\nu}}\, \delta(E_1 + E_2 - E_3 - E_4 - E_\nu - E_{\bar{\nu}}) \times$$
$$\times |\mathcal{M}|^2 (E_\nu + E_{\bar{\nu}}) f(E_1) f(E_2) (1 - f(E_3))(1 - f(E_4)) \tag{4.80}$$

Finally, the integration over $E_{\bar{\nu}}$ combined with the energy-conserving delta function $\delta(E_1 + E_2 - E_3 - E_4 - E_\nu - E_{\bar{\nu}})$, results in

$$\varepsilon_{\nu\bar{\nu}} = \frac{2^6}{(4\pi)^{10}} \int |\mathbf{p}_1| dE_1 \int |\mathbf{p}_2| dE_2 \int \frac{|\mathbf{p}_3|}{E_4}\, dE_3 \int \sin\theta_3 d\theta_3 \int d\phi_3 \int |\mathbf{q}_\nu| |\mathbf{q}_{\bar{\nu}}| dE_\nu \times$$
$$\times \int \sin\theta_\nu d\theta_\nu \int \sin\theta_{\bar{\nu}} d\theta_{\bar{\nu}} |\mathcal{M}|^2 (E_\nu + E_{\bar{\nu}}) f(E_1) f(E_2) (1 - f(E_3))(1 - f(E_4)) \tag{4.81}$$

Since energy and momentum are conserved in this process, we have

$$E_\nu = (E_1 + E_2 - E_3 - E_4)/2, \qquad \mathbf{p}_4 = -\mathbf{p}_3 \tag{4.82}$$

The remaining eight-dimensional integration is calculated numerically. As we have done in the case of direct Urca process, we are just integrating around the Fermi surfaces of the particles. By convention, the energies and momenta we are integrating over, are all in MeV. Hence the emissivity (4.81) is expressed in terms of MeV^5 and can be converted to $\mathrm{MeV/m}^3\mathrm{s}$ by dividing it by $\hbar^4 c^3$.

The above analysis can again be adapted to the case of $np\nu\bar{\nu}$ process. However, it will not longer be sensible to consider the process in the center-of-mass frame, i.e. the incoming nucleons are not identical particles. In this regard, the kinematics for the $np\nu\bar{\nu}$ process is rather modified. The incoming nucleons may be viewed as forming a system of total rest mass M_C, total energy E_C, and total momentum $\mathbf{p}_C$. Thus, we have

$$E_C = E_1 + E_2, \qquad \mathbf{p}_C = \mathbf{p}_1 + \mathbf{p}_2, \qquad M_C^2 = E_C^2 - |\mathbf{p}_C|^2 \tag{4.83}$$

By demanding conservation of energy and momentum for this process, one obtains for the above equalities

$$E_C = E_3 + E_4 + 2E_\nu \tag{4.84}$$

$$\mathbf{p}_C = \mathbf{p}_3 + \mathbf{p}_4 \tag{4.85}$$

We remind that the direction of $\mathbf{p}_2$ is the opposite of $\mathbf{p}_1$, and thus the square of $\mathbf{p}_C$ becomes

$$\begin{aligned} |\mathbf{p}_C|^2 = |\mathbf{p}_1 + \mathbf{p}_2|^2 &= |\mathbf{p}_1|^2 + |\mathbf{p}_2|^2 + 2|\mathbf{p}_1||\mathbf{p}_2|\cos\theta_2 \\ &= |\mathbf{p}_1|^2 + |\mathbf{p}_2|^2 - 2|\mathbf{p}_1||\mathbf{p}_2| \end{aligned} \tag{4.86}$$

From Eqs. (4.84) and (4.85) we find that

$$E_C - E_3 - 2E_\nu = E_4 = \sqrt{|\mathbf{p}_4|^2 + m_4^2} = \sqrt{|\mathbf{p}_C - \mathbf{p}_3|^2 + m_4^2} \tag{4.87}$$

Squaring the above equation results in

$$\begin{aligned} (E_C - E_3)^2 + 4E_\nu^2 - 4(E_C - E_3)E_\nu &= |\mathbf{p}_C - \mathbf{p}_3|^2 + m_4^2 \\ &= |\mathbf{p}_C|^2 + |\mathbf{p}_3|^2 - 2|\mathbf{p}_C||\mathbf{p}_3|\cos\theta_3 + m_4^2 \end{aligned} \tag{4.88}$$

We note that

$$E_C^2 = |\mathbf{p}_1|^2 + |\mathbf{p}_2|^2 + 2E_1E_2 + m_1^2 + m_2^2 \tag{4.89}$$

Substituting Eqs. (4.86) and (4.89) into Eq. (4.88), leads to an second-order equation in E_ν:

$$E_\nu^2 - (E_C - E_3)E_\nu + C = 0 \tag{4.90}$$

With

$$C = \left(m_1^2 + m_2^2 + m_3^2 - m_4^2 + 2E_1E_2 - 2E_CE_3 + 2|\mathbf{p}_C||\mathbf{p}_3|\cos\theta_3\right)/4 \tag{4.91}$$

the solution of Eq. (4.90) turns out to be

$$E_\nu = \frac{E_C - E_3}{2} - \sqrt{\frac{(E_C - E_3)^2}{4} - C} \tag{4.92}$$

Chapter 5

Numerical Results

In this chapter we present the numerical estimates obtained for neutrino emissivities due to the direct Urca process and neutrino pair bremsstrahlung. We are going to depict the produced rates of energy loss as a function of the number density of particles. In this context, we pick out two temperatures: 10^8 K and 10^9 K, which are of relevance for the emission of neutrinos. As discussed in the introduction, the emission of photons overtakes neutrinos when the internal temperature falls to $\sim 10^8$ K. As a first approach, we ignore the angle dependence of the emissivities, as a usual approximation in this field. We repeat this procedure for various equations of state and composition of matter. Finally, we briefly outline the main ideas behind the development of numerical algorithms.

5.1 Neutrino Emissivities

In the case of the direct Urca process, we compare our results with the approximate rates obtained by the expression of Prakash *et al.* (1991):

$$\varepsilon_{\rm Urca} = \frac{457\pi}{10080}\, G_F^2 \cos^2\theta_C (1+3g_A^2) \frac{m_n m_p \mu_e}{\hbar^{10} c^5} (k_B T)^6 \Theta_t \tag{5.1}$$

Here Θ_t is the threshold factor $\Theta(p_F^e + p_F^p - p_F^n)$, which is +1 if the argument exceeds 0, and is 0 otherwise. However, it ought to be stressed that the above result was derived by assuming $|\mathbf{p}|d|\mathbf{p}| \simeq mdE$ and that the participating particles are free. Interactions give rise to a number of changes. First, the neutron and proton single-particle energies are renormalized, which results in the masses m_n and m_p in Eq. (5.1) being replaced by effective masses m_n^* and m_p^*. A second effect is that in a nuclear medium the effective value of the *axial* vector coupling $|g_A|$ is quenched. At the saturation density $|g_A| \simeq 1$ and it is expected to remain at approximately this value at higher densities. Third, the effective weak-interaction matrix elements can be modified by the medium. These effects are expected to reduce the direct Urca rate (5.1), but probably by less than a factor of 10.

We now start with displaying the produced emissivities by the direct Urca process. We will hereafter refer to the energy loss rates computed by Eq. (5.1) as approximate rates. However, the numerical emissivities obtained for the direct Urca process, are all computed by implementing Eq. (3.44) from Chapter 3. In association with the energy loss rates, we have applied the EoS I – III, defined in Section 2.5, Chapter 2. Here we give the description of these three EoS:

- EoS I: pure nuclear matter with two-body interactions,
- EoS II: pure nuclear matter with three-body interactions,
- EoS III: the presence of hyperons in nuclear matter with two-body interactions.

In Figs. 5.1 and 5.2, we plot the rates of energy loss for pure nuclear matter with two-body interactions. From Figs. 5.1 and 5.2 we note that the numerical rates for the direct Urca process differ by a factor $2.2 - 2.8$ than the approximate rates. The main problem we had to face in our simulations was the right choice of the integration limits. As stated earlier, we consider only that region of phase space in which particle energies are within a few k_BT of the Fermi energies. But there is no unique method to trace the region of relevance in calculating the emissivities. Due to the assumption $|\mathbf{p}|d|\mathbf{p}| \simeq mdE$ in Eq. (5.1), we can expect a slight deviation in the approximate rates. We wish also to point out the relative slope seen in Figs. 5.1 and 5.2. Compared with the approximate rate, the numerical rate is slowly rising with increasing density.

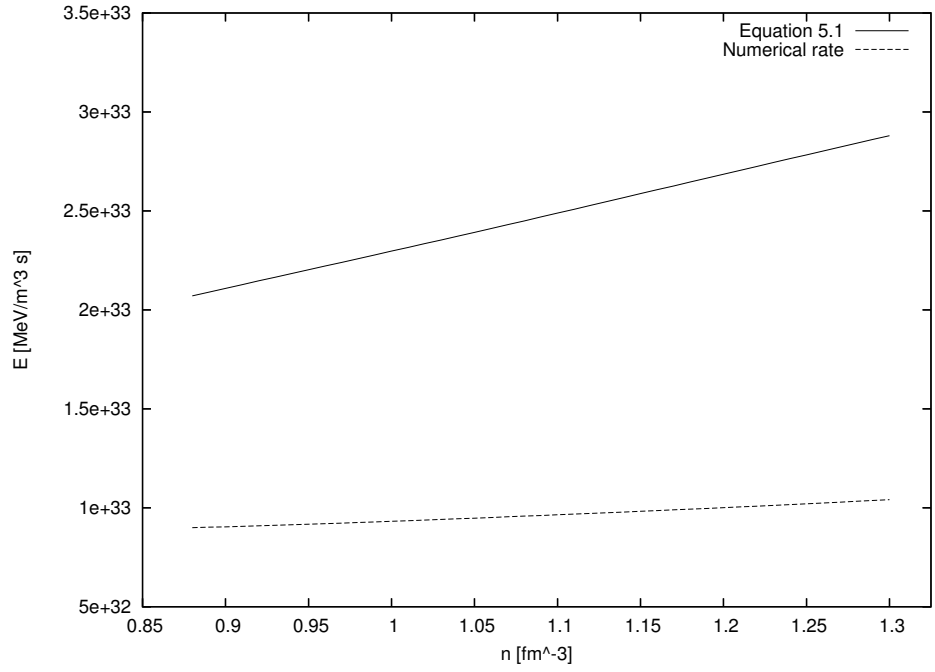

Figure 5.1: Emissivities for the direct Urca process at $T = 10^8$ K for EoS I. Angle dependence is excluded.

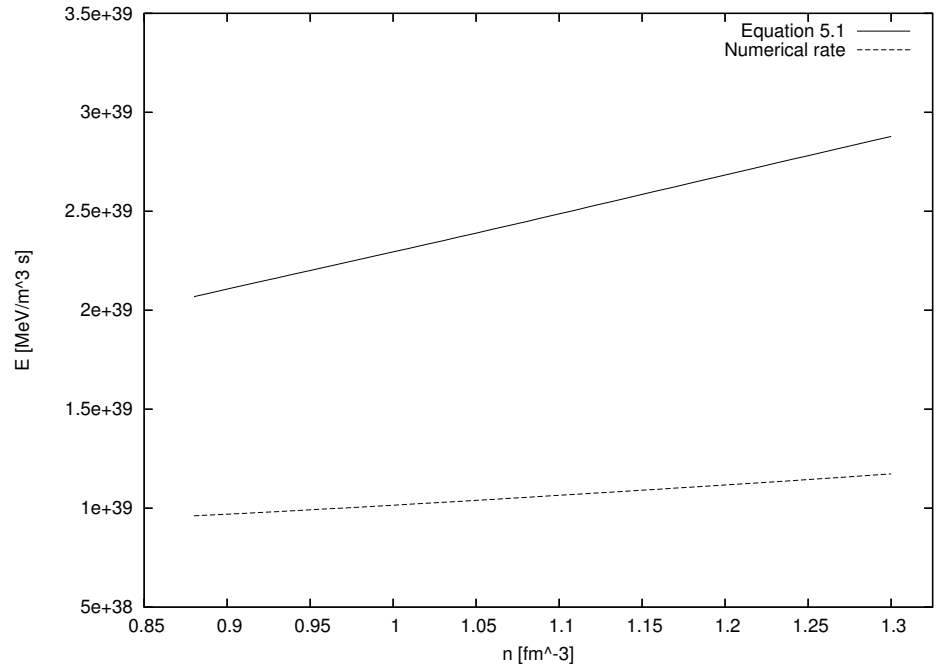

Figure 5.2: Emissivities for the direct Urca process at $T = 10^9\,\mathrm{K}$ for EoS I. Angle dependence is excluded.

In Figs. 5.3 and 5.4, we view the corresponding emissivities with the angle dependence. For comparison we have also included the results produced by the exclusion of angles. We have also taken into account the approximate rates by Eq. (5.1) in order to check the validity of the approximation. It is noteworthy to see that the rate of energy loss is rapidly increasing in proportion to the previous rates. When including the angle dependence the phase space of the interacting particles is expected to increase, resulting in larger energy loss rates. Although the densities range from $0.02\,\mathrm{fm}^{-3}$ to $1.3\,\mathrm{fm}^{-3}$, the direct Urca process starts only at a density $n = 5.5\,n_0 = 0.88\,\mathrm{fm}^{-3}$. This is due to the requirement of the minimum proton fraction, being $x_p = n_p/n \geqslant 14.08\%$. This means in turn that the triangle inequality, $p_F(e)+p_F(p) \geqslant p_F(n)$, is to be fulfilled so as to ensure simultaneous conservation of energy and momentum for the process. The rates with angle dependence get closer to the approximate rates, indicating that Eq. (5.1) is a reliable estimate for the emissivities. To my knowledge, this is the first time this has been checked.

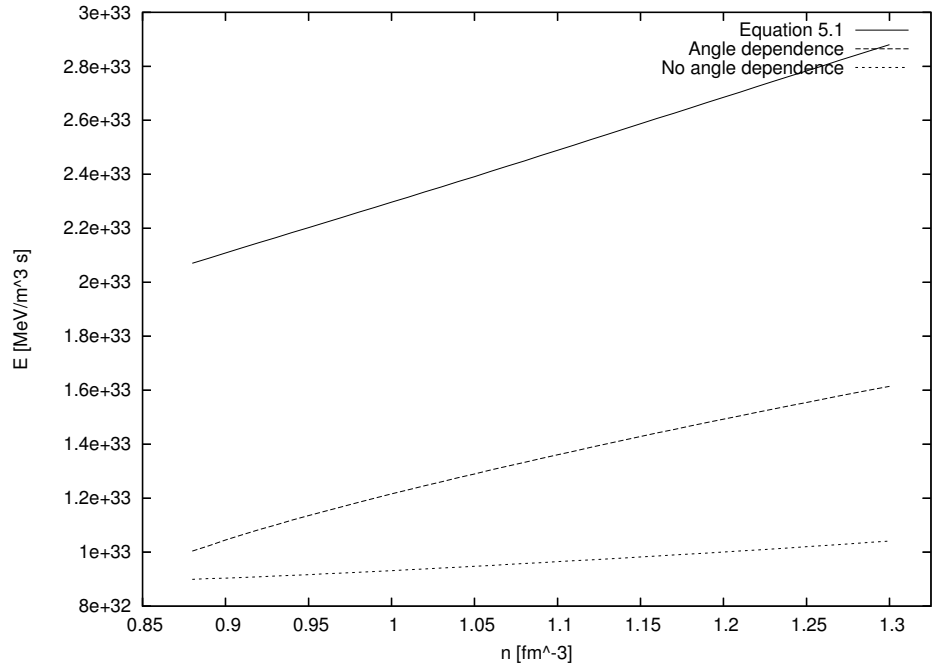

Figure 5.3: Emissivities for the direct Urca process at $T = 10^8\,\mathrm{K}$ for EoS I. Angle dependence is included.

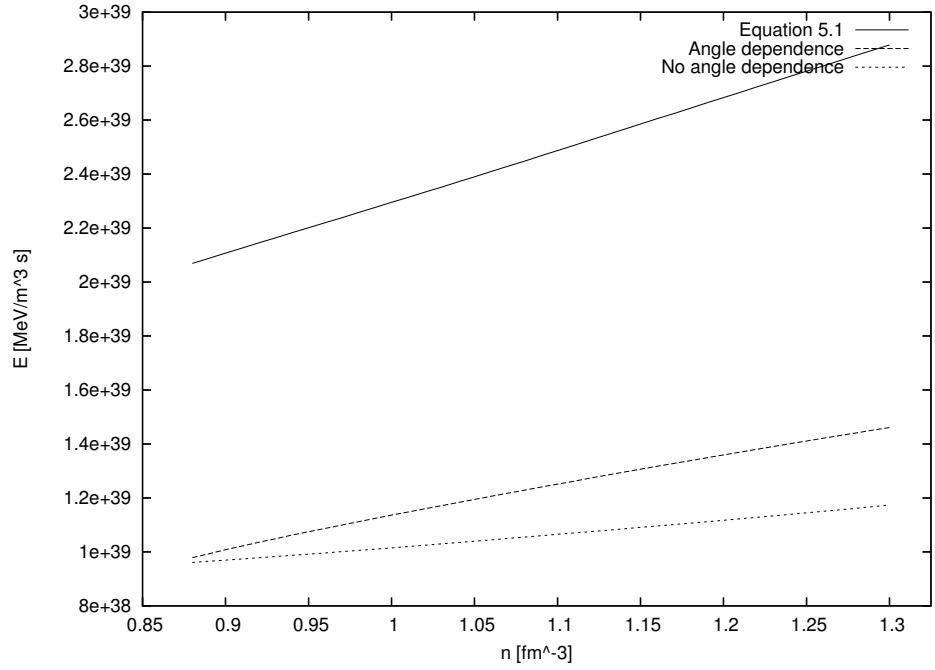

Figure 5.4: Emissivities for the direct Urca process at $T = 10^9\,\mathrm{K}$ for EoS I. Angle dependence is included.

For pure nuclear matter with three-body interactions we have plotted the direct Urca emissivities in Figs. 5.5 and 5.6. In this case, the numerical rates are in better agreement with the analytical results as the relative difference is given by a factor $1.4 - 1.6$. As expected, the three-body interactions tend to boost the energy loss by neutrino emission, yielding a rapid emission rate with increasing density. In addition, the EoS with three-body interactions reduces the threshold proton fraction to $x_p \geqslant 14.05\%$, causing the direct Urca process to start at $n = 5.25\, n_0 = 0.84\,\mathrm{fm}^{-3}$.

In Figs. 5.7 and 5.8, we show the corresponding emissivities with the inclusion of angles. Here we have also added the results obtained by ignoring the angle dependence. It seems that the angle dependence suppresses the energy loss by a factor of $1.9 - 2.7$ when compared with the omission of the angle dependence.

At the densities in the interior of neutron stars, the neutron chemical potential μ_n is likely to exceed the corresponding masses, modified by interactions of Σ, Λ and possibly Ξ-hyperons. Hence, in addition to nucleons, neutron star matter is expected to have significant populations of hyperons and possibly even Δ-isobars. If so, pure neutron matter would constitute an excited state relative to hyperon matter. As a next step, we attempted to calculate the direct Urca rate for the nuclear matter with the presence of Σ^- and Λ-hyperons in equilibrium. But it turned out to be that the conservation of Fermi momentum for this process was not possible whatever the density was.

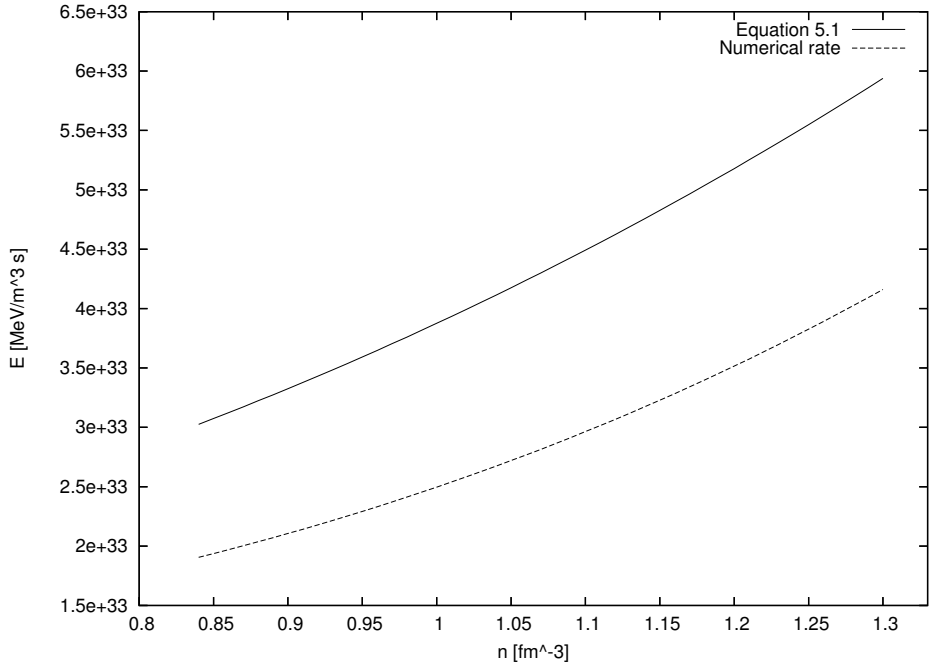

Figure 5.5: Emissivities for the direct Urca process at $T = 10^8\,\mathrm{K}$ for EoS II. Angle dependence is excluded.

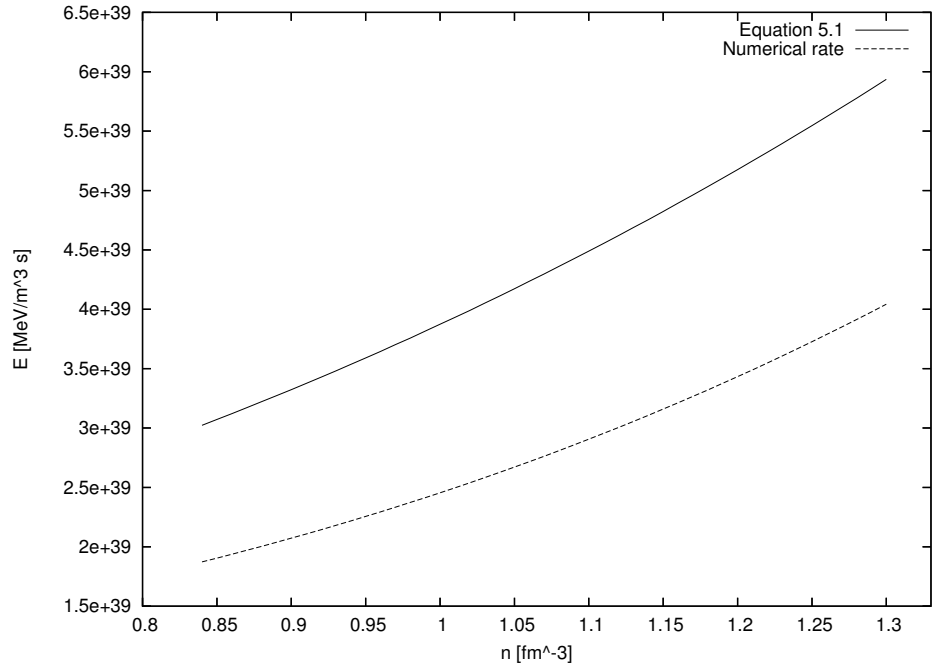

Figure 5.6: Emissivities for the direct Urca process at $T = 10^9\,\mathrm{K}$ for EoS II. Angle dependence is excluded.

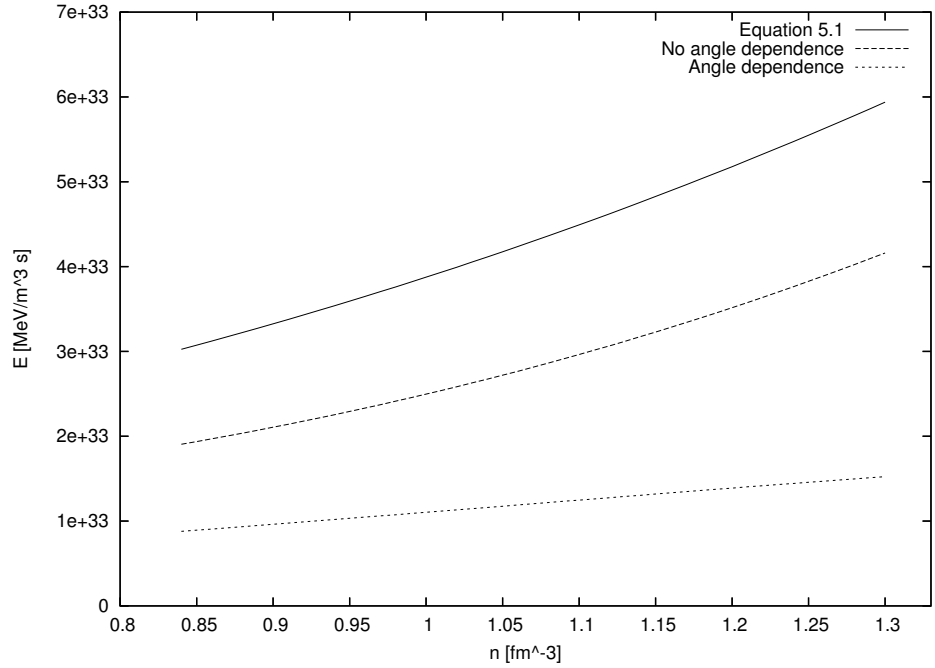

Figure 5.7: Emissivities for the direct Urca process at $T = 10^8\,\mathrm{K}$ for EoS II. Angle dependence is included.

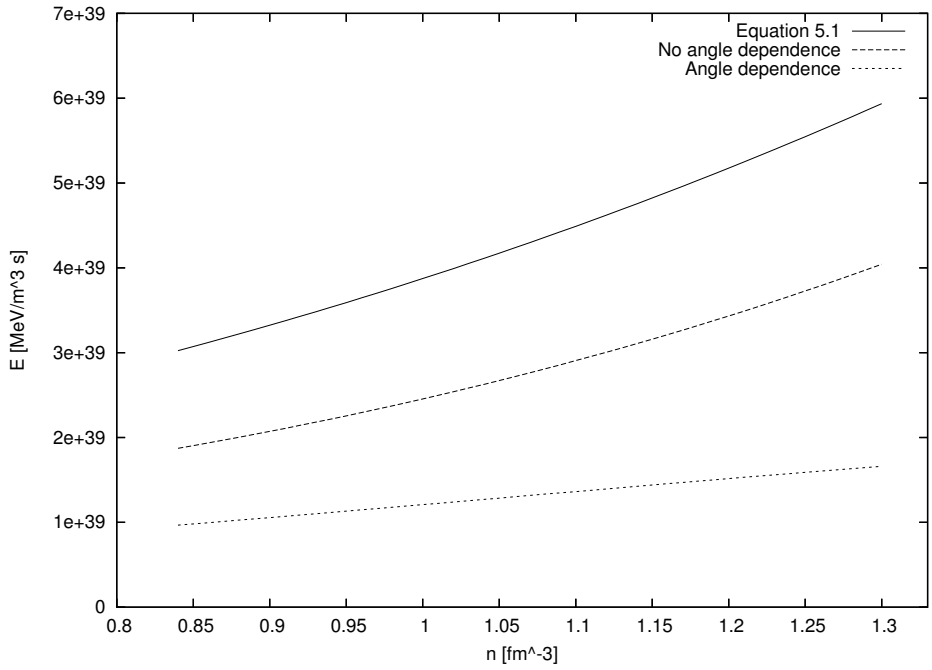

Figure 5.8: Emissivities for the direct Urca process at $T = 10^9\,\mathrm{K}$ for EoS II. Angle dependence is included.

In order to shed light on the effects from two-body and three-body interactions in nuclear matter, we confront the corresponding direct Urca emissivities in Figs. 5.9 and 5.10. Similarly, the energy loss rates with angle dependence are plotted in Figs. 5.11 and 5.12. It is clearly seen from Figs. 5.9 and 5.10 that the three-body interactions yield significant contributions to the energy loss when compared with two-body interactions. We also note that the EoS II allows the direct Urca process to start at $n = 5.25\,n_0 = 0.84\,\mathrm{fm}^{-3}$, while the EoS I ignite the process at $n = 5.5\,n_0 = 0.88\,\mathrm{fm}^{-3}$.

From Fig. 5.11 we see that the energy loss rate from the three-body interactions lie below that of two-body interactions. As Fig. 5.12 shows, the emissivity associated with the EoS II seems to be larger than the rate with two-body interactions.

From the results for the direct Urca process we deduce that the three-body interactions (EoS II) enhance the proton fraction considerably and thereby the increase of energy loss. As the proton fraction gets higher, the chemical potentials of the interacting particles become also larger. We here point out that the angle dependence plays a crucial role in the energy loss by neutrinos. The inclusion of angles extend the phase space of the particles which cause more neutrino emissions to take place.

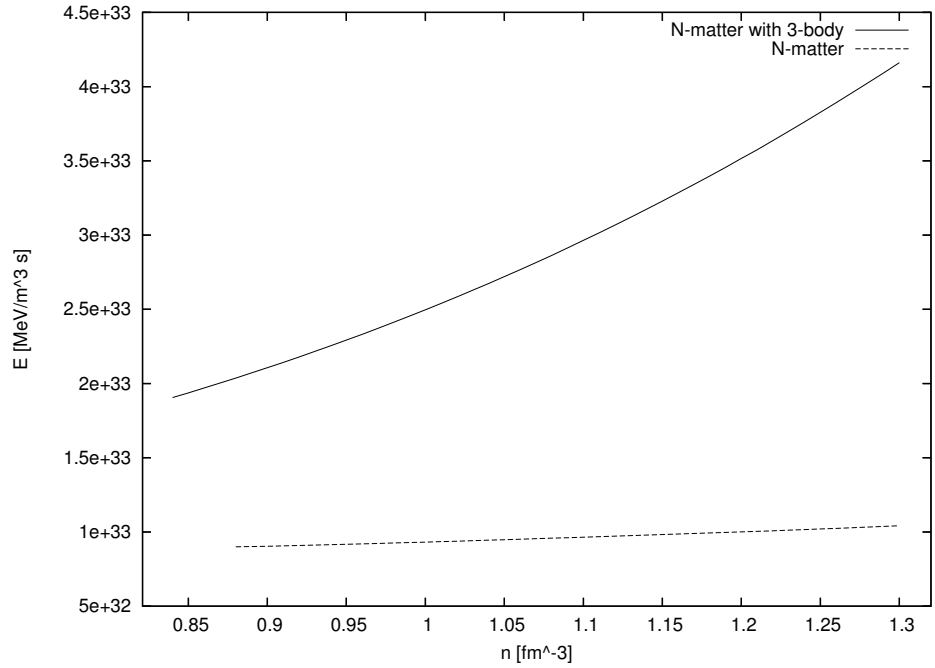

Figure 5.9: Emissivities for the direct Urca process at $T = 10^8\,\mathrm{K}$ for EoS I and II. Angle dependence is excluded.

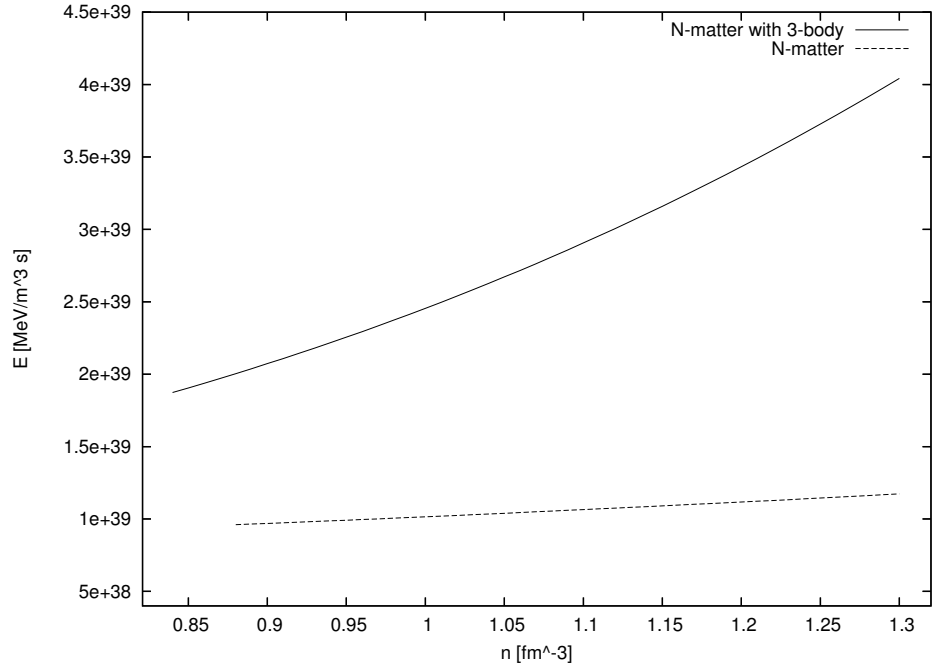

Figure 5.10: Emissivities for the direct Urca process at $T = 10^9\,\mathrm{K}$ for EoS I and II. Angle dependence is excluded.

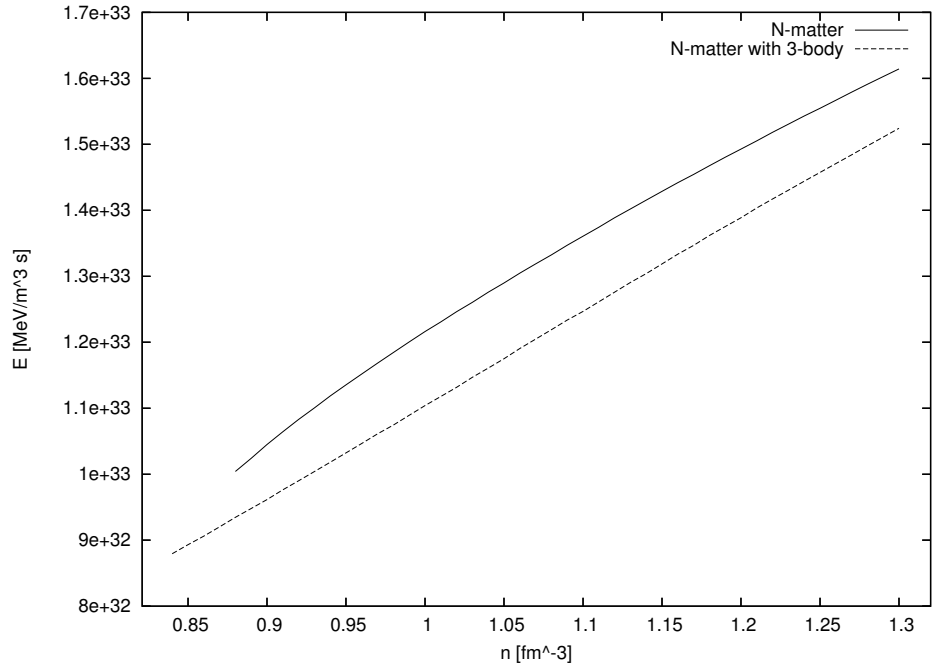

Figure 5.11: Emissivities for the direct Urca process at $T = 10^8\,\mathrm{K}$ for EoS I and II. Angle dependence is included.

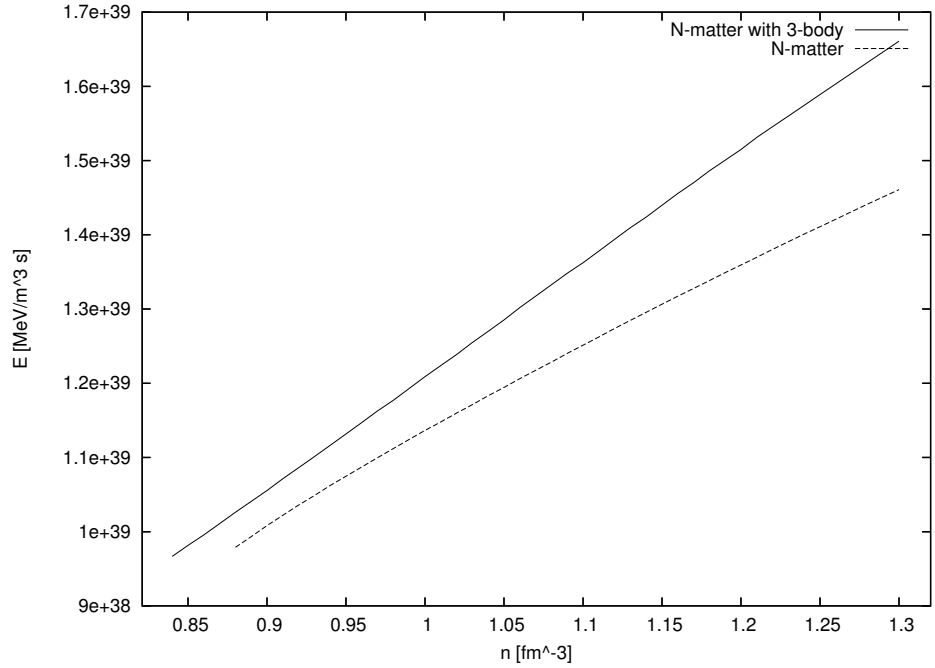

Figure 5.12: Emissivities for the direct Urca process at $T = 10^9\,\mathrm{K}$ for EoS I and II. Angle dependence is included.

We now go on to display the produced emissivities by the neutrino pair bremsstrahlung. By the way, we intended only to present the results for the $nn\nu\bar{\nu}$ process as it turns out to be the most relevant in concerning the bremsstrahlung process. In computing the emissivities, we took advantage of Eq. (4.81) from Chapter 4 and implemented the integrations numerically.

In Figs. 5.13 and 5.14, we plot the $nn\nu\bar{\nu}$ rates for pure nuclear matter with two-body interactions. For the sake of comparison we have also brought out the results with the angle dependence. It is interesting to notice that the $nn\nu\bar{\nu}$ process will take place no matter what the number density is. This is due to the presence of the additional neutron which increases the phase space of the interacting particles. This in turn implies that the conservation of energy and momentum is possible for the entire density range $n = 0.02 - 1.3\,\mathrm{fm}^{-3}$. As in the previous results, the angle dependence seems to enrich the phase space so that the rate of energy loss proceeds rapidly. The exclusion of angles seems to quench the emissivities with a factor of 20. However, we expect that the deviation will reduce by a factor of 3 as the number of integration points increases.

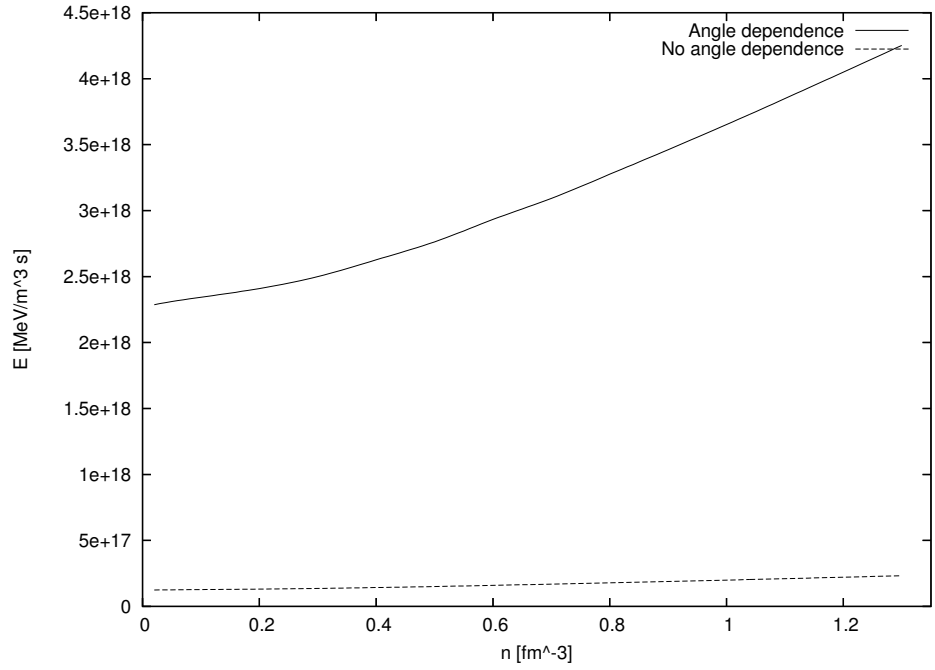

Figure 5.13: Emissivities for the $nn\nu\bar{\nu}$ process at $T = 10^8\,\mathrm{K}$ for EoS I.

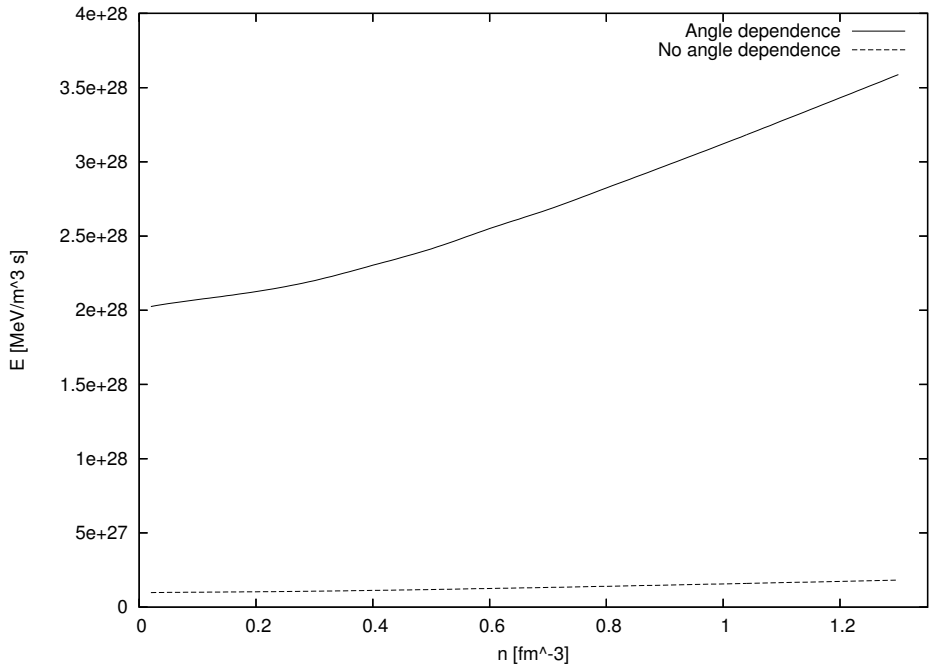

Figure 5.14: Emissivities for the $nn\nu\bar{\nu}$ process at $T = 10^9\,\mathrm{K}$ for EoS I.

Figs. 5.15 and 5.16 display the $nn\nu\bar{\nu}$ emissivities for the pure nuclear matter with three-body interactions. Here we have also included the rates with the exclusion of angles. As the results show, the angle dependence give rise to a more enhanced rate in proportion to those of no angles. This is again a result of the enlarged phase space accompanied by the angle dependence. We here observe an evident difference in the energy loss rates, being a factor of 18. As stated earlier, the results may be regulated by adding even more integration points. But the feeble aspect here is that the entire simulation would require an inconceivable computation time.

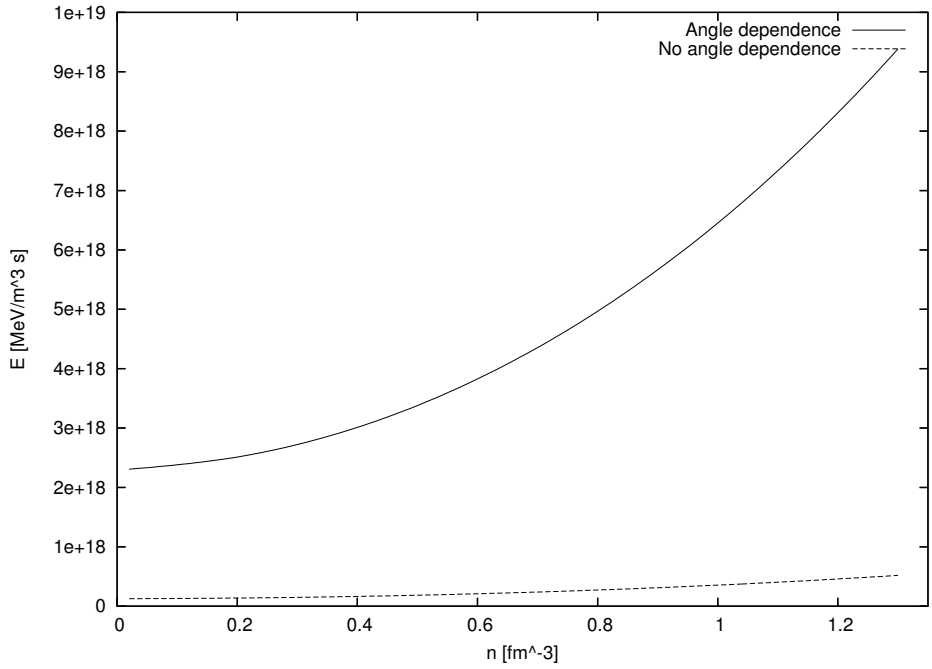

Figure 5.15: Emissivities for the $nn\nu\bar{\nu}$ process at $T = 10^8\,\mathrm{K}$ for EoS II.

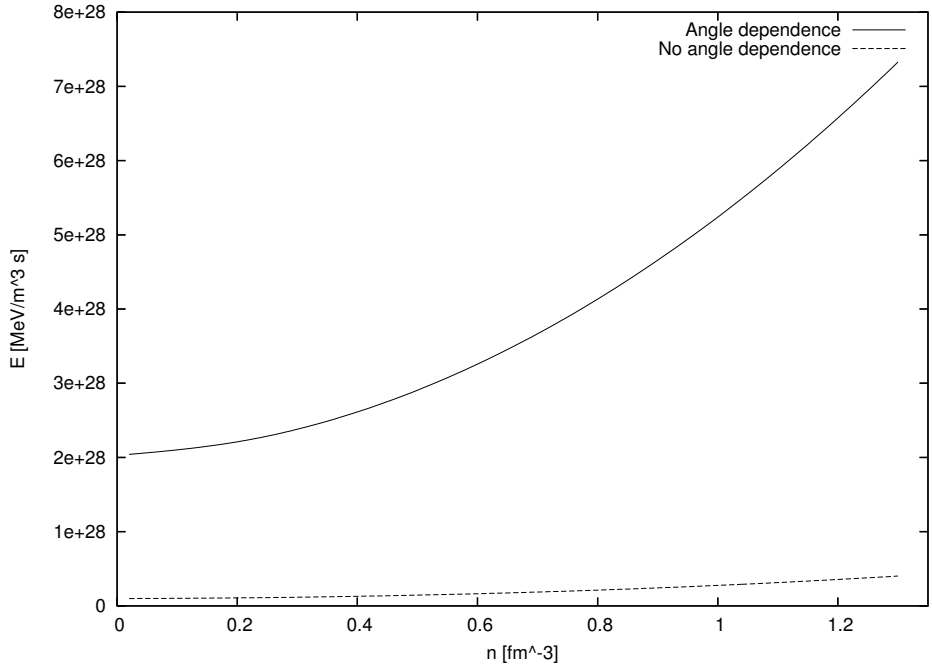

Figure 5.16: Emissivities for the $nn\nu\bar{\nu}$ process at $T = 10^9\,\mathrm{K}$ for EoS II.

In contrast to the direct Urca process considered earlier, the $nn\nu\bar{\nu}$ process takes place for the nuclear matter with Σ^- and Λ in equilibrium. Figs. 5.17 and 5.18 show the $nn\nu\bar{\nu}$ emissivities associated with the EoS III. The obtained rates by the exclusion of angles are also shown in Figs. 5.17 and 5.18. As the results show, the emissivities with the inclusion of angles progress slowly as the number density increases. However, the angle dependence gives relatively larger energy-loss rates than for the exclusion of angles. It seems that the relative difference here is by a factor of $18 - 20$.

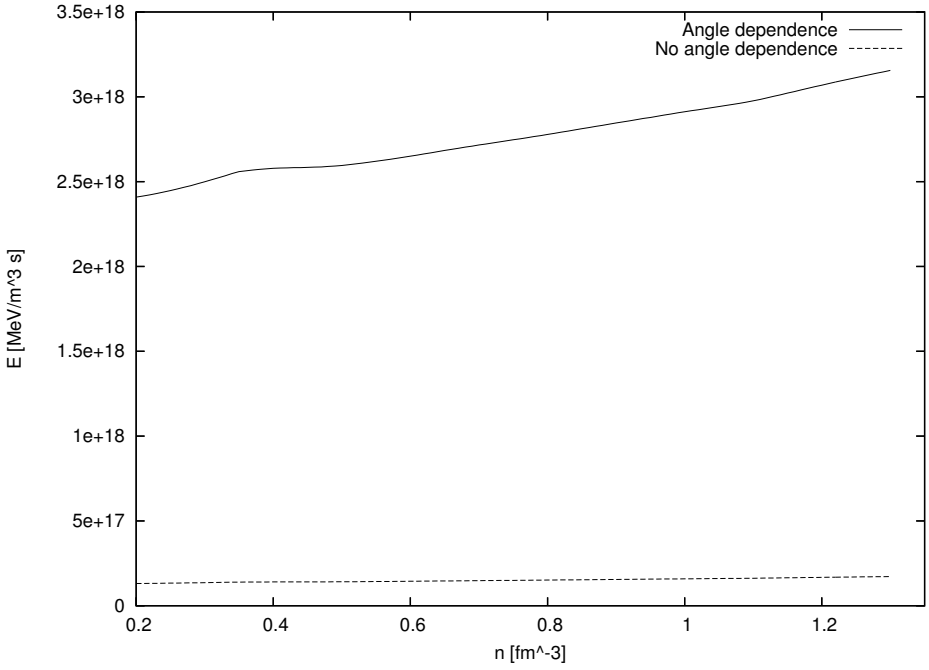

Figure 5.17: Emissivities for the $nn\nu\bar{\nu}$ process at $T = 10^8\,\mathrm{K}$ for EoS III.

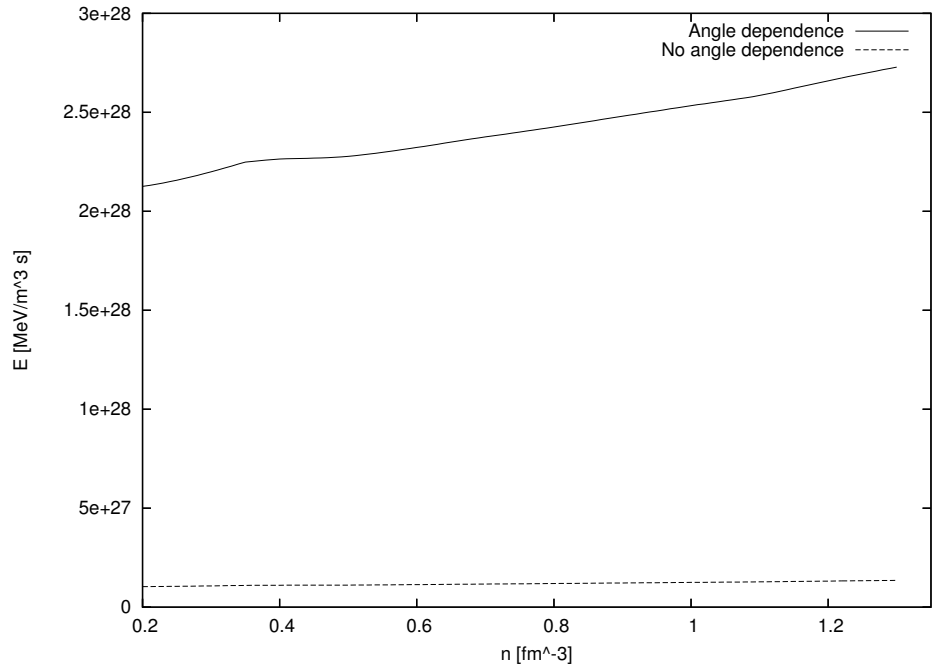

Figure 5.18: Emissivities for the $nn\nu\bar{\nu}$ process at $T = 10^9$ K for EoS III.

In Figs. 5.19 and 5.20, we confront the $nn\nu\bar{\nu}$ emissivities associated with the EoS I – III so as to bring out the effects from the appropriate EoS. The corresponding emissivities with the angle dependence are plotted in Figs. 5.21 and 5.22. It is evidently seen from Figs. 5.19–5.22 that the three-body interactions play a crucial role in the energy loss by neutrinos. On the next level we have the two-body interactions which amount to considerable energy-loss rates. At last, the hyperons with two-body interactions tend to give a rather constant energy loss through the entire density range. When including the angle dependence the energy losses by neutrinos speed up as the phase space of the interacting particles increases.

From the energy loss rates obtained for the $nn\nu\bar{\nu}$ process, we infer that the three-body interactions associated with the EoS II cause significant energy-loss rates when compared with EoS I and III. This is a consequence of the relative proton fractions presented in the neutron star. The three-body scheme tends to increase the relative proton fraction as the chemical potentials of the interacting particles get higher. On the other hand, the two-body interactions associated with the EoS I and III, yield a less stiffer energy loss by neutrinos.

Correspondingly, the emissivities associated with the $np\nu\bar{\nu}$ process may be calculated by implementing Eq. (4.81) from Chapter 4. In this regard, we just refer to the results presented for the $nn\nu\bar{\nu}$ process as the results would be of similar order. Since the neutrons are the most populated in the neutron stars, the $nn\nu\bar{\nu}$ process is usually being considered as the essential among the bremsstrahlung processes.

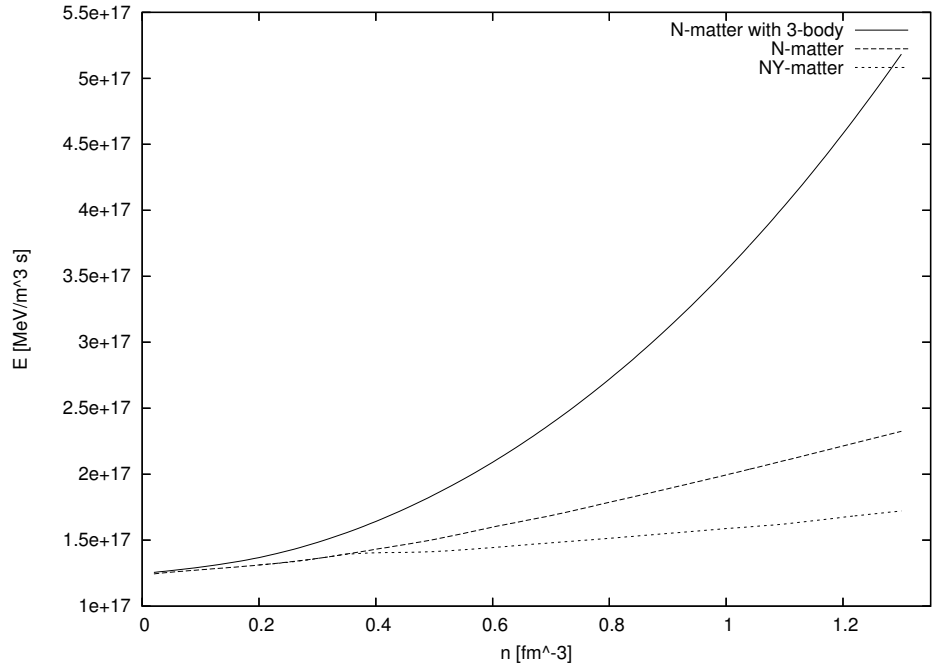

Figure 5.19: Emissivities for the $nn\nu\bar{\nu}$ process at $T = 10^8\,\mathrm{K}$ for EoS I – III. Angle dependence is excluded.

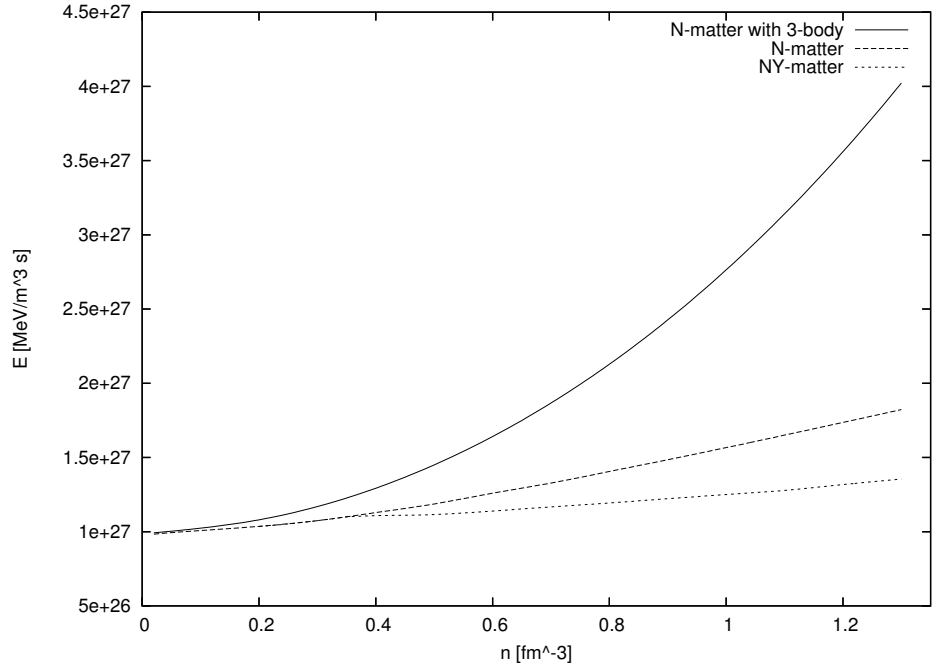

Figure 5.20: Emissivities for the $nn\nu\bar{\nu}$ process at $T = 10^9\,\mathrm{K}$ for EoS I – III. Angle dependence is excluded.

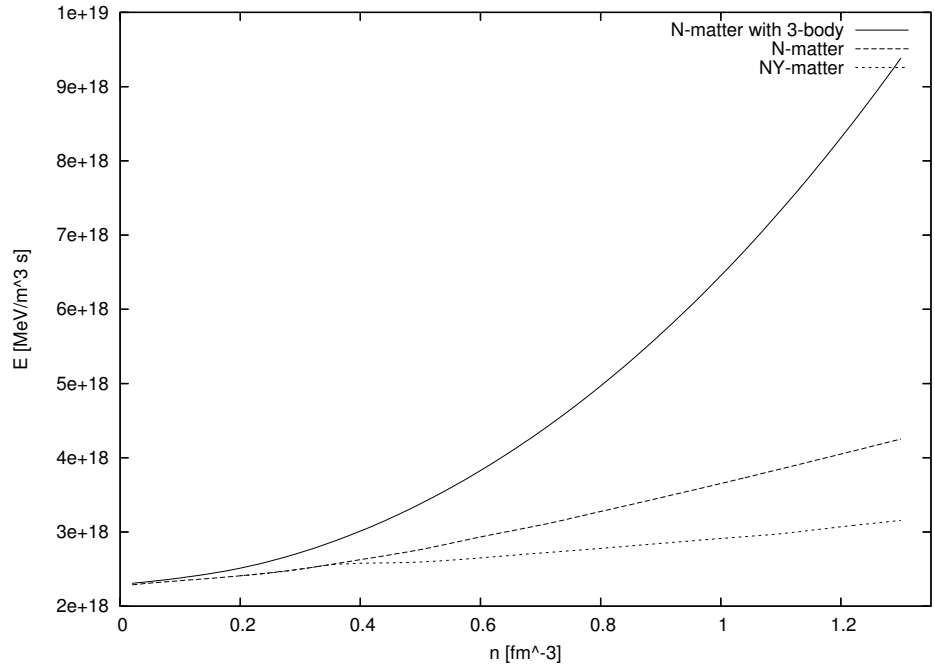

Figure 5.21: Emissivities for the $nn\nu\bar{\nu}$ process at $T = 10^8\,\mathrm{K}$ for EoS I – III. Angle-dependence is included.

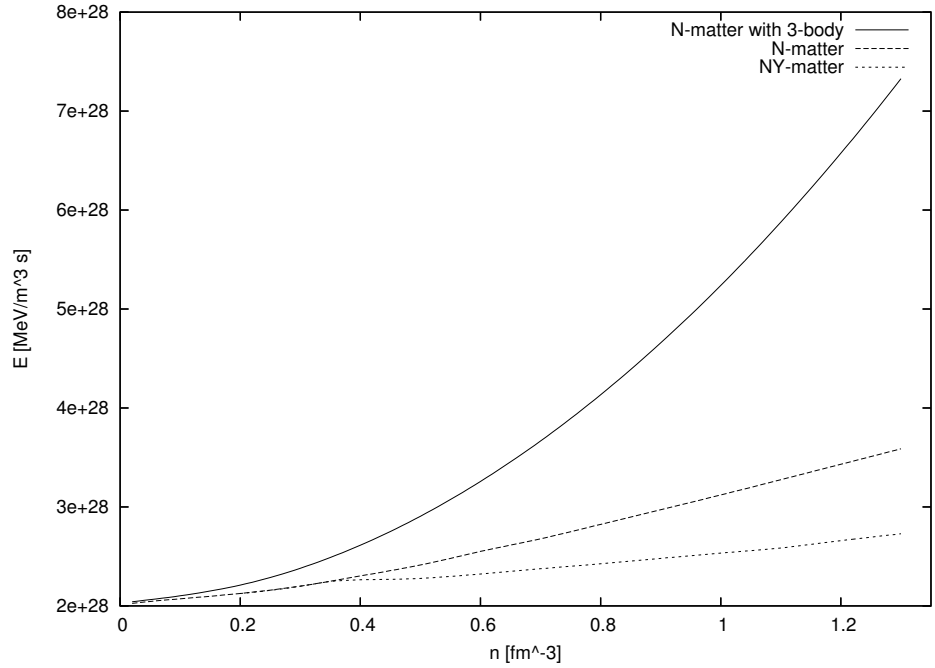

Figure 5.22: Emissivities for the $nn\nu\bar{\nu}$ process at $T = 10^9\,\mathrm{K}$ for EoS I – III. Angle-dependence is included.

5.2 Numerical Methods

As our first target, we went for the foundation of a generic program for calculating Feynman amplitudes. Generally, the Feynman amplitude may be viewed as a product of some 4×4 Dirac matrices, 4×1 spinors, and 1×4 spinors. However, it is not a straightforward task to perform this product numerically. The main reason is that we have to deal with the configuration of Dirac matrices and spinors in executing this product. On designing the generic code for Feynman amplitude, the emulative scheme was to compute $|\mathcal{M}|^2$ for every possible spin configuration, and then do the summing and averaging.

As a first step, we declared a class, called `Particle`, to represent the particles of all type. In order to manage the properties of particles, we had to define some member variables to this class. With the help of predefined member functions, we could access the properties of any particle and manipulate them in a desired way. Once we have defined this class, we were able to create a "particle" with given properties by calling the corresponding constructor. We further created classes to handle the spinors, vertices and propagators which enter into the Feynman amplitudes. The main purpose of these classes was to generate the appropriate spinors, vertices and propagators by the memory address of a particle. As a demonstration, we here put out the essential part of the developed code

```
class Spinor : public Element {
 public:
  Spinor(Particle &particle, int state=0);
  Tensor getFactor();
};

class Vertex : public Element {
 public:
  Vertex(Particle &boson, int indexNr=0);
  Vertex(Particle &boson, Particle &fermion, int indexNr=0);
  Tensor getFactor();
};

class Propagator : public Element {
 public:
  Propagator(Particle &particle, int indexNr1=0, int indexNr2=0);
  Tensor getFactor();
};
```

The constructors for these classes were designed to relate the spinors, vertices and propagators to the appropriate particles. In this context, we could also specify the spin states and free indices to each of these objects. By the way, it was the virtual function, `getFactor()`, that encapsulated the actual structure of spinors, vertices and propagators. The following program displays the implementation of this virtual function.

```
Spinor::Spinor(Particle &particle, int state) {
  p = &particle; // assigning p the address of particle
  b = 0;
  f = 0;
  m = 0;
  spin = state;
}

Tensor Spinor::getFactor() {
  Tensor U(2,1), L(2,1), DS(4,1), out(1,4), projection(2,2);
  CDouble K;

  K = 0;
  K = sqrt(p->getImpulse(0) + p->getMass());
  projection = 0;
  for (int i = 0; i < 3; i++) {
    projection += p->getImpulse(i+1)*S[i];
  }

  U = 0;
  U = K*C[spin];
  L = 0;
  L = product(projection,C[spin])/K;

  DS = 0;
  out = 0;
  if (p->getFrequency() == positive) {
    DS(Range(0,1)) = U;
    DS(Range(2,3)) = L;
    if (p->getLine() == outgoing) {
      out = product(adjoint(DS),G[0]);
      DS.resize(out.shape());
      DS = out;
    }
  }

  if (p->getFrequency() == negative) {
    DS(Range(0,1)) = L;
    DS(Range(2,3)) = U;
    if (p->getLine() == incoming) {
      out = product(adjoint(DS),G[0]);
      DS.resize(out.shape());
      DS = out;
    }
  }
  return DS;
}
```

```
Vertex::Vertex(Particle &boson, int indexNr) {
  p = 0;
  b = &boson;
  f = 0;
  m = 0;
  if (indexNr != 0) {
    freeIndex.push_back(indexNr);
  }
}

Vertex::Vertex(Particle &boson, Particle &fermion, int indexNr) {
  p = 0;
  b = &boson;
  f = &fermion;
  m = 0;
  if (indexNr != 0) {
    freeIndex.push_back(indexNr);
  }
}

Tensor Vertex::getFactor() {
  Tensor factor(4,4), projector(4,4);
  CDouble constant;

  int i = index(0);
  constant = 0;
  projector = 0;
  factor = 0;

  if (b->getG_e() != 0.0) {
    constant = I*b->getG_e();
    factor = constant*G[i];
  } else if (b->getG_W() != 0.0) {
    constant = -I*b->getG_W()/(2*sqrt(2.0));
    if (f) projector = I4 - 1.26*G5;
    else projector = I4 - G5;
    factor = constant*product(G[i],projector);
  } else if (b->getG_Z() != 0.0) {
    constant = -I*b->getG_Z()/2.0;
    projector = f->getC_V()*I4 - f->getC_A()*G5;
    factor = constant*product(G[i],projector);
  } else if (b->getG_pi() != 0.0) {
    constant = -I*b->getG_pi();
    factor = constant*G5;
  }
  return factor;
}
```

```
Propagator::Propagator(Particle &particle, int indexNr1, int indexNr2) {
  p = 0;
  b = 0;
  f = 0;
  m = &particle;
  if (indexNr1 != 0 && indexNr2 != 0) {
    freeIndex.push_back(indexNr1);
    freeIndex.push_back(indexNr2);
  }
}

Tensor Propagator::getFactor() {
  Tensor factor(1,1), bracket(4,4);
  CDouble constant, scalar;
  int i = index(0);
  int j = index(1);
  constant = 0;
  bracket = 0;
  factor = 0;

  scalar = 0;
  for (int i = 0; i < 4; i++) {
    scalar += g(i,i)*m->getImpulse(i)*m->getImpulse(i);
  }
  if (m->getG_e() != 0.0) {
    constant = -I*g(i,j)/scalar;
    factor = constant;
  } else if (m->getG_W() != 0.0) {
    constant = I*g(i,j)/(m->getMass()*m->getMass());
    factor = constant;
  } else if (m->getG_Z() != 0.0) {
    constant = I*g(i,j)/(m->getMass()*m->getMass());
    factor = constant;
  } else if (m->getG_pi() != 0.0) {
    constant = I/(scalar - m->getMass()*m->getMass());
    factor = constant;
  } else {
    constant = I/(scalar - m->getMass()*m->getMass());
    for (int i = 0; i < 4; i++) {
      bracket += m->getImpulse(i)*G[i];
    }
    bracket = bracket + m->getMass()*I4;
    factor.resize(bracket.shape());
    factor = constant*bracket;
  }
  return factor;
}
```

The principal stage was to create the class, `Amplitude`, to represent the entire Feynman amplitude. In concerning the configuration of spins and free indices, we had to define an abstract class called `Element`, which is inherited by the classes `Spinor`, `Vertex`, and `Propagator`. Specifically, the `Element` class was intended to represent each element of an given amplitude. By means of the pointers to `Particle`, one could relate each element of the amplitude to the appropriate particles. These two base classes were coded as follows

```
/* Representing each element of the Feynman amplitude. This abstract
class is being used only as a base class and in inheritance with the
derived classes: Spinor, Vertex and Propagator. */
class Element {
 protected:
  Particle *p, *b, *f, *m; // pointing to the particles of all type
  list<int> freeIndex; // containing the free indices to each element
  // representing the arrangement of summation indices
  Configuration index;
  int spin; // representing the two possible eigenstates of spin
 public:
  Element();
  virtual ~Element() {}
  virtual Tensor getFactor() = 0; // pure virtual function
  Particle* getParticle() { return p; }
  void setSpin(int state) { spin = state; }
  list<int> getFreeIndex() { return freeIndex; }
  int* getIndex(int position) { return &index(position); }
};

/* Representing the Feynman amplitude of any process and dealing with
the summation over spin states and the Dirac matrices. */
class Amplitude {
  list<Element*> M; // containing the entire Feynman amplitude
  Tensor amplitudes;
  int configurations;
 public:
  Amplitude():amplitudes(1,1) { amplitudes = 0; }
  void put(Element *element);
  double initialSpinStates();
  CDouble calculateAmplitude();
  CDouble indexSummation();
  void indexSummation(int instantIndex, CDouble &indexSum);
  CDouble spinSummation();
  void spinSummation(list<Element*>::iterator E, CDouble &spinSum);
  CDouble getAmplitudes(int i) { return amplitudes(i,0); }
  double polarizedAmplitude();
  double unpolarizedAmplitude();
};
```

Once an "amplitude" was created, it would first of all consist of pointers to `Element`. The key point here was that the objects of `Spinor`, `Vertex` and `Propagator`, were all placed at the locations pointed to by the `Element`'s pointers. In order to carry out the configuration of spins and free indices effectively, we implemented recursive functions that running through the `Element`'s pointers. According to the type of object pointed to by the pointer, the appropriate virtual function, `getFactor()`, would be executed. Here we show the recursive functions that carrying out the summations over spin states and free indices.

```
Element::Element():index(2) {
  index = 0, 0;
}

void Amplitude::put(Element *element) {
  M.push_back(element);
}

double Amplitude::initialSpinStates() {
  Particle *iP; // pointing to the interacting particles
  double multiplicity = 1;

  list<Element*>::iterator E = M.begin();
  while (E != M.end()) {
    iP = (*E)->getParticle();
    if (iP && iP->getLine() == incoming) {
      multiplicity *= iP->getStates();
    }
    E++;
  }
  return multiplicity;
}
```

```
CDouble Amplitude::calculateAmplitude() {
  // initializing an iterator to point to the start of the list
  list<Element*>::iterator E = M.begin();

  Tensor A, B, C;
  // making A the same size as the first element in the list
  A.resize(((*E)->getFactor()).shape());
  A = (*E)->getFactor();
  E++; // pointing to the next element in the list

  while (E != M.end()) {
    B.resize(((*E)->getFactor()).shape());
    // receiving the factor at the location pointed to by E
    B = (*E)->getFactor();

    if (A.size() == 1) {
      C.resize(B.shape());
    } else if (B.size() == 1) {
      C.resize(A.shape());
    } else {
      C.resize(A.rows(), B.columns());
    }
    C = product(A, B);
    A.resize(C.shape());
    A = C;

    if (A.size() == 1 && A(0,0) == 0.0) {
      break;
    }
    E++;
  }
  return A(0,0);
}
```

```
CDouble Amplitude::indexSummation() {
  int instantIndex = 1;
  CDouble indexSum = 0;
  indexSummation(instantIndex, indexSum);
  return indexSum;
}

void Amplitude::indexSummation(int instantIndex, CDouble &indexSum) {
  int position;
  int *address;

  list<int> indexList; // dealing with the free indices of each element
  list<int>::iterator F; // the corresponding iterator to indexList
  list<int*> indexPosition; // containing the address of index-position
  list<int*>::iterator P; // the corresponding iterator to indexPosition
  list<Element*>::iterator E = M.begin();

  while (E != M.end()) {
    indexList = (*E)->getFreeIndex();
    F = indexList.begin();
    position = 0;
    while (F != indexList.end()) {
      if ((*F) == instantIndex) {
        address = (*E)->getIndex(position);
        indexPosition.push_back(address);
      }
      position++;
      F++;
    }
    E++;
  }

  if (indexPosition.size() == 0) {
    indexSum += calculateAmplitude();
    return; // control statement
  }

  for (int index = 0; index < 4; index++) {
    P = indexPosition.begin();
    while (P != indexPosition.end()) {
      *(*P) = index;
      P++;
    }
    indexSummation(instantIndex + 1, indexSum);
  }
}
```

```
CDouble Amplitude::spinSummation() {
  Particle *iP; // pointing to the interacting particles
  CDouble spinSum = 0;
  configurations = 0;
  int particle = 0;
  list<Element*>::iterator E = M.begin();
  while (E != M.end()) {
    iP = (*E)->getParticle();
    if (iP) particle++;
    E++;
  }
  amplitudes.resize(pow(2.0, particle), 1);
  amplitudes = 0;
  E = M.begin();
  spinSummation(E, spinSum);
  return spinSum;
}

void Amplitude::spinSummation(list<Element*>::iterator E, CDouble
&spinSum) {
  Particle *iP; // pointing to the interacting particles
  CDouble polarizedSum = 0;
  list<Element*>::iterator N;
  while (E != M.end()) {
    iP = (*E)->getParticle();
    if (iP) {
      for (int state = 0; state < iP->getStates(); state++) {
        if (iP->getType() == undefined) {
          (*E)->setSpin(state);
        } else {
          if (iP->getFrequency() == positive) {
            (*E)->setSpin(state);
          } else {
            (*E)->setSpin(state);
          }
        }
        N = E;
        spinSummation(++N, spinSum);
      }
      return;
    }
    E++;
  }
  polarizedSum = indexSummation();
  spinSum += polarizedSum*conj(polarizedSum);
  amplitudes(configurations++, 0) = polarizedSum;
}
```

```
double Amplitude::polarizedAmplitude() {
  CDouble amplitude, squaredAmplitude;
  amplitude = squaredAmplitude = 0;

  amplitude = indexSummation();
  squaredAmplitude = amplitude*conj(amplitude);
  return real(squaredAmplitude);
}

double Amplitude::unpolarizedAmplitude() {
  CDouble squaredAmplitude = 0;

  squaredAmplitude = spinSummation()/initialSpinStates();
  return real(squaredAmplitude);
}
```

Chapter 6

Concluding Remarks

This thesis started with an overview of the dominant modes of energy loss from a neutron star. In this regard, we studied the direct Urca process and neutrino pair bremsstrahlung in detail so as to estimate the associated energy-loss rates. In Chapters 3 and 4, we developed a calculational scheme that may be carried out to determine the neutrino emissivities of any process. The principal stage was here to design a generic code for calculating the Feynman amplitude of any process. We have also succeeded in combining the EoS with the calculation of emissivities to which we introduced the many-body correlations in an effective way. The one-boson interactions we have considered, may be defined as follows

$$V = \bar{u}(\mathbf{p}_1{}')\bar{u}(\mathbf{p}_2{}') \left(\sum_{j=1}^{5} v_j(\mathbf{k}) F_j \right) u(\mathbf{p}_1) u(\mathbf{p}_2),$$

where F_j $(j = 1, ..., 5)$ denote the Fermi invariant quantities, being

$$S = 1^{(1)}1^{(2)}, \quad V = \gamma_\mu^{(1)}\gamma_\mu^{(2)}, \quad T = \frac{1}{2}\sigma_{\mu\nu}^{(1)}\sigma_{\mu\nu}^{(2)},$$

$$A = i\gamma_5^{(1)}\gamma_\mu^{(1)} i\gamma_5^{(2)}\gamma_\mu^{(2)}, \quad P = \gamma_5^{(1)}\gamma_5^{(2)}.$$

In the case of a pseudovector coupling for the pseudoscalar mesons one has to replace P with the on-shell equivalent pseudovector invariant

$$P' \propto (\gamma_\mu^{(1)} \cdot \partial^\mu)\gamma_5^{(1)}(\gamma_\nu^{(2)} \cdot \partial^\nu)\gamma_5^{(2)},$$

with the labels $(1, 2)$ meaning the interacting baryons 1 and 2. The $v_j(\mathbf{k})$ term refers to the appropriate meson propagator defined like $i/(-\mathbf{k}^2 - m_\alpha^2)$, including the appropriate coupling constants. In general, the coefficients $v_j(\mathbf{k})$ are functions of the three Mandelstam invariants s, t and u, though one can choose the interaction to depend on the momentum transfer. In our treatment, the $v_j(\mathbf{k})$ was given by the meson propagators only. The only medium effects we have included, are the effective masses for the various baryons, and their corresponding densities and chemical potentials. The next is to use the EoS to parametrize $v_j(\mathbf{k})$, in order to obtain an effective medium

dependent interaction consistent with the associated EoS.

The main objective of this thesis was to calculate the emissivities associated with the direct Urca process and neutrino pair bremsstrahlung. From the results we obtained for the energy loss rates, we conclude that the direct Urca process would lead to more rapid cooling than the bremsstrahlung process. The modified Urca process discussed in Chapter 1, is expected to give energy losses similar to that of the bremsstrahlung process. While an exact treatment of neutron star cooling lies still in the future, it is clear already what the important physical principles are and how the calculation will be done.

The lesson of the recent studies of neutrino processes is that there are many possible physical conditions that could result in neutron stars cooling fast. One of these is proton concentrations that were regarded as unacceptably high some time ago, but that are not outside the range currently regarded as being physically possible. Another is the presence of hyperons or Δ-isobars. In addition, there are the exotic states considered earlier.

Energy losses by the nucleon direct Urca process, if allowed, exceed those for any of the other processes previously considered. In addition, there are numerous other possible processes for which the losses have the same temperature dependence as that of the direct Urca process, and whose magnitudes are simply related to, but generally smaller than, that of the nucleon direct Urca process. It is therefore tempting to regard it, rather than the modified Urca process, as the standard one.

In summary, the study of neutron star cooling has the potential for giving information about neutron star interiors. It is unlikely that observations alone will be sufficient to identify the states of dense matter, but coupled with theoretical studies of dense matter and information to be obtained from observational data, they are likely to lead to important insights. In the years to come, one can look forward to a continuing interplay between astrophysical observations, the theoretical study of neutron stars, nuclear theory, and laboratory nuclear physics.

Appendix A

The Dirac Equation

In this appendix we introduce the Dirac equation and derive the main results relating to this equation. In evaluating the Feynman diagrams we are often dealing with polarization sums and traces of γ-matrices. The very powerful and elegant methods for performing these polarization sums are to be worked out here. Moreover, we develop some useful techniques for calculating the traces of products of γ-matrices.

A.1 The Dirac Equation

The Dirac equation for particles of rest mass m can be written

$$i\hbar\frac{\partial\psi(x)}{\partial t} = \left[c\boldsymbol{\alpha}\cdot(-i\hbar\boldsymbol{\nabla}) + \beta mc^2\right]\psi(x) \tag{A.1}$$

where $\boldsymbol{\alpha} = (\alpha_1, \alpha_2, \alpha_3)$ and β are 4×4 Hermitian matrices satisfying

$$[\alpha_i, \alpha_j]_+ = 2\delta_{ij}, \qquad [\alpha_i, \beta]_+ = 0, \qquad \beta^2 = 1, \qquad i,j = 1,2,3. \tag{A.2}$$

With

$$\gamma^0 = \beta, \qquad \gamma^i = \beta\alpha_i \tag{A.3}$$

the Dirac equation becomes

$$(i\hbar\gamma^\mu\partial_\mu - mc)\,\psi(x) = 0 \tag{A.4}$$

with the 4×4 Dirac matrices γ^μ, $\mu = 0, ..., 3$, satisfying the anticommutation relations

$$[\gamma^\mu, \gamma^\nu]_+ = 2g^{\mu\nu} \tag{A.5}$$

and the Hermiticity conditions $\gamma^{0\dagger} = \gamma^0$ and $\gamma^{j\dagger} = -\gamma^j$ for $j = 1,2,3$, which can be combined into

$$\gamma^{\mu\dagger} = \gamma^0\gamma^\mu\gamma^0 \tag{A.6}$$

Note that we express the partial derivative in Eq. (A.4) in shorthand by $\partial_\mu = \partial/\partial x^\mu$.

Correspondingly, $\psi(x)$ is a spinor wavefunction with four components $\psi_\alpha(x)$, $\alpha = 1, ..., 4$. The adjoint field $\bar{\psi}(x)$ is defined by

$$\bar{\psi}(x) = \psi^\dagger(x)\gamma^0 \tag{A.7}$$

and satisfies the adjoint Dirac equation

$$(i\hbar\partial_\mu\gamma^\mu + mc)\,\bar{\psi}(x) = 0 \tag{A.8}$$

The Dirac equations (A.4) and (A.8) can be derived from the Lagrangian density[12]

$$\mathscr{L} = c\bar{\psi}(x)\,(i\hbar\gamma^\mu\partial_\mu - mc)\,\psi(x) \tag{A.9}$$

to which we may let act by the Euler-Lagrange equation

$$\frac{\partial\mathscr{L}}{\partial\psi(x)} - \partial_\mu\left(\frac{\partial\mathscr{L}}{\partial(\partial_\mu\psi(x))}\right) = 0 \tag{A.10}$$

A fifth anticommuting γ-matrix is defined by

$$\gamma^5 \equiv i\gamma^0\gamma^1\gamma^2\gamma^3, \tag{A.11}$$

and γ^5 has the properties

$$[\gamma^\mu, \gamma^5]_+ = 0, \qquad \left(\gamma^5\right)^2 = 1, \qquad \gamma^{5\dagger} = \gamma^5. \tag{A.12}$$

We also define the matrix γ_5 through

$$\gamma_5 \equiv \frac{i}{4!}\epsilon_{\rho\mu\sigma\nu}\gamma^\rho\gamma^\mu\gamma^\sigma\gamma^\nu = \gamma^5, \tag{A.13}$$

where the totally antisymmetric Levi-Civita symbol $\epsilon_{\rho\mu\sigma\nu}$ is equal to $+1$ if (ρ, μ, σ, ν) is an even permutation of $(0, 1, 2, 3)$, -1 if it is an odd permutation, and 0 if any index is repeated.

There exists several representations of γ-matrices. One of the most frequently used representations for γ-matrices is the original Dirac representation. In terms of the Pauli 2×2 spin matrices

$$\sigma_1 = \begin{pmatrix} 0 & 1 \\ 1 & 0 \end{pmatrix}, \qquad \sigma_2 = \begin{pmatrix} 0 & -i \\ i & 0 \end{pmatrix}, \qquad \sigma_3 = \begin{pmatrix} 1 & 0 \\ 0 & -1 \end{pmatrix}, \tag{A.14}$$

the Dirac matrices can in this representation be written as

$$\gamma^0 = \begin{pmatrix} 1 & 0 \\ 0 & -1 \end{pmatrix}, \qquad \gamma^i = \begin{pmatrix} 0 & \sigma^i \\ -\sigma^i & 0 \end{pmatrix}, \qquad i = 1, 2, 3, \tag{A.15}$$

and

$$\gamma^5 = \begin{pmatrix} 0 & 1 \\ 1 & 0 \end{pmatrix}. \tag{A.16}$$

In fact, these five γ-matrices form the Dirac basis and this, in turn, are appropriate for acting on Dirac spinors written in this basis.

The γ-matrices act like a vector, and their contraction with a vector acts like a scalar. So, it is common to write a covariant four-vector using Feynman slash notation, defined by

$$\not{p} \equiv p_\mu \gamma^\mu \tag{A.17}$$

A.2 Solutions to the Dirac Equation

The Dirac equation (A.4) possesses free-particle solutions

$$\psi^+(x) = K^+ u(p,s)\mathbf{e}^{-ipx/\hbar}, \qquad \psi^-(x) = K^- v(p,s)\mathbf{e}^{ipx/\hbar} \tag{A.18}$$

where $K^\pm$ are normalization factors, given by

$$K^\pm = \sqrt{\frac{c}{2EV}} \tag{A.19}$$

Note that $p = (E/c, \mathbf{p})$, $E = \sqrt{|\mathbf{p}|^2c^2 + m^2c^4}$ and $px = Et - \mathbf{p}\cdot\mathbf{x}$. By putting the solutions (A.18) into the Dirac equation (A.4), we obtain the momentum space Dirac equations

$$(\not{p} - mc)u(p,s) = 0, \qquad (\not{p} + mc)v(p,s) = 0 \tag{A.20}$$

These has two positive energy solutions

$$u(p,s) = N^+ \begin{pmatrix} \chi_s \\ \frac{c\boldsymbol{\sigma}\cdot\mathbf{p}}{E+mc^2}\chi_s \end{pmatrix}, \qquad s = 1,2, \tag{A.21}$$

and two negative energy solutions

$$v(p,s) = N^- \begin{pmatrix} \frac{c\boldsymbol{\sigma}\cdot\mathbf{p}}{E+mc^2}\chi'_s \\ \chi'_s \end{pmatrix}, \qquad s = 1,2, \tag{A.22}$$

which are then interpreted as positive energy antiparticle solutions. Here $N^\pm$ are some other normalization factors, defined by

$$N^\pm = \sqrt{\frac{E+mc^2}{c}} \tag{A.23}$$

The index $s = 1,2$ signifies the two possible eigenstates of spin of a spin-1/2 particle: spin up and spin down. These two spin states are represented by the Pauli spinors

$$\chi_1 \equiv \chi'_2 \equiv \begin{pmatrix} 1 \\ 0 \end{pmatrix}, \qquad \chi_2 \equiv \chi'_1 \equiv \begin{pmatrix} 0 \\ 1 \end{pmatrix} \tag{A.24}$$

which are mutually orthogonal, and consequently the Dirac spinors $u(p,s)$ and $v(p,s)$ involving these two states become also orthogonal. Furthermore, we normalize the spinors $u(p,s)$ and $v(p,s)$ so that

$$u^\dagger(p,s)u(p,s) = v^\dagger(p,s)v(p,s) = \frac{2E}{c} \tag{A.25}$$

They then satisfy the orthonormality relations

$$u^\dagger(p,s)u(p,s') = v^\dagger(p,s)v(p,s') = \frac{2E}{c}\delta_{ss'}$$
$$u^\dagger(p,s)v(-p,s') = 0 \tag{A.26}$$

It might seem that $u(p,s=1)$ describes a particle with spin up, $u(p,s=2)$ a particle with spin down, and so on, but this is not quite the case. For Dirac particles the spin matrices are

$$\mathbf{S} = \frac{\hbar}{2}\mathbf{\Sigma}, \qquad \text{with } \mathbf{\Sigma} \equiv \begin{pmatrix} \boldsymbol{\sigma} & 0 \\ 0 & \boldsymbol{\sigma} \end{pmatrix} \tag{A.27}$$

and the Dirac spinors $u(p,s)$ and $v(p,s)$ are not eigenstates of Σ_z. As a matter of fact, it is impossible to construct spinors that satisfy Eq. (A.20) and are, at the same time, eigenstates of S_z. The reason is that $\mathbf{S}$ by itself is not a conserved quantity; only the total angular momentum, $\mathbf{L}+\mathbf{S}$, is conserved here. However, if we orient the z-axis so that it points along the direction of motion (in which case $p_x = p_y = 0$) then $u(p,s)$ and $v(p,s)$ are eigenspinors of S_z.

A.3 Completeness Relations

In most practical situations, the interacting particles are unpolarized, i.e. the initial and final spin orientations are arbitrary. It then becomes necessary to average and sum over polarization states of initial and final particles respectively. For this purpose, we here show explicitly how to perform the summation over spin states.

To start with, we take the transpose conjugate of the positive energy spinor $u(p,s)$ (A.21):

$$\bar{u}(p,s) = u^\dagger(p,s)\gamma^0 = N^{+*}\begin{pmatrix} \chi_s^\dagger & -\chi_s^\dagger \frac{c\boldsymbol{\sigma}\cdot\mathbf{p}}{E+mc^2} \end{pmatrix} \tag{A.28}$$

We are ready now to sum over the two spin states of a particle:

$$\begin{aligned}\sum_s u(p,s)\bar{u}(p,s) &= \sum_s |N^+|^2 \begin{pmatrix} \chi_s \\ \frac{c\boldsymbol{\sigma}\cdot\mathbf{p}}{E+mc^2}\chi_s \end{pmatrix}\begin{pmatrix} \chi_s^\dagger & -\chi_s^\dagger \frac{c\boldsymbol{\sigma}\cdot\mathbf{p}}{E+mc^2} \end{pmatrix} \\ &= \frac{E+mc^2}{c}\begin{pmatrix} 1 & -\frac{c\boldsymbol{\sigma}\cdot\mathbf{p}}{E+mc^2} \\ \frac{c\boldsymbol{\sigma}\cdot\mathbf{p}}{E+mc^2} & -\frac{c^2(\boldsymbol{\sigma}\cdot\mathbf{p})^2}{(E+mc^2)^2} \end{pmatrix}\end{aligned} \tag{A.29}$$

where in the last step we have applied $\chi_s\chi_s^\dagger = 1$. From the last equation, we notice that

$$(\boldsymbol{\sigma}\cdot\mathbf{p})^2 = \mathbf{p}^2 = \frac{(E+mc^2)(E-mc^2)}{c^2} \tag{A.30}$$

where we have used the properties $\sigma_i^2 = 1$ and $[\sigma_i,\sigma_j]_+ = 2\delta_{ij}$.

On substituting Eq. (A.30) in Eq. (A.29), we obtain

$$\begin{aligned}\sum_s u(p,s)\bar{u}(p,s) &= \begin{pmatrix} \frac{E+mc^2}{c} & -\boldsymbol{\sigma}\cdot\mathbf{p} \\ \boldsymbol{\sigma}\cdot\mathbf{p} & -\frac{E-mc^2}{c} \end{pmatrix} \\ &= \gamma^0\frac{E}{c} - \boldsymbol{\gamma}\cdot\mathbf{p} + \mathbf{1}\cdot mc \\ &= \gamma^\mu p_\mu + mc \equiv \not{p} + mc \end{aligned} \tag{A.31}$$

We follow the same lines of reasoning in order to show the summation over spin states of an antiparticle. Firstly, we take the adjoint of the negative energy spinor $v(p,s)$ (A.22):

$$\bar{v}(p,s) = v^\dagger(p,s)\gamma^0 = N^{-*}\begin{pmatrix} \chi_s^\dagger\frac{c\boldsymbol{\sigma}\cdot\mathbf{p}}{E+mc^2} & -\chi_s^\dagger \end{pmatrix} \tag{A.32}$$

We now go on to sum over the two spin states of an antiparticle:

$$\begin{aligned}\sum_s v(p,s)\bar{v}(p,s) &= \sum_s |N^-|^2 \begin{pmatrix} \frac{c\boldsymbol{\sigma}\cdot\mathbf{p}}{E+mc^2}\chi_s \\ \chi_s \end{pmatrix}\begin{pmatrix} \chi_s^\dagger\frac{c\boldsymbol{\sigma}\cdot\mathbf{p}}{E+mc^2} & -\chi_s^\dagger \end{pmatrix} \\ &= \frac{E+mc^2}{c}\begin{pmatrix} \frac{c^2(\boldsymbol{\sigma}\cdot\mathbf{p})^2}{(E+mc^2)^2} & -\frac{c\boldsymbol{\sigma}\cdot\mathbf{p}}{E+mc^2} \\ \frac{c\boldsymbol{\sigma}\cdot\mathbf{p}}{E+mc^2} & -1 \end{pmatrix} \end{aligned} \tag{A.33}$$

where the last step follows by $\chi_s\chi_s^\dagger = 1$. On proceeding the spin sum, we make use of Eq. (A.30)

$$\begin{aligned}\sum_s v(p,s)\bar{v}(p,s) &= \begin{pmatrix} \frac{E-mc^2}{c} & -\boldsymbol{\sigma}\cdot\mathbf{p} \\ \boldsymbol{\sigma}\cdot\mathbf{p} & -\frac{E+mc^2}{c} \end{pmatrix} \\ &= \gamma^0\frac{E}{c} - \boldsymbol{\gamma}\cdot\mathbf{p} - \mathbf{1}\cdot mc \\ &= \gamma^\mu p_\mu - mc \equiv \not{p} - mc \end{aligned} \tag{A.34}$$

A.4 Casimir's Trick

The summations over polarization states are easily performed using the following trick. The Casimir's trick reduces everything down to a problem of calculating the trace of some complicated product of γ-matrices. In contrast to the spin sums from the last section, we now deal with summands of the form $\bar{u}(p,s)\mathcal{A}u(p,s)$, in which the spin states are to be summed up. Here $\mathcal{A}$ is some product of γ-matrices. First we write the summand $\bar{u}(p,s)\mathcal{A}u(p,s)$ with explicit spinor indices $i,j = 1,2,3,4$:

$$\begin{aligned}\mathbf{Tr}(\widetilde{\mathcal{A}}) = \sum_s \bar{u}(p,s)\mathcal{A}u(p,s) &= \sum_s\sum_i\sum_j \bar{u}_i(p,s)\mathcal{A}_{ij}u_j(p,s) \\ &= \sum_i\sum_j \mathcal{A}_{ij}\sum_s u_j(p,s)\bar{u}_i(p,s) \end{aligned} \tag{A.35}$$

where in the last step we have moved $\bar{u}_i(p,s)$ behind $u_j(p,s)$ ($\bar{u}_i(p,s)$ is just a number, element of vector $\bar{u}(p,s)$, so it commutes with everything).

Using the completeness relation (A.31), we have

$$\begin{aligned}\mathbf{Tr}(\widetilde{\mathcal{A}}) &= \sum_s \bar{u}(p,s)\mathcal{A}u(p,s) = \sum_i \sum_j \mathcal{A}_{ij}\left(\not{p}+m\right)_{ji} \\ &= \sum_i \sum_j \left(\not{p}+m\right)_{ji}\mathcal{A}_{ij} = \mathbf{Tr}\left[\left(\not{p}+m\right)\mathcal{A}\right] \end{aligned} \tag{A.36}$$

Notice that there are no spinors left; once we do the summation over spins, it all reduces to matrix multiplication and taking the trace. If either positive energy spinor $u(p,s)$ (in Eq. (A.36)) is replaced by a negative energy spinor $v(p,s)$, the corresponding mass on the right-hand side switches sign.

A.5 Contraction Identities and Traces

The manipulation of expressions involving γ-matrices is often greatly facilitated by the use of the following algebraic identities, which follow easily from the anticommutation relations (A.5). In terms of the metric

$$g^{\mu\nu} \equiv \begin{pmatrix} 1 & 0 & 0 & 0 \\ 0 & -1 & 0 & 0 \\ 0 & 0 & -1 & 0 \\ 0 & 0 & 0 & -1 \end{pmatrix} \tag{A.37}$$

we have:

a) $\gamma^\mu\gamma_\mu = \frac{1}{2}g_{\mu\nu}\big(\gamma^\mu\gamma^\nu + \gamma^\nu\gamma^\mu\big) = g_{\mu\nu}g^{\mu\nu} = 4$

b) $\gamma^\mu\gamma^\alpha\gamma_\mu = \big(2g^{\mu\alpha} - \gamma^\alpha\gamma^\mu\big)\gamma_\mu = 2\gamma^\alpha - 4\gamma^\alpha = -2\gamma^\alpha$

c) $\gamma^\mu\gamma^\alpha\gamma^\beta\gamma_\mu = \big(2g^{\mu\alpha} - \gamma^\alpha\gamma^\mu\big)\gamma^\beta\gamma_\mu = 2\gamma^\beta\gamma^\alpha + 2\gamma^\alpha\gamma^\beta = 4g^{\alpha\beta}$

d) $\gamma^\mu\gamma^\alpha\gamma^\beta\gamma^\eta\gamma_\mu = \big(2g^{\mu\alpha} - \gamma^\alpha\gamma^\mu\big)\gamma^\beta\gamma^\eta\gamma_\mu = 2\gamma^\beta\gamma^\eta\gamma^\alpha - 4\gamma^\alpha g^{\beta\eta} = -2\gamma^\eta\gamma^\beta\gamma^\alpha$

e) $\gamma^\mu\gamma^\alpha\gamma^\beta\gamma^\eta\gamma^\delta\gamma_\mu = \big(2g^{\mu\alpha} - \gamma^\alpha\gamma^\mu\big)\gamma^\beta\gamma^\eta\gamma^\delta\gamma_\mu = 2\big(\gamma^\beta\gamma^\eta\gamma^\delta\gamma^\alpha + \gamma^\alpha\gamma^\delta\gamma^\eta\gamma^\beta\big)$

The completely antisymmetric Levi-Civita symbol $\epsilon_{\rho\mu\sigma\nu}$, introduced in Eq. (A.13), satisfies the following contraction identity:

$$\epsilon^{\alpha\mu\beta\nu}\epsilon_{\rho\mu\sigma\nu} = -2\big(g^\alpha_\rho g^\beta_\sigma - g^\alpha_\sigma g^\beta_\rho\big) \tag{A.38}$$

We next list some rules and relations which are extremely useful in evaluating the trace of a product of γ-matrices.

1. For any two $n \times n$ matrices A and B, and any scalar c, we have

$$\begin{aligned}\mathbf{Tr}(A+B) &= \mathbf{Tr}(A) + \mathbf{Tr}(B) \\ \mathbf{Tr}(AB) &= \mathbf{Tr}(BA) \\ \mathbf{Tr}(cA) &= c\mathbf{Tr}(A)\end{aligned} \tag{A.39}$$

2. The trace of the product of an odd number of γ-matrices is zero. If $(\gamma^\alpha\gamma^\beta...\gamma^\mu\gamma^\nu)$ contains an odd number of γ-matrices, then

$$\begin{aligned}\mathbf{Tr}\big(\gamma^\alpha\gamma^\beta...\gamma^\mu\gamma^\nu\big) &= \mathbf{Tr}\big(\gamma^\alpha\gamma^\beta...\gamma^\mu\gamma^\nu\gamma^5\gamma^5\big)\\ &= -\mathbf{Tr}\big(\gamma^5\gamma^\alpha\gamma^\beta...\gamma^\mu\gamma^\nu\gamma^5\big)\end{aligned} \tag{A.40}$$

where the last step follows by moving the γ^5-matrix in the front of the γ-matrices. By the cyclic property of the traces (Eq. (A.39)), we realize that

$$\begin{aligned}\mathbf{Tr}\big(\gamma^\alpha\gamma^\beta...\gamma^\mu\gamma^\nu\big) &= -\mathbf{Tr}\big(\gamma^\alpha\gamma^\beta...\gamma^\mu\gamma^\nu\gamma^5\gamma^5\big)\\ &= -\mathbf{Tr}\big(\gamma^\alpha\gamma^\beta...\gamma^\mu\gamma^\nu\big) = 0\end{aligned} \tag{A.41}$$

3. For a product of an even number of γ-matrices:

$$\mathbf{Tr}\big(\gamma^\alpha\gamma^\beta\big) = \mathbf{Tr}\big(2g^{\alpha\beta} - \gamma^\beta\gamma^\alpha\big) = 2g^{\alpha\beta}\mathbf{Tr}(1) - \mathbf{Tr}\big(\gamma^\beta\gamma^\alpha\big) = 8g^{\alpha\beta} - \mathbf{Tr}\big(\gamma^\alpha\gamma^\beta\big)$$

with $\mathbf{Tr}(1) = 4$. Moving the last term over to the left-hand side results in

$$\mathbf{Tr}\big(\gamma^\alpha\gamma^\beta\big) = 4g^{\alpha\beta} \tag{A.42}$$

Correspondingly

$$\begin{aligned}\mathbf{Tr}\big(\gamma^\alpha\gamma^\beta\gamma^\rho\gamma^\sigma\big) &= \mathbf{Tr}\big[\gamma^\alpha\gamma^\beta\big(2g^{\rho\sigma} - \gamma^\sigma\gamma^\rho\big)\big] = 2g^{\rho\sigma}\mathbf{Tr}\big(\gamma^\alpha\gamma^\beta\big) - \mathbf{Tr}\big(\gamma^\alpha\gamma^\beta\gamma^\sigma\gamma^\rho\big)\\ &= 8g^{\rho\sigma}g^{\alpha\beta} - \mathbf{Tr}\big[\gamma^\alpha\big(2g^{\beta\sigma} - \gamma^\sigma\gamma^\beta\big)\gamma^\rho\big]\\ &= 8g^{\rho\sigma}g^{\alpha\beta} - 2g^{\beta\sigma}\mathbf{Tr}\big(\gamma^\alpha\gamma^\rho\big) + \mathbf{Tr}\big(\gamma^\alpha\gamma^\sigma\gamma^\beta\gamma^\rho\big)\\ &= 8g^{\rho\sigma}g^{\alpha\beta} - 8g^{\beta\sigma}g^{\alpha\rho} + \mathbf{Tr}\big[\big(2g^{\alpha\sigma} - \gamma^\sigma\gamma^\alpha\big)\gamma^\beta\gamma^\rho\big]\\ &= 8g^{\rho\sigma}g^{\alpha\beta} - 8g^{\beta\sigma}g^{\alpha\rho} + 2g^{\alpha\sigma}\mathbf{Tr}\big(\gamma^\beta\gamma^\rho\big) - \mathbf{Tr}\big(\gamma^\sigma\gamma^\alpha\gamma^\beta\gamma^\rho\big)\\ &= 8g^{\rho\sigma}g^{\alpha\beta} - 8g^{\beta\sigma}g^{\alpha\rho} + 8g^{\alpha\sigma}g^{\beta\rho} - \mathbf{Tr}\big(\gamma^\alpha\gamma^\beta\gamma^\rho\gamma^\sigma\big)\end{aligned}$$

Rearranging the last equation provides

$$\mathbf{Tr}\big(\gamma^\alpha\gamma^\beta\gamma^\rho\gamma^\sigma\big) = 4\big(g^{\alpha\beta}g^{\rho\sigma} - g^{\alpha\rho}g^{\beta\sigma} + g^{\alpha\sigma}g^{\beta\rho}\big) \tag{A.43}$$

4. Since γ^5 is the product of an even number of γ-matrices, it follows that $\mathbf{Tr}(\gamma^5\gamma^\alpha) = \mathbf{Tr}(\gamma^5\gamma^\alpha\gamma^\beta\gamma^\rho) = 0$. When γ^5 is multiplied by an even number of γ's, we find

$$\begin{aligned}\mathbf{Tr}\big(\gamma^5\big) &= \mathbf{Tr}\big(\gamma^5\gamma^\alpha\gamma^\beta\big) = 0\\ \mathbf{Tr}\big(\gamma^5\gamma^\alpha\gamma^\beta\gamma^\rho\gamma^\sigma\big) &= -4i\epsilon^{\alpha\beta\rho\sigma}\end{aligned} \tag{A.44}$$

As an important application of the above relations we here demonstrate the evaluation of the traces (3.5) and (3.6) from Chapter 3. We first look at the trace (3.5) and write out the factors explicitly

$$\begin{aligned}\mathbf{Tr}(\widetilde{\mathcal{A}}) &= \mathbf{Tr}\left[\left(\not{p}_4 + m_e\right)\gamma^\mu\left(1-\gamma^5\right)\left(\not{p}_2 - m_{\bar{\nu}_e}\right)\left(1+\gamma^5\right)\gamma^\nu\right]\\ &= \mathbf{Tr}\left[\not{p}_4\gamma^\mu\left(1-\gamma^5\right)\not{p}_2\left(1+\gamma^5\right)\gamma^\nu\right] - m_{\bar{\nu}_e}\mathbf{Tr}\left[\not{p}_4\gamma^\mu\left(1-(\gamma^5)^2\right)\gamma^\nu\right] +\\ &\quad + m_e\mathbf{Tr}\left[\gamma^\mu\left(1-\gamma^5\right)\not{p}_2\left(1+\gamma^5\right)\gamma^\nu\right] - m_e m_{\bar{\nu}_e}\mathbf{Tr}\left[\gamma^\mu\left(1-(\gamma^5)^2\right)\gamma^\nu\right]\end{aligned} \tag{A.45}$$

When applying the identities (A.12) and rule 2, the last three terms cancel out, and we are left with

$$\mathbf{Tr}(\widetilde{\mathcal{A}}) = \mathbf{Tr}\left[(1-\gamma^5)^2 \not{p}_4 \gamma^\mu \not{p}_2 \gamma^\nu\right] = 2p_{4\alpha}p_{2\beta}\mathbf{Tr}\left[\left(1-\gamma^5\right)\gamma^\alpha\gamma^\mu\gamma^\beta\gamma^\nu\right] \tag{A.46}$$

where we have used $(1-\gamma^5)^2 = 2(1-\gamma^5)$. From Eqs. (A.43) and (A.44), we finally obtain for the trace (3.5)

$$\begin{aligned}\mathbf{Tr}(\widetilde{\mathcal{A}}) &= 8p_{4\alpha}p_{2\beta}\big(g^{\alpha\mu}g^{\beta\nu} - g^{\alpha\beta}g^{\mu\nu} + g^{\alpha\nu}g^{\mu\beta} + i\epsilon^{\alpha\mu\beta\nu}\big) \\ &= 8\left[p_4^\mu p_2^\nu - (p_4\cdot p_2)g^{\mu\nu} + p_4^\nu p_2^\mu + i\epsilon^{\alpha\mu\beta\nu}p_{4\alpha}p_{2\beta}\right]\end{aligned} \tag{A.47}$$

In the same manner, we have for the trace (3.6)

$$\begin{aligned}\mathbf{Tr}(\widetilde{\mathcal{B}}) &= \mathbf{Tr}\left[(\not{p}_3 + m_p)\,\gamma_\mu\left(1-c_A\gamma^5\right)(\not{p}_1 + m_n)\left(1+c_A\gamma^5\right)\gamma_\nu\right] \\ &= \mathbf{Tr}\left[\not{p}_3\gamma_\mu\left(1-c_A\gamma^5\right)\not{p}_1\left(1+c_A\gamma^5\right)\gamma_\nu\right] + m_n\mathbf{Tr}\left[\not{p}_3\gamma_\mu\left(1-c_A^2\right)\gamma_\nu\right] + \\ &\quad + m_p\mathbf{Tr}\left[\gamma_\mu\left(1-c_A\gamma^5\right)\not{p}_1\left(1+c_A\gamma^5\right)\gamma_\nu\right] + m_pm_n\mathbf{Tr}\left[\gamma_\mu\left(1-c_A^2\right)\gamma_\nu\right]\end{aligned} \tag{A.48}$$

Here the second and third term contains three γ-matrices, and hence falls off in accordance with rule 2. On proceeding, we take advantage of the relations (A.12) and (A.42)

$$\begin{aligned}\mathbf{Tr}(\widetilde{\mathcal{B}}) &= \mathbf{Tr}\left[(1-c_A\gamma^5)^2\not{p}_3\gamma_\mu\not{p}_1\gamma_\nu\right] + m_pm_n\left(1-c_A^2\right)\mathbf{Tr}\left[\gamma_\mu\gamma_\nu\right] \\ &= \left(1+c_A^2\right)p_3^\rho p_1^\sigma\mathbf{Tr}\left[\gamma_\rho\gamma_\mu\gamma_\sigma\gamma_\nu\right] - 2c_Ap_3^\rho p_1^\sigma\mathbf{Tr}\left[\gamma^5\gamma_\rho\gamma_\mu\gamma_\sigma\gamma_\nu\right] + \\ &\quad + 4m_pm_n\left(1-c_A^2\right)g_{\mu\nu}\end{aligned} \tag{A.49}$$

and using Eqs. (A.43) and (A.44) this reduces to

$$\begin{aligned}\mathbf{Tr}(\widetilde{\mathcal{B}}) &= 4\left(1+c_A^2\right)p_3^\rho p_1^\sigma\left(g_{\rho\mu}g_{\sigma\nu} - g_{\rho\sigma}g_{\mu\nu} + g_{\rho\nu}g_{\mu\sigma}\right) + 8c_Ai\epsilon_{\rho\mu\sigma\nu}p_3^\rho p_1^\sigma + \\ &\quad + 4m_pm_n\left(1-c_A^2\right)g_{\mu\nu} \\ &= 4\left(1+c_A^2\right)\left[p_{3\mu}p_{1\nu} - (p_3\cdot p_1)g_{\mu\nu} + p_{3\nu}p_{1\mu}\right] + 8c_Ai\epsilon_{\rho\mu\sigma\nu}p_3^\rho p_1^\sigma + \\ &\quad + 4m_pm_n\left(1-c_A^2\right)g_{\mu\nu}\end{aligned} \tag{A.50}$$

Bibliography

[1] B. L. Friman and O. V. Maxwell. Neutrino emissivities of neutron stars. *Astrophys. J.*, 232:541–557, September 1979.

[2] H. Heiselberg and M. Hjorth-Jensen. Phases of dense matter in neutron stars. *Phy. Rep.*, 328, 2000.

[3] G. Baym and Frederick K. Lamb. Neutron stars. *arXiv:physics*, 0503245 v2, Apr 2005.

[4] James M. Lattimer and M. Prakash. The physics of neutron stars. *arXiv:astro-ph*, 0405262 v1, May 2004.

[5] Richard R. Silbar and Sanjay Reddy. Neutron stars for undergraduates. *Am. J. Phys.*, 72(7), July 2004.

[6] N. Iwamoto. Neutrino emissivities and mean free paths of degenerate quark matter. *Ann. Phys.*, 141(1):1–49, June 1982.

[7] C. J. Pethick. Cooling of neutron stars. *Rev. Mod. Phys.*, 64(4):1133–1140, Oct 1992.

[8] Stuart L. Shapiro and Saul A. Teukolsky. Black holes, white dwarfs, and neutron stars. 1983.

[9] Steven Weinberg. Effects of a neutral intermediate boson in semileptonic processes. *Phys. Rev.*, D5:1412–1417, 1972.

[10] J. A. M. Vermaseren. New features of FORM. 1989.

[11] James M. Lattimer, C. J. Pethick, Madappa Prakash, and Pawel Haensel. Direct urca process in neutron stars. *Phys. Rev. Lett.*, 66(21):2701–2704, May 1991.

[12] F. Mandl and G. Shaw. Quantum field theory. 1988.